Dating blueschist-facies metamorphism within the Naga ophiolite, Northeast India, using sheared carbonate veins

Journal:	*International Geology Review*
Manuscript ID	TIGR-2021-0265.R3
Manuscript Type:	Data Article
Date Submitted by the Author:	n/a
Complete List of Authors:	Maibam, Bidyananda; Manipur University, Earth Sciences Palin, Richard M; University of Oxford, Department of Earth Sciences Gerdes, Alex; University of Frankfurt, Geosciences; Goethe-University Frankfurt White, Richard; University of St Andrews, School of Earth and Environmental Sciences Foley, Stephen; Macquarie University, Department of Earth & Planetary Sciences
Keywords:	blueschist, dynamic recrystallisation, exhumation, petrological modelling, U-Pb carbonate geochronology

Dating blueschist-facies metamorphism within the Naga ophiolite, Northeast India, using sheared carbonate veins

Bidyananda Maibam[a]*, Richard M. Palin[b], Axel Gerdes[c,d], Richard W. White[e], Stephen Foley[f]

[a]*Department of Earth Sciences, Manipur University, Canchipur, Imphal-795003, India*

[b]*Department of Earth Sciences, University of Oxford, Oxford, OX1 3AN, United Kingdom*

[c]*Department of Geosciences, Goethe-University Frankfurt, 60438 Frankfurt, Germany*

[d]*Frankfurt Isotope and Element Research Center (FIERCE), Goethe-University Frankfurt, 60438 Frankfurt, Germany*

[e]*School of Earth and Environmental Sciences, University of St. Andrews, KY16 9AL, United Kingdom*

[f]*ARC Centre of Excellence for Core to Crust Fluid Systems, Department of Earth & Environmental Sciences, Macquarie University NSW 2109, Australia*

**corresponding author: bmaibam@yahoo.com*

Keywords: blueschist; dynamic recrystallisation; exhumation; petrological modelling; U–Pb carbonate geochronology

ABSTRACT

The tectonic significance of blueschist-facies rocks associated with the Indo-Myanmar ophiolite belt is uncertain, given lack of detailed petrological study and the paucity of reliable

age data for different stages in their geological evolution. Here, we present new integrated petrological and geochronological data for samples from the Nagaland complex of the Indo-Myanmar ophiolite belt, northeastern India, which constrains the pressure–temperature conditions and absolute ages of peak and retrograde metamorphism. Several samples of blueschist were collected from the region, which have been variably deformed and subjected to shear recrystallization. Based on microstructural constraints and mineral geochemistry, garnet, omphacite, barroisite, chlorite and muscovite are interpreted to represent a high-pressure prograde-to-peak metamorphic assemblage, and omphacite, actinolite, hornblende and albite represent a lower-pressure retrograde metamorphic assemblage that formed during shear-related exhumation. Petrological modelling and thermobarometry indicates that unsheared samples equilibrated at ~1.9 GPa and ~480–520 °C at peak metamorphism, indicating subduction to ~60 km depth, whereas sheared and recrystallised samples re-equilibrated at ~0.6 GPa and ~470 °C during retrograde metamorphism associated with obduction of the Naga ophiolite onto the Indian foreland. U–Pb *in-situ* analysis of carbonate grains (aragonite–calcite) and associated silicate phases (epidote, prehnite, amphibole etc.) in different microstructural positions, including within dynamically recrystallised shear bands that cross-cut older metamorphic fabrics and cogenetic silicate phases, constrains the age of peak metamorphism to be c. 95 Ma and retrograde metamorphism to be c. 90 Ma. Based on the overall progression of ages in the sheared and unsheared samples, we interpret that the area experienced exhumation at a time-averaged rate of ~1 cm/year in the order of Phanerozoic period plate tectonic rate. which is in the order of rates of plate tectonic processes on the Phanerozoic Earth

1. Introduction

High-pressure metamorphic belts provide a critical record of the geological evolution of paleo-plate boundaries, and provide valuable constraints on tectonothermal models of both modern and ancient orogeneses (e.g. Ernst 1973; Carswell 1990). Blueschist-facies rocks form at high-pressure–low-temperature (H*P*–L*T*) metamorphic conditions characteristic of subduction zones (Miyashiro 1961; Cloos 1985; Palin and White 2016) or ephemerally in the embryonic stages of collisional orogeny (Wang and Foley, 2020), where they may subsequently recrystallize to greenschists or amphibolites under higher temperatures and/or lower pressures (Ernst 1973). Combining mineral equilibria constraints on the thermobarometric conditions under which sequential assemblages formed with absolute ages obtained via *in-situ* geochronology, can elucidate the timing and timescales of geodynamic processes that control the subduction–exhumation cycle (e.g. Terry *et al*. 2000; Rubatto and Hermann 2001; St-Onge *et al*. 2013).

The power of this integrated technique is demonstrated here in the case of the Indo-Myanmar ophiolite belt, a part of the Indo-Myanmar Range that extends to the east and southeast of the Himalayan orogen. The geological history and tectonic evolution of this belt is currently poorly understood, such that more precise constraints on the pressure–temperature–time (*P*–*T*–*t*) path of key lithologies are necessary to improving our geological understanding of this part of southeast Asia. Much of the current uncertainty concerning the tectonic evolution and significance of these Indian-plate ophiolitic rocks stems from a lack of reliable petrochronological data. In particular, the timing and *P*–*T* conditions of high-pressure metamorphism in the Indo-Myanmar belt is poorly constrained due to the general absence of datable mineral phases in mafic igneous rocks that are reactive at subsolidus subduction-zone H*P*–L*T* metamorphic conditions. Zircon from jadeitites in this region have previously yielded U–Pb ages ranging from Late Jurassic (c. 147 Ma: Shi *et al*. 2008) to Late Cretaceous (c. 77

Ma: Yui *et al*. 2013), although all of these data show significant scatter due to incomplete recrystallization of magmatic grains and metasomatic/hydrothermal activity during subduction and exhumation, which can partially reset isotope systems (Wang and Griffin 2004). Furthermore, these former studies performed geochronology on zircon grains separated from the host rocks, which inhibits direct correlation of age data with *P–T* conditions derived from metamorphic assemblages and microstructures, leading to potentially unreliable geological interpretations.

The zircon U–Pb isotope system is widely applied for dating the crystallization and re-crystallization of mineral assemblages during high-temperature metamorphic events (e.g. Williams and Claesson, 1987; Parrish, 1990; Robb *et al*. 1999, Rubatto et al., 2001). However, some lithologies and/or geological processes often cannot be dated directly by this technique due to the absence of appropriate minerals that incorporate measurable amounts of radiogenic nuclides. Examples of such rocks can be found in shear zones, but this issue also extends to H*P*–L*T* metamorphic rocks, ore mineralisations, diagenetic minerals and cements, some sedimentary rocks, and some alteration assemblages (e.g. Gilley *et al*. 2003). Recent studies have focused on the application of *in-situ* U–Pb isotope analyses of low-U minerals in thin section by laser ablation inductively coupled plasma mass spectrometry (LA-ICP-MS) for geochronological study (Millonig *et al*. 2012; Coogan *et al*. 2016; Ring and Gerdes 2016; Roberts and Walker 2016; Li *et al*. 2014). Thus, instead of dating single accessory mineral domains, millimetre-sized minerals and mineral assemblages (e.g., carbonate, epidote, amphibole etc.) that recrystallised and equilibrated during a single tectonic event and which contain measurable amounts of U and Pb can be used to determine crystallization ages (e.g. Burisch *et al*. 2017; Ring and Gerdes 2016).

Here we apply the isochron method to dynamically recrystallised carbonate veins and selected mineral assemblages in blueschists within the Kiphiere District of the Nagaland

ophiolite belt and integrate these ages with thermobarometric data to produce new constraints on the timing and rates of subduction and exhumation of Neo-Tethyan crust in the Indo-Myanmar region.

2. Geological background

The Indo-Myanmar Range is thought to represent a relict eastward-dipping subduction zone that runs from the eastern edge of the Himalayan Range in southeast Tibet to the island of Sumatra in the south (Allen *et al*. 2008; Fig. 1). The Eastern Himalayas, about 700 km long, trends ENE-WSW. Broadly N-S trending to sigmoid IMR has subdivided into three sectors from north to south of about 400 km length each e.g., Naga Hills, Chin Hills and Arakan Yoma (Acharyya 2015). The belt continues as the Anadaman Nicobar island arc in the south. Belts of narrow tectonised but nearly continues, late Mesozoic-Eocene ophiolite and associated sediments skirt along the northern margin of the Himalayas (Indus-Tsangpo Ophiolite-ITO) and the eastern margin of the Himalayas IMR. Structural relationships show that Indian-plate oceanic crust was overridden by units of the West Burma Block (e.g. Holt *et al*. 1991; Mitchell *et al*. 2007; Searle *et al*. 2007), although its age of formation and the timing of its obduction are poorly known. The Indo-Myanmar ophiolite belt separates subducted Indian-plate oceanic lithosphere to the west from a closely associated high-pressure metamorphic belt and Jurassic to Cretaceous magmatic arc–forearc complex of the Burmese plate to the east (Mitchell *et al*. 2012). The Naga Hills ophiolite is represented by peridotite, cumulate mafic-ultramafic, mafic volcanics, eclogite, glaucophane schist, amphibolite and late felsic intrusives. The ophiolite sequence has an east-dipping thrust contact with the underlying flysch-like sediments of the Disang and Barail Formations exposed to the west, and are overthrust from the east by continental metamorphic rocks of the Naga Metamorphics consisting of quartz mica-schist, garnet mica-schist, quartzite, and

granitic gneiss (Brunnschweiler, 1966). The mid-Cretaceous, fossil-bearing Nimi Formation occurs at the contact between the ophiolite and the Naga Metamorphics (Chatterjee and Ghose, 2010). Within this belt, blueschist- and eclogite-facies mafic rocks occur as tectonic slices (or detached layers and lenses) intercalated with unmetamorphosed mafic and ultramafic units. Basement lithologies underlie Palaeogene sediments in the ophiolite belt, although their geological history and lithological constitution are uncertain (Acharyya 2015). Ophiolitic rocks within the Indo-Myanmar belt have been subdivided into two parallel groups: the 'Eastern' and 'Western' belts (Mitchell 1993), although both show similar structural and petrological characteristics. Accretion of the Eastern Belt, which contains metamorphosed ultramafic rocks in northern Myanmar that host world-famous jadeitites, is thought to have occurred sometime after the Mesozoic (Gansser 1980; Mitchell 1993; Shi *et al*. 2008). The Western Belt along the Naga and Manipur hills, which forms part of the Indo-Myanmar Range, formed due to collision between India and the Burmese microplate during the late Oligocene (Sengupta *et al*. 1990).

There is still controversy about emplacement ages of ophiolites in these two belts: the 'Eastern Belt' is inferred to mark the locus of the subduction zone into which the ophiolites were accreted since Mesozoic, whilst the 'Western Belt' was inferred to have been caused by a late Oligocene terminal collision between the Indian and the Burmese continental blocks (Shit et al., 2014 and references therein). In the 'Western Belt' a combination of radiolarian biostratigraphy and whole-rock K–Ar geochronology suggests an Upper Jurassic age (Kimmeridgian–Lower Tithonian) for marine sedimentation and volcanism in the Nagaland ophiolite belt (Sarkar *et al*. 1996; Baxter *et al*. 2011). The mid-Cretaceous, fossiliferous Nimi Formation occurs at the contact between the ophiolite and the Naga metamorphic units, and so gives a maximum age constraint on the initiation of obduction. Recently, Singh et al. (2017) reported U–Pb zircon ages ranging between 116 and 119 Ma from the plagiogranite of

the studied ophiolite. In the 'Eastern Belt' falling in the Mynamar Shi *et al*. (2008) reported a sensitive high-resolution ion microprobe (SHRIMP) U–Pb zircon age of 146.5 ± 3.4 Ma for jadeitites of the Jade Mines area, Myanmar, and proposed that subduction may have begun during the Late Jurassic. Mitchell (1993) suggested that the Manipur ophiolitic nappe was emplaced along the Indo-Myanmar ranges during the Mid-Eocene and was followed by a switch to east-dipping subduction from the mid-Miocene onwards. Recently, Liu *et al*. (2016) reported a c. 125 Ma U–Pb zircon crystallisation age for rodingite associated with formation of the ophiolite, and a c. 115 Ma age for garnet amphibolites within the Kalaymo ophiolite belt, which lies adjacent to the Indo-Myanmar ophiolite belt. Shi et al. (2014) reported superimposed tectono-metamorphic ages of phengitic mica Ar-Ar ages from blueschist-facies rocks in the Tagaung-Myitkyina Belt. They interpreted a Jurassic age (152.4 ± 1.5 Ma) obtained from glaucophane as the lower limit of the subduction age and suggested that Eocene (45.0 ± 1.3 Ma) ages recorded an intra-continental shearing deformation event.

Chatterjee and Ghose (2010) documented eclogite- and blueschist-facies rocks present as thrust slices and lenses within the volcanic and ultramafic rocks of the Naga ophiolite belt. Ao and Bhowmik (2014) deduced the thermal history of the eclogite and blueschist rocks ranging from ~1.15 GPa and ~340 °C to 0.6 GPa and 335 °C. Despite an improved understanding of the tectonic evolution of the Indian ophiolite belt, a paucity of reliable geochronological age data has hindered the correlation of sutures and collisional deformation episodes within the region.

3. Analytical methods

The eclogites and blueschists rocks of Naga Hills occur as NE–SW to N–S oriented, steeply east-dipping shear fault-bound tectonic slices or detached layers and lenses intercalated with basaltic and ultramafic units parallel to the shear faults in the Naga Hills ophiolite of Phek

district, Nagaland (Chatterjee and Ghose, 2010). In the area eclogite constitutes the core of some lenses, which are surrounded by successive layers of garnet-blueschist, glaucophanite and greenschist. Twenty metamorphosed samples were collected between Longkhimong and Moya villages, after systematic petrographic study six samples were selected for detailed study. Mineral compositional data for all samples were obtained on a JEOL JXA-8200 electron microprobe housed at the Institute of Geosciences, Johannes-Gutenberg University of Mainz, Germany. Operating conditions included an acceleration voltage of 15 kV, a beam current of 12 nA, and a 2 μm spot size. A matrix correction for atomic number (Z), absorption (A), and fluorescence (F) was automatically applied to all analyses. For the data presented below, mineral compositions were recalculated to standard numbers of oxygens per formula unit (pfu) using the software AX (Holland 2009), with OH assumed to be present in stoichiometric amounts. The proportion of ferric iron in different mineral species was also calculated using AX. Mineral proportions for each sample were determined using the software JmicroVision (Roduit 2010), with each individual count consisting of five hundred points randomly distributed over a digitally scanned thin-section image. Calculated volume proportions of minerals in each sample are given below. These bulk compositions are given in Supplementary Table 3. Mineral abbreviations are after Kretz (1983). Representative compositions of major minerals for all samples are given in Supplementary Table 2 and photomicrographs of microstructural features and assemblages are shown in Figures 2 and 3.

Bulk-rock compositions for use in petrological modelling were obtained from X-ray fluorescence (XRF) via the production of glass beads in order to guarantee standardised and reproducible analyses. Powdered rock samples were initially dried overnight at 105 °C. Approximately 5.2 g of lithium tetraborate ($Li_2B_4O_7$) flux and 0.4 g of powdered rock sample were then weighed, homogenized, and melted in a Vulcan AMA melting device to produce each glass beads. These beads were then analyzed in a Philips MagXPRO spectrometer with

a rhenium X-ray tube housed in the Institute of Geoscience, Johannes Gutenberg University of Mainz, Germany. Detection limits are estimated to be 100 μg g^{-1} for light elements (Na, Mg, Al) and 10 μg g^{-1} for heavy elements (K to U). Analysed major oxides comprised SiO_2, Al_2O_3, total Fe_2O_3, MnO, MgO, CaO, Na_2O, K_2O, TiO_2, P_2O_5, SO_3, Cr_2O_3, and NiO.

All U–Pb ages for the analysed carbonate grains and silicate phases were acquired *in situ* from polished thin sections by laser ablation-inductively coupled plasma-mass spectrometry (LA-ICP-MS) at the Goethe University Frankfurt (GUF), using a Element2 (Thermo-Scientific) sector field ICP-MS coupled to a RESOlution ArF Excimer laser (Compex Pro 102). The applied method was similar as described in Ring and Gerdes (2016), Burisch *et al*. (2017), Hansman *et al*. (2018) and Salih *et al*. (2019). Ablation spot size was 213 μm and crater depth was ~20 μm. Samples were screened by LA-ICP-MS for suitable Pb and U concentration and variability, and selected spots were subsequently analysed in fully automated mode. Spot analyses consisted of 20 s background acquisition followed by 20 s sample ablation. Surface contamination was removed prior to each spot analysis via a 3-s pre-ablation. Soda-lime glass SRM-NIST 614 was used as a reference material together with two carbonate reference materials – WC-1 and a Zechstein dolomite – to bracket sample analysis. SRM-NIST 614 yielded a depth penetration of about 0.5 μm s^{-1} and an average sensitivity of 280,000 cps/μg g^{-1} for ^{238}U. The detection limits for ^{206}Pb and ^{238}U were ~0.1 and 0.05 ng g^{-1}, respectively. All data were corrected using an MS Excel spreadsheet program (Gerdes and Zeh, 2006, 2009). NIST 614 was used as a standard for the analysis of silicate phases. The possible offset related to sample matrix is within the analytical uncertainty of the quoted ages.

The $^{207}Pb/^{206}Pb$ ratio was corrected for mass bias (0.3%) and the $^{206}Pb/^{238}U$ ratio for inter-element fraction (ca. 5%) using SRM-NIST 614. An additional correction of 4% was applied on the $^{206}Pb/^{238}U$ to correct for difference in the fractionation due to the carbonate

matrix. This resulted in a lower intercept age of 23 WC-1 spot analyses of 254.1 ± 1.5 (MSWD = 1.5; anchored at $^{207}Pb/^{206}Pb$ of 0.851) and 253.9 ± 3.4 (MSWD = 1.5; n = 17) for the Zechstein dolomite used as an in-house reference material in Frankfurt. Data were plotted on a Tera-Wasserburg diagram and ages calculated as lower intercepts using Isoplot 3.71 (Ludwig 2007). All uncertainties are reported at the 2 sigma level.

According to Rasbury and Cole (2009), a linear regression taken through a group of samples from the same system produces a slope from which an age can be calculated using the accepted decay rate for the parent isotope. If the system being analysed has no initial heterogeneity, and it remained closed throughout the duration of the decay process, all scatter of data points about the isochron can be explained by analytical uncertainties. Closed isotopic systems will plot as a line, giving a precise age and low mean squared weighted deviate (MSWD) of ~1, while systems that have not remained closed will show scatter and have a high MSWD (>>1).

4. Sample petrology

Out of the twenty collected samples we have selected four metabasite samples for systematic study and thermobarometry Six metabasite samples were collected from. Locality information and GPS co-ordinates for each outcrop are given in Supplementary Table 1 and location map is presented in Figure 1C. Field photographs of the studied samples are presented in Figure 1D. The samples occur as meter-sized boulder blocks, which occur individually and in clusters (Figures 1 D1, D3) within serpentinites. Samples are thus classified as either sheared or unsheared based on the occurrence of key deformational features present at the field, hand sample, and microscopic scale. Samples N5 and 14 lack evidence of post-peak shear-driven recrystallization and likely represent relics of

undeformed, peak metamorphic blueschists. By contrast, samples 7c, 13, 3b, and 11 are strongly sheared and represent subsequently deformed equivalents of these older units.

4.1. Sample description

4.1.1. Unsheared samples N5 and 14

Unsheared samples N5 and 14 exhibit a largely unfoliated microstructure and show no evidence of pervasive retrogression following peak blueschist-facies metamorphism during subduction, though localised retrogression does occur. Sample N5 is a blueschist that contains abundant sodic amphibole (38%) and epidote (37%), with minor quartz (9%), garnet (6%), sodic–calcic amphibole (4%), phengite (3%), and rutile (2%). Accessory pyrite, zircon, and apatite also occur. Garnet porphyroblasts are between 0.5 and 2 mm in diameter (Figures 2a–b) and exhibit no substantial major element compositional zoning, with core compositions of $Alm_{56–58}Prp_{12–14}Grs_{21–22}Sps_{7–8}$ and rim compositions of $Alm_{60–61}Prp_{15–16}Grs_{22–23}Sps_{3–4}$ (Supplementary Table 2 and Fig. 4). Core regions contain inclusions of pumpellyite, phengite, epidote, barroisite, actinolite, and quartz, and rims contain inclusions of phengite, epidote, actinolite, rutile, and quartz. Some grains show replacement by chlorite at their outermost rims. Matrix phengite has Si = 3.34–3.38 pfu (on a 11 O basis; Supplementary Table 2) and grains included in the outer rims of garnet has Si = 3.32–3.35 pfu. Epidote shows no significant compositional zoning from core to rim, with a minor range in pistacite content [XPs = $Fe^{3+}/(Al^{3+}+Fe^{3+})$] of 0.18–0.21 (Supplementary Table 2). According to the classification scheme of Hawthorne *et al*. (2012), sodic and sodic-calcic amphiboles in the matrix are glaucophane and winchite–katophorite, respectively (Figure 5).

Sample 14 is modally dominated by epidote (50%) and quartz (35%), with lesser garnet (1%), sodic-calcic amphibole (10%), phengite (2%), rutile (0.5%), titanite (0.5%), and carbonate (1%). Accessory minerals include chlorite, apatite, and zircon (all <<1%).

Although sample 14 displays no foliation, it is mildly anisotropic, with alternating centimetre-scale quartz- and epidote-rich domains. In contrast to the large porphyroblasts present in sample N5, garnet forms <0.1 mm diameter grains that are restricted to quartz-rich regions (Figure 2). These garnet grains have no inclusions and are compositionally homogeneous ($Alm_{36–39}Prp_{10–13}Grs_{31–36}Sps_{36–39}$). Epidote shows no significant zoning, with core and rim compositions both having similar pistacite contents of 0.20–0.24 (Supplementary Table 2). Matrix rutile is partially or fully replaced by titanite (Figure 2), though rare inclusions in sodic-calcic amphibole lack such pseudomorph textures. Phengite contains Si = 3.34–3.35 pfu (Supplementary Table 2) and in places is intimately intergrown with chlorite, though the extremely fine-grained nature of these intergrowths prohibited reliable compositional analysis of either phase. Sodic-calcic amphibole in the matrix is barroisite–winchite–katophorite (Hawthorne *et al*. 2012; Figure 5), with rare tremolite**,** likely representing minor post-peak retrograde mineralogical transformation.

4.1.2. Sheared samples 11 and 7c

In contrast to N5 and 14, sheared samples 11 and 7c contain distinct spaced foliations that are truncated by carbonate- and quartz-filled veins. These crosscutting veins commonly form shear bands (Figures 3e–f) and locally deflect the main metamorphic foliations at their boundaries (Figure 3b), indicating that shearing and vein formation post-dated subduction metamorphism. The host rock domains in sample 7c are dominated by epidote (39%), calcic amphibole (32%), and sodic–calcic amphibole (18%), with minor phengite (4%), albite (2%), K-feldspar (2%), titanite (1%), and quartz (2%). Apatite and zircon occur as accessory phases. The main metamorphic foliation is defined by elongate and aligned crystals of epidote and amphibole (Figure 3a). Large green calcic amphibole is mostly pargasite with thin magnesiohornblende outer rims, and sodic-calcic amphibole is winchite (Figure 5).

Matrix phengite has Si = 3.39–3.43 pfu and epidote cores have *X*Ps = 0.19–0.25 and rims have *X*Ps = 0.26–0.33 (Supplementary Table 2). Quartz- and carbonate -filled veins crosscut and offset this epidote- and amphibole-defined metamorphic foliation (Figure 3b).

Sample 11 contains abundant sodic amphibole (33%), quartz (34%), carbonate (14%), and sodic pyroxene (11%), with subsidiary sodic–calcic amphibole (2%), phengite (1%), garnet (2%), and albite (1%). Accessory pyrite, titanite, apatite, and zircon (all <<1%) also occur. Alternating sodic amphibole (glaucophane) and quartz-rich bands define a spaced foliation that wraps around porphyroblasts of pyroxene and garnet (Figure 3c). Grains of the latter are commonly less than 1 mm in diameter and are variably replaced by aggregates of carbonate, albite and/or quartz (Figure 3d). Though individual grains lack any significant major-element compositional zoning from core to rim, compositions vary significantly between grains; the majority are spessartine-rich ($Alm_{19–24}Prp_{10–14}Grs_{17–20}Sps_{45–51}$), while others are richer in almandine and grossular ($Alm_{26–29}Prp_{12}Grs_{23–32}Sps_{28–37}$). Minor sodic-calcic amphibole in the matrix is winchite, and sodic pyroxene porphyroblasts are compositionally classified as aegirine–augite (X_{Jd} = 0.04–0.23) (Morimoto *et al*. 1988).

5. Phase equilibria modelling

Constraints on the *P–T* conditions of peak subduction-zone metamorphism were obtained from unsheared samples N5 and 14, whereas constraints on the *P–T* conditions of subsequent ductile shearing were obtained from sheared sample 7c. Preliminary investigation of phase equilibria stability in sample 11 did not allow for reliable thermobarometry to be performed due to the high variance of the interpreted peak mineral assemblage. Phase diagrams showing the *P–T* conditions over which equilibrium mineral assemblages are calculated to occur in a specific bulk-rock composition (pseudosections) were constructed using THERMOCALC v3.40i and the internally consistent thermodynamic data set ds55 (Powell and Holland 1988;

Holland and Powell 1998; updated to August 2004) in the Na_2O–CaO–K_2O–FeO–MgO–Al_2O_3–SiO_2–H_2O–TiO_2–O (NCKFMASHTO) compositional system. The following activity–composition relations for solid-solution phases were used: clinoamphibole (calcic, sodic-calcic, and sodic amphibole; Diener and Powell 2012), clinopyroxene (diopside and omphacite, Diener and Powell 2012), muscovite and paragonite (Coggon and Holland 2002), talc and epidote (Holland and Powell 1998), chlorite (Holland *et al*. 1998), biotite and garnet (White *et al*. 2007), plagioclase and K-feldspar (Holland and Powell 2003), ilmenite and hematite (White *et al*. 2000). Albite, lawsonite, rutile, titanite, quartz, kyanite, and H_2O were treated as pure phases.

5.1. Metamorphic mineral equilibria modelling parameters

Bulk-rock compositions used for modelling were obtained via XRF analysis, as discussed previously (Supplementary Table 2). Point counting was applied to the entire thin section image, aside from areas that do not actually contain pieces of the rock (e.g. as it is not a perfect rectangle). 500 points were sufficient in this case, as we kept track of the evolving proportions during analyses and the values converged on final results after ~300 points or so. For sample 7c, areas adjacent to shear bands were excluded from consideration during point counting such that the proportions obtained represent unsheared portions of the sample that equilibrated prior to deformation.

The fluid contents for each bulk rock composition during metamorphism were calculated using the proportions of hydrous phases present in each equilibrium mineral assemblage, assuming H_2O was present in stoichiometric amounts. Mixed-component fluids were not considered due to the lack of reliable a-x relations for C–O–H fluids at elevated pressures; nonetheless, however, this should not have any significant effects on our calculated diagrams, as unsheared sample N5 does not contain carbonate, unsheared sample 14 contains only a minor proportion (2.2 vol. %), and carbonate veins in sheared sample 7c are

interpreted from microstructural constraints to post-date final metamorphism and textural equilibration. Pressure uncertainties for assemblage field boundaries are approximately ±0.1 GPa (Powell and Holland 2008; Palin *et al*. 2016).

5.1.1. Unsheared samples

Calculated mineral assemblages matching those observed in unsheared samples N5 and 14 constrain peak *P–T* conditions of subduction-zone metamorphism to ~1.8–2.0 GPa and ~420–560 °C, with the calculated proportions and compositions of major minerals best matching observed values at ~1.9 GPa and ~480–520 °C. These conditions lie along the global range of *P–T* conditions predicted to occur at the surface of subducted oceanic crust in modern-day subduction zones (Syracuse *et al*. 2010; Penniston-Dorland *et al*. 2015).

5.1.2. Sheared sample

In contrast with the undeformed samples, the observed mineral assemblage in sample 7c was calculated to be stable at the notably lower pressure and slightly lower temperature conditions of ~0.2–0.6 GPa and ~420–490 °C, with observed and calculated mineral proportions and compositions matching best at ~0.6 GPa and ~470 °C. Semi-independent constraints on *P–T* conditions using the avPT function of THERMOCALC for each sample produced similar and statistically robust results of 2.05 ± 0.22 GPa and 489 ± 39 °C for N5, 1.95 ± 0.18 GPa and 541 ± 34 °C for 14, and 0.60 ± 0.23 GPa and 464 ± 76 °C for 7c (Supplementary Table 4) corroborating the results obtained by phase diagram modelling.

6. U–Pb geochronology

U–Pb isotopic analysis of carbonate grains was carried out on metabasite samples 14 (unsheared), 11 (sheared), 3b and 13, which equilibrated at different stages of the subduction–exhumation cycle. Carbonate crystals within dynamically recrystallised veins

were preferentially selected for analyses; however, suitable matrix minerals were also investigated in order to perform a check on the analysed carbonates, which generally have a low U content. Results of the isotopic composition of the Nagaland blueschists are presented in Supplementary Table 5 and isochrons are shown in Figure 9. Measured $^{207}Pb/^{206}Pb$ ratios range from 0.205 to 0.836 (sample 3b), 0.735 to 0.848 (sample 13), 0.776 to 0.845 (sample 11) and 0.809 to 0.846 (sample 14), and measured $^{238}U/^{206}Pb$ ratios range from 0.361 to 9.752 (sample 3b), 0.043 to 10.53 (sample 13), 0.118 to 5.474 (sample 11) and 0.809 to 0.846 (sample 14). All data for each sample lie on a single array on an isochron diagram, indicating that each attained isotopic equilibrium, and give well-defined least squares fit indices with MSWD values of 0.35–1.17 (Figure 9). The U concentrations in the minerals range between 0 and 3 ppb and model Th/U ratios show a wide variation, with most lying between 0.015 and 5, but some reaching up to ~46. These analyses show that unsheared samples 14 and 11 equilibrated at 95.3 ± 5.9 Ma and 93.7 ± 4.0 Ma, respectively, and sheared samples 3b and 13 experienced exhumation-related shear deformation at 90.6 ± 3.4 Ma and 88.8 ± 2.7 Ma, respectively. Although the unsheared sample dataset is within uncertainty of all the sheared sample dates, an overall age progression may be reconstructed from the sheared and unsheared samples. Considering the well-behaved dataset in the studied samples with a low MSWD, it can be broadly inferred that the analysed phases had the same initial isotopic ratio and that the system was at equilibrium during closure of the isotopic system.

7. Discussion and implications

Most natural carbonate occurs in the form of calcite and can be transported to the Earth's interior via subduction of carbonate-rich sediments or metasomatized oceanic crust (Zhang *et al*. 2018). Calcite transforms to aragonite at high pressure. Although may revert back to calcite during exhumation if there are no kinetic limitations. At the *P–T* conditions of peak metamorphism for samples N5 and 14, the carbonate likely stabilised in the form of aragonite,

whereas carbonate in sheared samples 11 and 7c is calcite, which indicates polymorphic transformation following exhumation from peak depths. Representative BSE images showing the analysed spots are presented in Figure 10.

The tectonothermal evolution of the Indo-Myanmar Tethyan ophiolite belt is poorly understood owing to a lack of integrated thermobarometry and geochronology. Here, we have combined microstructurally constrained U–Pb data with *P–T* conditions calculated for peak and retrograde metamorphism in order to constrain the exhumation history of the Nagaland region of this ophiolite complex (Figure 11). The investigated samples show considerable microstructural variation, ranging from largely undeformed (N5 and 14) to sheared (11, 3b, 7c, and 13). The contrasting textures and ages of the studied rocks, together with reported metamorphic recrystallizations ages in the adjoining ophiolite belts in Myanmar (Shi *et al*. 2008; Yui *et al.* 2013; Liu *et al*. 2016) suggest that the terrain has undergone several metamorphic events. In terms of texture, the blueschist facies rocks (N5 and 14) do not show any obvious preferred orientation that they were formed predominantly under near-hydrostatic conditions, without apparent shear deformation. By contrast, the sheared samples record deformation and post-tectonic (annealing) recrystallization, as the constituent minerals display preferred orientation, bending, and curving.

Mineral assemblages in the unsheared samples N5 and 14 constrain peak *P–T* conditions of subduction-zone metamorphism to ~1.8–2.0 GPa and ~420–560 °C, with the calculated proportions and compositions of major minerals matching observed values at ~1.9 GPa and ~480–520 °C (Figure 6).

By contrast, the observed mineral assemblage in sheared (sample 7c) was calculated to be stable at notably lower *P–T* conditions of ~0.2–0.6 GPa and ~420–490 °C, with observed and calculated mineral proportions and compositions matching best at ~0.6 GPa and ~470 °C. The calculated peak metamorphic conditions for the unsheared samples agree with *P–T*

conditions previously reported for the area (Chatterjee and Ghose 2010). The *P–T* conditions are far-removed from the slab-top range for modern-day subduction reported by Syracuse *et al*. (2010). The calculated pressures of ~1.9 GPa for peak metamorphism and ~0.6 GPa for retrograde equilibration are approximately equivalent to depths of 60 km and 15 km, respectively, assuming no significant tectonic overpressure. In Figure 10, the *P–T* path calculated here is compared with published examples for other blueschist samples from the Naga ophiolites and other studies with thermal models of the global active subduction zones (Syracuse *et al*. 2010).

The age of the high-*P* metamorphic event is crucial to the reconstruction of the geological history of this little-known terrain; however, reliable metamorphic age data has been lacking, and ages for the Nagaland ophiolite are poorly resolved whereas it is not so in the Eastern Belt. We have integrated our new age and *P–T* data into a revised tectonic model for the evolution of the Naga ophiolite belt, as shown in Figure 12. Only one whole-rock K–Ar isotopic age of 148 ± 4 Ma (Upper Jurassic) has been reported from a volcanic rock in this area (Sarkar *et al*. 1996), which is supported by a radiolarian age (Baxter *et al*. 2011), whereas recently, a younger U–Pb zircon age of 115 Ma (Lower Cretaceous) has been reported from a plagiogranite (Singh *et al*. 2017). Based on the available geochronological and radiolarian ages, the formation age of the Nagaland ophiolite crust thus likely ranges between Early Cretaceous (Liu *et al*. 2016; our unpublished data) and Late Jurassic (Figure 12a). Past plate reconstructions during this period suggest that early subduction off the coast of Myanmar dipped to the west during the Jurassic, but there was a reversal in polarity immediately prior to the Early Cretaceous (Figure 12b; Bhowmik and Ao, 2015). This reversal caused the proto-Nagaland ophiolite complex oceanic crust to experience subduction along an eastern-dipping convergent margin during the Early Cretaceous, with U–Pb ages of the blueschist associated with the Nagaland ophiolite

suggesting that peak high-pressure metamorphism was reached at around this time (Figure 12c).

Utilizing the integrated petrologically constrained *in situ* ages and thermobarometry shows that the unsheared sample 14 yielded a U–Pb age of 95.3 Ma while sheared samples yielded ages ranging between 93.7 Ma (sample 11) and 88.8 Ma (sample 13) Ma, illustrating an age difference between the sheared and unsheared samples. This suggests that the Mesozoic ophiolite underwent H*P*–L*T* subduction-related metamorphism c. 95 Ma and that exhumation was a continuous process that lasted until c. 89 Ma (Figure 12d). This age range is in agreement with the Guillot *et al*. (2008)'s H*P* metamorphic age inferred from K–Ar whole rock and mineral (phengite, glaucophane) ages of 100 to 80 Ma for the western Himalayan Tethyan ophiolites. Based on a zircon isotopic study, an older age of 115 Ma has been reported from the garnetiferous amphibolite of the adjoining Myanmar ophiolite (Liu *et al*. 2016). However, no petrological information was presented, making it hard to evaluate the significance of this age. As a consequence, it is unclear whether the available ages record a prolonged emplacement event, discrete metamorphic events or if the older amphibolite represents remnants of metamorphic sole of the ophiolite belt. Although the unsheared sample dataset is within uncertainty of the sheared sample dates, an overall age progression is evident from the studied sheared and unsheared samples. Based on the combined U–Pb age dataset and the calculated *P–T* regime**,** it can be inferred that the Nagaland blueschist rocks were exhumed at a rate of ~1 cm/year (~45 km in 5 Ma), which is in the order of rates of plate tectonic processes on the Phanerozoic Earth. However, exhumation along the slab interface would imply overall faster transport rates to achieve this vertical rate.

U–Pb dating of low-uranium minerals such as calcite, prehnite, epidote, amphibole at small scale is a new and promising geochronological method. In the present study, we focussed on both carbonate and other cogenetic silicate phases such as prehnite, epidote,

amphibole etc. formed at the same time and the isotopic systems seem to be closed since the metamorphic event. The reported age uncertainty could be improved by using well characterised specific with less scatter age and matrix matched standards (e.g., carbonate minerals normalisation of Pb–Pb isotope is currently achieved using a synthetic glass other than a carbonate, Roberts et al. 2020) reference materials (both carbonate and silicate phases) Although the behaviour of uranium in carbonates that have undergone high *P*/low *T* is not clear because of the lack of studies in natural and synthetic systems, our study suggest that the U–Pb systematics of carbonate can withstand temperatures up to 500 °C without resetting. These data thus encourage the ongoing development of in-situ dating of carbonates and low uranium silicate minerals as a tool to understand the rates and ages of tectonic processes.

Acknowledgements

BM began this work during his visits to JGU Mainz on a BOYSCAST Fellowship and continued during the INSA-DFG Exchange programme visit to Bonn. BM thanks the Council of Scientific and Industrial Research, Government of India for financial support in the form of a project. Sample processing equipment were procured under a Department of Science and Technology, Government of India FIST program. This is FIERCE contribution XX. BM acknowledges Yhunyulo Tep for the help during the field work. Lorenzo Fedele (Napoli) and four anonymous journal reviewers are appreciated for their insightful comments.

References

Acharyya S.K., 2015, Indo-Burman Ranges: a belt of accreted microcontinents, ophiolites and Mesozoic–Paleogene flyschoid sediments: International Journal of Earth Sciences, v. 104, p. 1235–1251.

Allen, R., Najman, Y., Carter, A., Barfod, D., Bickle, M.J., Chapman, H.J., Garzanti, E., Vezzoli, G., Ando, S., and Parrish, R.R., 2008, Provenance of the Tertiary sedimentary rocks of the Indo-Burman Ranges, Burma (Myanmar): Burman arc or Himalayan-derived?: Journal of the Geological Society of London, v. 165, p. 1045–1057.

Anon., 1986, Geology of Nagaland ophiolite: Geological Survey of India Memoir, v. 119, 113 pp.

Ao, A., Bhowmik, S.K., 2014, Cold subduction of the Neotethys: the metamorphic record from finely banded lawsonite and epidote blueschists and associated metabasalts of the Nagaland Ophiolite Complex, India: Journal of Metamorphic Geology, v. 32, p. 829–860.

Baxter, A.T., Aitchison, J.C., Zyabrev, S.V., and Ali, J.R., 2011, Upper Jurassic radiolarians from the Naga Ophiolite, Nagaland, northeast India: Gondwana Research, v. 20, p. 638–644.

Bhowmik, S.K., and Ao, A., 2016, Subduction initiation in the Neo-Tethys: constraints from counterclockwise P–T paths in amphibolite rocks of the Nagaland Ophiolite Complex, India: Journal of Metamorphic Geology, v. 34, p. 17–44.

Brunnschweiler, R.O., 1966, On the geology of the Indoburman ranges — Arakan Coast and Yoma, Chin Hills, Naga Hills: Journal of the Geological Society of Australia, v. 13, p. 137–194.

Burisch, M., Gerdes, A., Walter, B.F., Neumann, U., Fettel, M. and Markl, G., 2017, Methane and the origin of five-element veins: Mineralogy, age, fluid inclusion chemistry and ore forming processes in the Odenwald, SW Germany: Ore Geology Reviews, v. 81, p. 42–61.

Carswell, D.A., 1990, Eclogite-Facies Rocks. Blackie, London.

Chatterjee, N., and Ghose, N.C., 2010, Metamorphic evolution of the Naga Hills eclogite and blueschist, North India: implications for early subduction of the Indian plate under the Burma microplate: Journal of Metamorphic Geology, v. 28, p. 209–225.

Cloos, M., 1985, Thermal evolution of convergent margins: Thermal modelling and evaluation of isotopic Ar-ages for blueschists in the Franciscan Complex of California: Tectonics, v. 4, p. 421–433.

Coggon, R., and Holland, T.J.B., 2002, Mixing properties of phengitic micas and revised garnet–phengite thermobarometers: Journal of Metamorphic Geology, v. 20, p. 683–696.

Coogan, L.A., Parrish, R.R. and Roberts, N.M., 2016, Early hydrothermal carbon uptake by the upper oceanic crust: Insight from in situ U–Pb dating: Geology, v. 44(2), p. 147–150.

Diener, J.F.A., and Powell, R., 2012, Revised activity–composition models for clinopyroxene and amphibole: Journal of Metamorphic Geology, v. 30, p. 131–142.

Ernst, W.G., 1973, Blueschist metamorphism and P–T regimes in active subduction zones: Tectonophysics, v. 17, p. 255–272.

Gansser, A., 1980, The significance of the Himalayan suture zone: Tectonophysics, v. 62, p. 37–52.

Gilley, L.D., Harrison, T.M., Leloup, P.H., Ryerson, F.J., Lovera, O.M. and Wang, J.H., 2003, Direct dating of left-lateral deformation along the Red River shear zone, China and Vietnam: Journal of Geophysical Research: Solid Earth, v. 108(B2), 2127.

Guillot, S., Mahéo, G., de Sigoyer, J., Hattori, K.H. and Pêcher, A., 2008, Tethyan and Indian subduction viewed from the Himalayan high- to ultrahigh-pressure metamorphic rocks: Tectonophysics, v. 451, p. 225–241.

Hansman, R.J., Albert, R., Gerdes, A., and Ring, U., 2018, Absolute ages of multiple generations of brittle structures by U-Pb dating of calcite: Geology, v. 6(3), p. 207–210.

Hawthorne, F.C., Oberti, R., Harlow, G.E., Maresch, W.V., Martin, R.F., Schumacher, J.C. and Welch, M.D., 2012. Nomenclature of the amphibole supergroup. American Mineralogist, v. 97, p. 2031–2048.

Hernández-Uribe, D., Palin, R.M., Cone, K.A. and Cao, W., 2020. Petrological implications of seafloor hydrothermal alteration of subducted mid-ocean ridge basalt: Journal of Petrology, v. 9, p. egaa086, doi: 10.1093/petrology/egaa086

Holland, T.J.B., 2009, AX: A program to calculate activities of mineral end-members from chemical analyses. http://www.esc.cam.ac.uk/research/research-groups/holland/ax. Accessed June 2015.

Holland, T.J.B., and Powell, R., 1998, An internally consistent thermodynamic dataset for phases of petrological interest: Journal of Metamorphic Geology, v. 16, p. 309–344.

Holland, T.J.B., and Powell, R., 2003, Activity-composition relations for phases in petrological calculations: an asymmetric multicomponent formulation: Contributions to Mineralogy and Petrology, v. 145, p. 492–501.

Holland, T.J.B., Baker, J.M., and Powell, R., 1998, Mixing properties and activity–composition relationships of chlorites in the system MgO–FeO–Al_2O_3–SiO_2–H_2O: European Journal of Mineralogy, v. 10, p. 395–406.

Holt, W.E., Ni, J.F., Wallace, T.C., and Haines, A.J., 1991, The active tectonics of the Eastern Himalayan syntaxis and surrounding regions: Journal of Geophysical Research, v. 96, p. 14595–14632.

Johannes, W., and Puhan, D., 1971, The calcite-aragonite transition, reinvestigated. Contributions to Mineralogy and Petrology, v. 31(1), p. 28–38.

Khogenkumar, S., Singh, A.K., Kumar, S., Lakhan, N., Chaubey, M., Imtisunep, S., Dutt, A. and Oinam, G., 2021, Subduction versus non-subduction origin of the Nagaland-Manipur Ophiolites along the Indo-Myanmar Orogenic Belt, northeast India: Fact and fallacy. Geological Journal, v. 56(4), p. 1773–1794.

Kretz, R., 1983, Symbols for rock-forming minerals: American Mineralogist, 68, 277–279.

Li, Q., Parrish, R.R., Horstwood, M.S.A., and McArthur, J.M., 2014, U–Pb dating of cements in Mesozoic ammonites: Chemical Geology, v.376, p. 76–83.

Liu, C.-Z., Chung, S.-L., Wu, F.-Y., Zhang, C., Xu, Y., Wang, J.-G., Chen, Y. and Guo, S., 2016, Tethyan suturing in Southeast Asia: Zircon U–Pb and Hf–O isotopic constraints from Myanmar ophiolites: Geology, v. 44, p. 311–314.

Ludwig, K., 2007, Isoplot 3.62, Berkley Geochronology Centre Special Publication 4, p. 70.

Morimoto, N. *et al*. 1988, Nomenclature of pyroxenes: American Mineralogist, v. 73, p. 1123–1133.

Millonig, L.J., Gerdes, A., and Groat, L.A., 2012, U–Th–Pb geochronology of meta-carbonatites and meta-alkaline rocks in the southern Canadian Cordillera: a geodynamic perspective: Lithos, v. 152, p. 202–217.

Mitchell, A.H.G., 1993, Cretaceous–Cenozoic tectonic events in the western Myanmar–Assam region: Journal of the Geological Society of London, v. 150, p. 1089–1102.

Mitchell, A.H.G., Htay, M.T., Htun, K.M., Win, M.N., Oo, T., and Hlaing, T., 2007, Rock relationships in the Mogok Metamorphic Belt, Tatkon to Mandalay, central Myanmar: Journal of Asian Earth Sciences, v. 29, p. 891–910.

Mitchell, A.H.G., Chung, S.-L., Oo, T., Lin, T.-H., and Hung, C-H., 2012, Zircon U-Pb ages in Myanmar: magmatic-metamorphic events and the closure of a Neo-Tethys Ocean?: Journal of Asian Earth Sciences, v. 56, p. 1–23.

Miyashiro, A., 1961, Evolution of metamorphic belts. Journal of Petrology, v. 2, p. 277–311.

Palin, R.M., and White, R.W., 2016, Emergence of blueschists on Earth linked to secular changes in oceanic crust composition: Nature Geoscience, v. 9, p. 60–64.

Palin, R.M., Weller, O.M., Waters, D.J., and Dyck, B., 2016, Quantifying geological uncertainty in metamorphic phase equilibria modelling; a Monte Carlo assessment and implications for tectonic interpretations: Geoscience Frontiers, v. 7, p. 591–607.

Penniston-Dorland, S. C., Kohn, M. J., and Manning, C. E., 2015, The global range of subduction zone thermal structures from exhumed blueschists and eclogites: Rocks are hotter than models: Earth and Planetary Science Letters, v. 428, p. 243–254.

Powell, R., and Holland, T.J.B., 1988, An internally consistent thermodynamic dataset with uncertainties and correlations: 3. Application to geobarometry, worked examples, and a computer program: Journal of Metamorphic Geology, v. 6, p. 173–204.

Powell, R., and Holland, T.J.B., 1994, Optimal geothermometry and geobarometry: American Mineralogist, v. 79, p. 120–133.

Rasbury, E.T., Cole, J.M., 2009, Directly dating geologic events: U–Pb dating of carbonates: Reviews of Geophysics v. 47, RG3001.

Ring, U., and A. Gerdes, 2016, Kinematics of the Alpenrhein-Bodensee graben system in the Central Alps: Oligocene/Miocene transtension due to formation of the Western Alps arc: Tectonics, v. 35, doi:10.1002/2015TC004085.

Robb, L.J., Armstrong, R.A., and Waters, D.J., 1999, The history of granulite-facies metamorphism and crustal growth from single zircon U–Pb geochronology: Namaqualand, South Africa: Journal of Petrology, v. 40, p. 1747–1770.

Roberts, N.M.W. and Walker, R.J., 2016. U-Pb geochronology of calcite-mineralized faults: Absolute timing of rift-related fault events on the northeast Atlantic margin: Geology, v. 44, p. 531–534.

Roberts, N.M.W., Drost, K., Horstwood, M.S.A., Condon, D.J., Chew, D., Drake, H., Milodowski, A.E., McLean, N.M., Smye, A.J., Walker, R.W., Haslam, R., Hodson, K., Imber, J., Beaudoin, N., and Lee, J.K., 2020. Laser ablation inductively coupled plasma mass spectrometry (LA-ICP-MS) U–Pb carbonate geochronology: strategies, progress, and limitations: Geochronology, v. 2, p. 33–61,

Roduit, N., 2010. JMicroVision: un logiciel d'analyse d'images pétrographiques innovant: Étude sur différentes méthodes de quantification et de caractérisation des roches. Éditions universitaires Européennes, 136 pp.

Rubatto, D., and Hermann, J., 2001, Exhumation as fast as subduction?: Geology, v. 29, p. 3–6.

Rubatto, D., Williams, I.S. and Buick, I.S., 2001, Zircon and monazite response to prograde metamorphism in the Reynold Range, Central Australia: Contribution to Mineralogy and Petrology, v. 140, p. 458–468.

Sarkar, A., Datta, A.K., Poddar, B.C., Bhattacharyya, B.K., Kollapuri, V.K., and Sanwal, R., 1996, Geochronological studies of Mesozoic igneous rocks from eastern India: Journal of Southeast Asian Earth Sciences, v. 13, p. 77–81.

Salih, N., Mansurbeg, H., Kolo, K., Gerdes, A., and Préat, A., 2019, In situ U-Pb dating of hydrothermal diagenesis in tectonically controlled fracturing in the Upper Cretaceous Bekhme Formation, Kurdistan Region-Iraq: International Geology Review, v. 62, p. 2261–2279.

Schmidt, M.W., and Poli, S., 1998, Experimentally based water budgets for dehydrating slabs and consequences for arc magma generation: Earth and Planetary Science Letters, v. 163, p. 361–379.

Searle, M.P., Noble, S.R., Cottle, J.M., Waters, D.J., Mitchell, A.H.G., Hlaing, T., and Horstwood, M.S.A., 2007, Tectonic evolution of the Mogok metamorphic belt, Burma

(Myanmar) constrained by U–Th–Pb dating of metamorphic and magmatic rocks: Tectonics, v. 26, p. TC3014.

Sengupta, S., Ray, K.K., Acharyya, S.K., and de Smeth, J.B., 1990, Nature of ophiolite occurrence along eastern margin of Indian plate and their tectonic significance: Geology, v. 18, p. 439–442.

Shi, G.H., Cui, W.Y., Cao, S.M., Jiang, N., Jian, P., Liu, D.Y., Miao, L.C., and Chu, B.B., 2008, Ion microprobe zircon U–Pb age and geochemistry of the Myanmar jadeitite: Journal of the Geological Society of London, v. 165, p. 221–234.

Shi, G., Lei, W., He, H., Nok Ng, Y., Liu, Y., Liu Y., Yuan, Y., Kang, Z., and Xie, G., 2014, Superimposed tectono-metamorphic episodes of Jurassic and Eocene age in the jadeite uplift, Myanmar, as revealed by $^{40}Ar/^{39}Ar$ dating. Gondwana Research, v. 26, p. 464–474.

Singh, A.K., Chung, S.L., Bikramaditya, R.K. and Lee, H.Y., 2017, New U–Pb zircon ages of plagiogranites from the Nagaland-Manipur Ophiolites, Indo-Myanmar Orogenic Belt, NE India: Journal of Geological Society of London, v. 174, p. 170–179.

St-Onge, M.R., Rayner, N., Palin, R.M., Searle, M.P., Waters, D.J., 2013, Integrated pressure-temperature-time constraints for the Tso Morari dome (NW India): Implications for the burial and exhumation path of UHP units in the western Himalaya: Journal of Metamorphic Geology, v. 31, p. 469–504.

Stacey, J.S., and Kramers, J.D., 1975, Approximation of terrestrial lead isotope evolution by a two-stage model: Earth and Planetary Science Letters, v. 26, p. 207–221.

Syracuse, E.M., van Keken, P.E., and Abers, G.A., 2010, The global range of subduction zone thermal models. Physics of the Earth and Planetary Interiors, v. 183, p. 73–90.

Terry, M.P., Robinson, P. and Ravna, K., 2000, Kyanite eclogite thermobarometry and evidence for thrusting of UHP over HP metamorphic rocks, Nordøyane, Western Gneiss Region, Norway: American Mineralogist, v. 85, p. 1637–1650.

Wang, X. and Griffin, W.L., 2004, Unusual Hf contents in metamorphic zircon from coesite-bearing eclogites of the Dabie Mountains, east-central China: implications for the dating of ultrahigh-pressure metamorphism: Journal of Metamorphic Geology, v. 22, p. 629–637.

Wang, Y., and Foley, S.F., 2020, The role of blueschist stored in shallow lithosphere in the generation of post-collisional orogenic magmas: Journal of Geophysical Research, v. 125, doi.org/10.1029/2020JB019910.

White, R.W., Powell, R., and Holland, T.J.B., 2007, Progress relating to calculation of partial melting equilibria for metapelites: Journal of Metamorphic Geology, v. 25, p. 511–527.

White, R.W., Powell, R., Holland, T.J.B., and Worley, B.A., 2000, The effect of TiO_2 and Fe_2O_3 on metapelitic assemblages at greenschist and amphibolite facies conditions: mineral equilibria calculations in the system K_2O–FeO–MgO–Al_2O_3–SiO_2–H_2O–TiO_2–Fe_2O_3: Journal of Metamorphic Geology, v. 18, p. 497–511.

Williams, I.S., and Claesson, S., 1987, Isotopic evidence for Precambrian provenance and Caledonian metamorphism of high grade paragneisses from the Seve Nappes, Scandanavian Caledonides. II, Ion microprobe zircon U-Th-Pb: Contribution to Mineralogy and Petrology, v. 97, p. 205–217.

Yui, T.F., Fukoyama, M., Iizuka, Y., Wu, C.M., Wu, T.W., Liou, J.G. and Grove, M., 2013, Is Myanmar jadeitite of Jurassic age?: A result from incompletely recrystallised inherited zircon. Lithos, v. 160–161, p. 268–282.

Zhang, Zh., Mao, Zh., Liu, X., Zhang, Y., and Brodholt, J., 2018, Stability and Reactions of $CaCO_3$ Polymorphs in the Earth's Deep Mantle: Journal of Geophysical Research, Solid Earth, v. 123(8), p. 6491–6500.

Figure captions

Figure 1. (A) Regional geological map of Indo-Myanmar Range and part of Myanmar (after Acharyya 2015). (B) Geological map of the Indo-Myanmar ophiolite belt (after Geological Survey of India M.N.C. DRG No. 42/87) (C) Geological map of the Nagaland ophiolite belt showing sample locations (after Anon. 1986, Ao and Bhowmick, 2016). (D) Field photographs (1) Unfoliated/Unsheared sample occur as boulders. Person for reference. (2) Unsheared sample showing the slicken sided face, chisel is for reference. (3) Blueschist samples present as blocky boulders. (4) Sheared sample showing foliation on a freshly broken face. Pen shows the foliation trend.

Figure 2. Thin-section photomicrographs showing representative mineral assemblages and microstructures for undeformed samples N5 (a–b) and 14 (c–d). All thin section images are shown under plane-polarized light. Scale bar is 1 mm. (a–b) Glaucophane- and epidote-rich matrix in sample N5, with minor garnet porphyroblasts associated with quartz and muscovite. (c) Small millimetre-scale garnet in sample 14 mostly occurs in quartz-rich domains that are relatively epidote- and barroisite-poor. (d) Barroisite grains enclose epidote crystals. Mineral use in 2(a) Gln – Glaucophane, Grt – Garnet, Ep – Epidote, Ms – Muscovite. 2(b) Gln – Glaucophane, Grt – Garnet, Ep – Epidote, Ms – Muscovite, Qtz – quartz, 2(c) Brs – Barroisite, Carb – Carbonate, Grt – Garnet, Ep – Epidote. 2(d) Brs – Barroisite, Ep – Epidote, Ms – Muscovite, Qtz – quartz, Ttn – Titanite.

Figure 3. Thin-section photomicrographs showing representative mineral assemblages and microstructures in sheared samples 7c (a–b) and 11 (c–f). All thin section images are shown under plane-polarized light (unless stated otherwise) and oriented perpendicular to the dominant metamorphic foliation. Scale bar is 1 mm. (a) The metamorphic foliation in sample 7c is defined by aligned crystals of epidote, sodic-calcic amphibole, and calcic amphibole, (b) and is crosscut by quartz- and carbonate-filled veins that also cause localized deflections at their intersections. Sample 11 contains olive-green aegirine–augite (c) and garnet (d) porphyroblasts that are wrapped by a glaucophane–magnesioriebeckite foliation defined by alternating glaucophane- and quartz-rich bands. Sheared veins filled with carbonate (e) and quartz (f) exhibit ductile deformation microstructures and dynamic recrystallization. Mineral abbreviation use in Figure 3(a) Brs – Wnc: Barroisite – Winchite, Ep – Epidote, Prg – Ed: Pargsite – Edinite, Ttn: Titanite, Figure 3(b) Qtz – Quartz, Carb – Carbonate, Brs – Barroisite, Wnc – Winchite, Ep – Epidote, Ms – Muscovite, Kfs – K-feldspar, Ab – Albite, 3(c) Agt – Aegirine augite, Gln: Glaucophane, Fgl – Ferroglacuphane, Grt – Garnet, Qtz – Quartz, Ms – Muscovite, Figure 3(d) Alb – Albite, Carb – Carbonate, Gln – Glaucophane, Fgl – Ferroglaucophane, Quartz – Quartz, Figure 3(e) Carb – Carbonate, Ms – Muscovite, Qtz – Quartz, Figure 3(f) Carb – Carbonate, Qtz – Quartz.

Figure 4. Compositional line profile for a garnet porphyroblast of from the unsheared sample N5, running from rim to rim (~0.75 mm diameter). (a) Cation mole fractions of divalent cations. (b) X-ray compositional map of divalent cations showing relative concentrations from core to rim. Colours do not represent equivalent cation concentrations between images.

Figure 5. Compositions of amphiboles from all studied samples, classified according to the classification scheme of Hawthorne *et al*. (2012). Discrimination between calcic (group 2),

calcic-sodic (group 3), and sodic (group 4) amphiboles is based upon the Na content of the M4 crystallographic site, with the ranges <0.5, 0.5–1.5, and >1.5, respectively for a 23-oxygen recalculation. Representative compositions are given in Supplementary Table 2.

Figure 6. Results of mineral equilibria modelling for unsheared sample N5. (a) Pressure–temperature (*P*–*T*) pseudosection constructed for the bulk composition given in Supplementary Table 3. Dotted overlay represents the global range of *P*–*T* conditions modelled to occur at the surface of subducting ocean crust in present-day subduction zones (Syracuse *et al*. 2010). Gray star and associated dashed ellipses represent the results of avPT calculations (Supplementary Table 4) and are shown at 1 and 2 S.D. Bold line marks the extent of H_2O-bearing assemblage fields. Numbered fields are as follows: 1 – Grt Ms Cld Tlc Omp, 2 – Grt Ms Cld Tlc Omp Gln, 3 – Grt Ms Cld Tlc Omp Gln Lws, 4 – Grt Ms Cld Tlc Omp Ky Lws, 5 – Grt Ms Act Cld Tlc Ky Lws, 6 – Grt Ms Bt Cld Act Gln, 7 – Grt Chl Bt Cld Act Gln, 8 – Grt Bt Act Gln Mag, 9 – Grt Bt Chl Hbl Gln, 10 – Bt Omp Hbl Pl H_2O, 11 – Bt Omp Hbl Pl Ab H_2O, 12 – Grt Ms Omp Hbl H_2O, 13 – Grt Ms Gln H_2O, 14 – Grt Chl Ms Omp Gln, 15 – Grt Chl Ms Brs Gln, 16 – Grt Chl Ms Omp Gln Lws, 17 – Grt Ms Cld Omp Gln Lws. Some small, minor fields are unlabelled for clarity. (b) Interpreted peak assemblage field showing isolines of modal proportions of selected phases. Red star indicates the best match between observed and calculated mineral abundances. Dashed line labelled $XNaM_4Act$ = 0.25 marks the division between actinolite (<0.25) at low-*T* and barroisite (>0.25) at high-*T*. (c) Bar chart showing degree of correlation between observed volume proportions (%) of minerals and calculated proportions at 1.9 GPa and 485 °C (red star in b).

Figure 7. Results of mineral equilibria modelling for unsheared sample 14. (a) Pressure–temperature (*P*–*T*) pseudosection constructed for the bulk composition given in

Supplementary Table 3. Dotted overlay represents the global range of *P–T* conditions modelled to occur at the surface of subducting ocean crust in present-day subduction zones (Syracuse *et al*. 2010). Gray star and associated dashed ellipses represent the results of avPT calculations (Supplementary Table 4) and are shown at 1 and 2 S.D. Bold line marks the extent of H_2O-bearing assemblage fields. Numbered fields are as follows: 1 – Grt Ms Pg Omp Act Gln, 2 – Grt Ms Bt Omp Act Gln, 3 – Grt Bt Omp Act Gln Ab, 4 – Grt Bt Omp Act Gln Ilm Mag Ab (–Rt), 5 – Grt Bt Omp Act Gln Mag Ab (–Rt), 6 – Grt Bt Omp Brs Gln Mag, 7 – Bt Omp Brs Gln Hbl Mag, 8 – Grt Bt Omp Brs Hbl, 9 – Bt Di Brs Hbl H_2O, 10 – Bt Di Hbl Ttn H_2O (–Rt), 11 – Bt Di Hbl, 12 – Grt Ms Bt Omp Act H_2O, 13 – Grt Ms Tlc Omp Act H_2O, 14 – Grt Ms Tlc Omp H_2O, 15 – Grt Ms Tlc Omp Brs Lws, 16 – Grt Chl Ms Omp Brs, 17 – GrtChl Ms Omp Brs H_2O. Some small, minor fields are unlabelled for clarity. (b) Red star indicates the best match between observed and calculated mineral abundances. Interpreted peak assemblage field showing isolines of modal proportions of selected phases. Dashed line labelled $XNaM_4Act = 0.25$ marks the division between actinolite (<0.25) at low-T and barroisite (>0.25) at high-T. (c) Bar chart showing degree of correlation between observed volume proportions (%) of minerals and calculated proportions at 2.0 GPa and 525 °C (red star in part b).

Figure 8. Results of phase equilibria modelling for sheared sample 7c. (a) Pressure–temperature (*P–T*) pseudosection constructed for the bulk composition given in Supplementary Table 3. Dotted overlay represents the global range of *P–T* conditions modelled to occur at the surface of subducting ocean crust in present-day subduction zones (Syracuse *et al*. 2010). Gray star and associated dashed ellipses represent the results of avPT calculations (Table 4) and are shown at 1 and 2 S.D. Bold line marks the extent of H_2O-bearing assemblage fields. Numbered fields are as follows: 1 – Omp Act Gln Mag Rt Hem (–

Ttn), 2 – Omp Act Gln Mag Rt, 3 – Omp Act Gln Mag, 4 – Omp Act Gln Mag Ab, 5 – Act Gln Mag Ab, 6 – Omp Act Hbl Gln Mag Rt (–Ttn), 7 – Omp Act Hbl Gln Ab, 8 – Act Hbl Gln Mag Ab, 9 – Chl Act Hbl Mag Ab, 10 – Chl Act Hbl Ab H_2O, 11 – BrsHbl Ab, 12 – Omp Act Hbl Ab, 13 – Di Act Hbl Ab H_2O, 14 – Di Hbl Ab H_2O, 15 – Di Act Hbl Pl, 16 – Di Hbl Pl Mag Hem (–Ttn, Ep), 17 – Omp Act Hbl Gln Rt Hem (–Ttn), 18 – Omp Brs Hbl Gln Rt Hem (–Ttn), 19 – Omp Brs Hbl Gln Rt (–Ttn), 20 – Omp Act Hbl Gln Rt (–Ttn), 21 – Omp Brs Hbl Gln, 22 – Omp Act Hbl Gln, 23 – Omp Brs Gln Rt Hem (–Ttn), 24 – Omp Act Hem (–Ttn), 25 – Omp Act (–Ttn). Some small, minor fields are unlabelled for clarity. (b) Red star indicates the best match between observed and calculated mineral abundances. Interpreted peak assemblage field showing isolines of modal proportions of selected phases. Dashed line labelled $XNaM_4Act = 0.25$ marks the division between actinolite (<0.25) at low-T and barroisite (>0.25) at high-T. (c) Bar chart showing degree of correlation between observed volume proportions (%) of minerals and calculated proportions at 0.6 GPa and 465 °C (red star in b).

Figure 9. Isochrons for all dated samples. A: Unsheared sample 14. B: Sheared sample 11. C: Sheared sample 3b. D: Sheared sample 13. All ellipses are shown at the 2σ confidence interval and n = number of analyses.

Figure 10. Representative back scattered electron images of analysed samples 14 (a), 11 (b), 3b (c) and 13 (d). U–Pb analysed spots are showing in ellipse (white: silicate phases and yellow: carbonates).

Figure 11. Pressure–temperature diagram summarizing the proposed model for the tectonometamorphic evolution of blueschist-facies rocks from the Nagaland ophiolite complex. Red boxes represent calculated conditions of metamorphism and thick grey arrow

represents the interpreted *P–T–t* evolution. Paths for Nagaland blueschists reported by Chatterjee and Ghose (2010) and Ao and Bhowmik (2014) are shown (CG10 and AB14, respectively) for comparison. Aragonite-calcite stability curve is from Johannes and Puhan (1971).

Figure 12. Schematic tectonic model for formation and exhumation of the Nagaland ophiolite belt and its metamorphic suite. (a) Westward-dipping subduction away from Myanmar during the Jurassic, with future Nagaland ophiolite belt oceanic crust on the overlying plate. (b) Reversal in the subduction dip direction prior to the Early Cretaceous, leading to burial of future Nagaland ophiolitic crust and mantle. (c) Peak metamorphism of the studied samples was achieved during the Middle Cretaceous, with (d) slab break-off and buoyancy-driven exhumation and associated shearing of these units during the Middle to Late Cretaceous. (e) the final configuration of the Indo-Myanmar plates and suture zone between following collisional orogenesis (modified after Khogenkumar *et al*. 2021). Yellow star indicates locations of the studied samples during metamorphism and deformation.

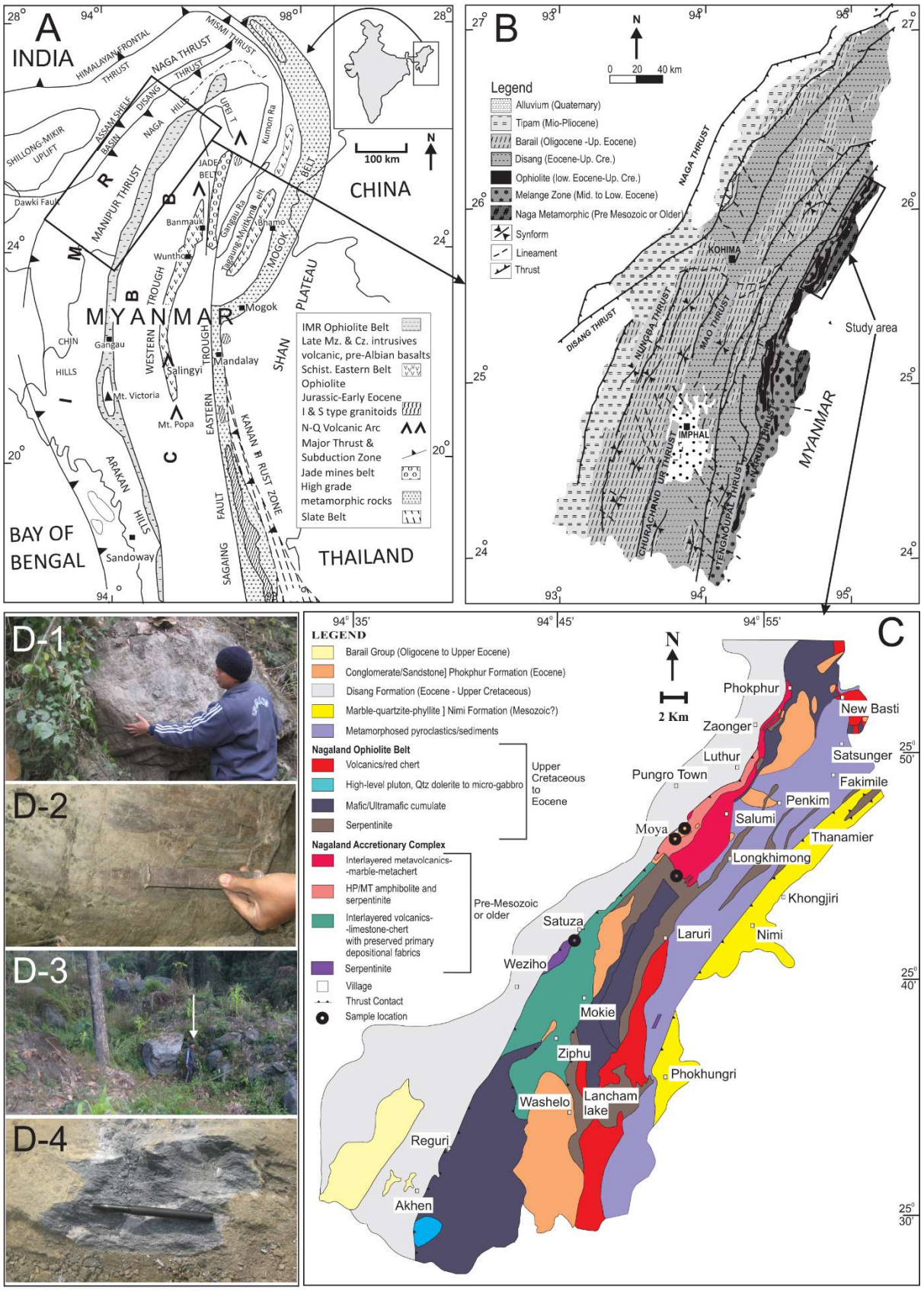
A
INDIA
HIMALAYAN FRONTAL THRUST
NAGA THRUST
MISMI THRUST
ASSAM SHELF
DISANG
HILLS
UPPER T
SHILLONG-MIKIR UPLIFT
NAGA
Kumon Ra
BELT
100 km
N
CHINA
Dawki Fault
MANIPUR THRUST
JADE BELT
Gangau Ra
Jade mine
Hkamo
MOGOK
Banmauk
Wuntho
TROUGH
PLATEAU
MYANMAR
Mogok
CHIN
Gangau
WESTERN
TROUGH
Salingyi
Mandalay
SHAN
HILLS
Mt. Victoria
EASTERN
Mt. Popa
KANAN RUST ZONE
FAULT
ARAKAN
HILLS
BAY OF BENGAL
Sandoway
SAGAING
THAILAND
IMR Ophiolite Belt
Late Mz. & Cz. intrusives volcanic, pre-Albian basalts
Schist. Eastern Belt
Ophiolite
Jurassic-Early Eocene I & S type granitoids
N-Q Volcanic Arc
Major Thrust & Subduction Zone
Jade mines belt
High grade metamorphic rocks
Slate Belt
B
N
0 20 40 km
Legend
Alluvium (Quaternary)
Tipam (Mio-Pliocene)
Barail (Oligocene -Up. Eocene)
Disang (Eocene-Up. Cre.)
Ophiolite (low. Eocene-Up. Cre.)
Melange Zone (Mid. to Low. Eocene)
Naga Metamorphic (Pre Mesozoic or Older)
Synform
Lineament
Thrust
NAGA THRUST
KOHIMA
DISANG THRUST
NUNGBA THRUST
MAO THRUST
Study area
IMPHAL
CHURACHAND UR THRUST
TENGNOUPAL THRUST
KARUM THRUST
MYANMAR
D-1
D-2
D-3
D-4
C
LEGEND
Barail Group (Oligocene to Upper Eocene)
Conglomerate/Sandstone] Phokphur Formation (Eocene)
Disang Formation (Eocene - Upper Cretaceous)
Marble-quartzite-phyllite] Nimi Formation (Mesozoic?)
Metamorphosed pyroclastics/sediments
Nagaland Ophiolite Belt
Volcanics/red chert
High-level pluton, Qtz dolerite to micro-gabbro
Mafic/Ultramafic cumulate
Serpentinite
Upper Cretaceous to Eocene
Nagaland Accretionary Complex
Interlayered metavolcanics--marble-metachert
HP/MT amphibolite and serpentinite
Interlayered volcanics--limestone-chert with preserved primary depositional fabrics
Serpentinite
Pre-Mesozoic or older
Village
Thrust Contact
Sample location
N
2 Km
Phokphur
New Basti
Zaonger
Luthur
Satsunger
Pungro Town
Fakimile
Penkim
Salumi
Moya
Thanamier
Longkhimong
Khongjiri
Satuza
Laruri
Nimi
Weziho
Mokie
Ziphu
Phokhungri
Washelo
Lancham lake
Reguri
Akhen

Fig. 1

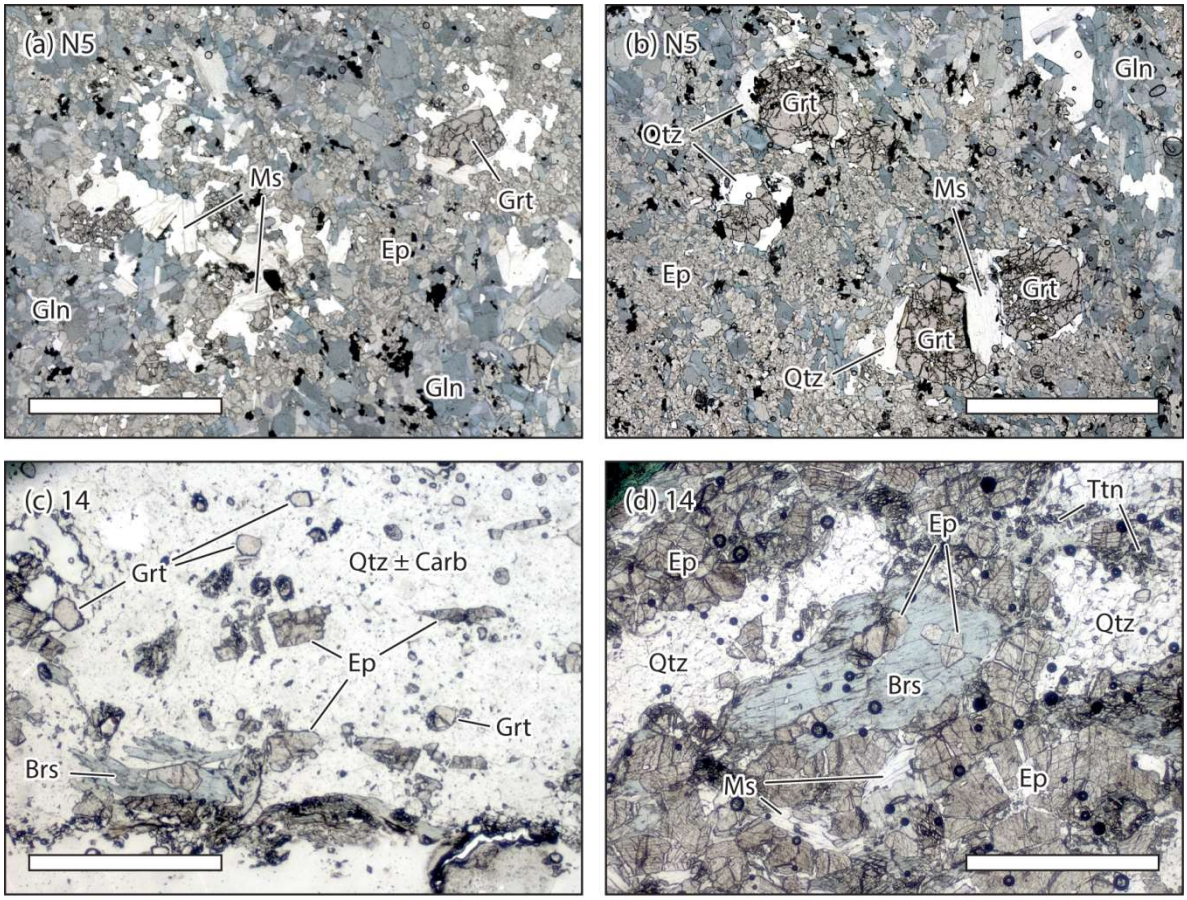

Fig. 2

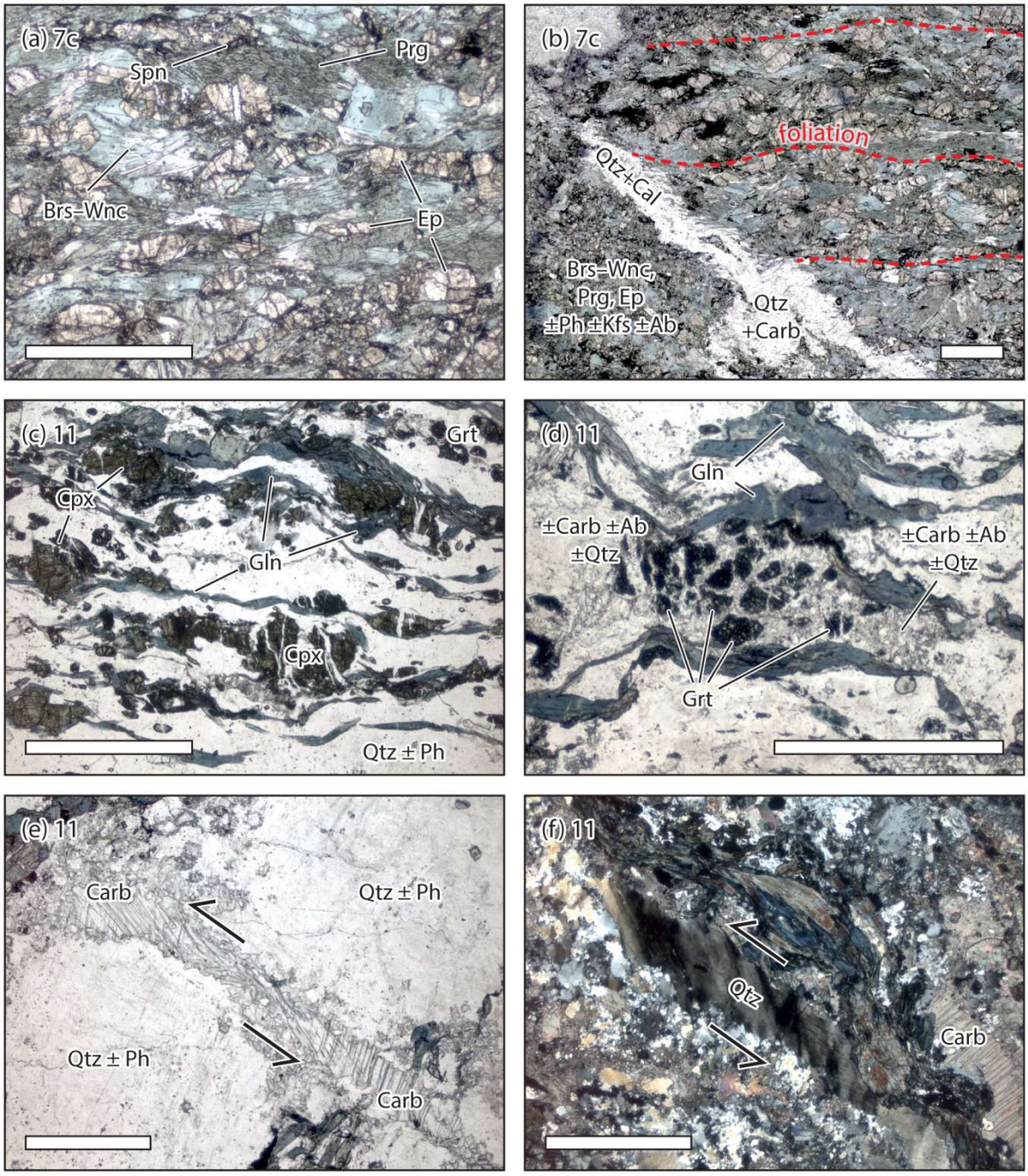
(a) 7c
Spn
Prg
Brs–Wnc
Ep
(b) 7c
foliation
Qtz±Cal
Brs–Wnc,
Prg, Ep
±Ph±Kfs ±Ab
Qtz
+Carb
(c) 11
Grt
Cpx
Gln
Cpx
Qtz ± Ph
(d) 11
Gln
±Carb ±Ab
±Qtz
±Carb ±Ab
±Qtz
Grt
(e) 11
Carb
Qtz ± Ph
Qtz ± Ph
Carb
(f) 11
Qtz
Carb

Fig. 3

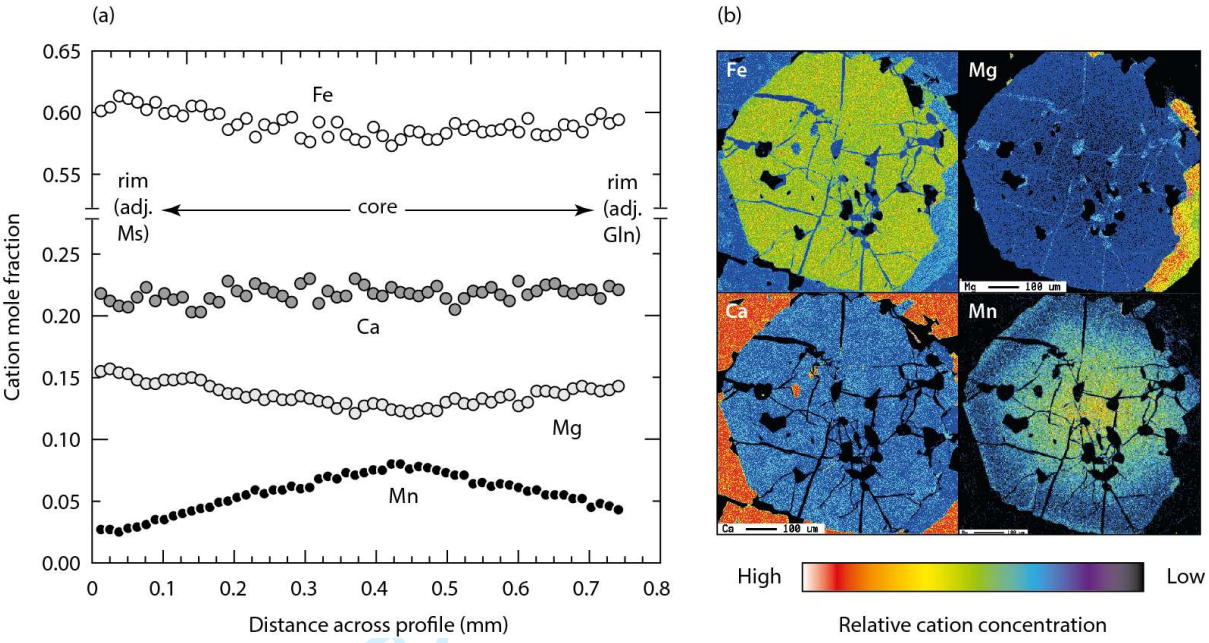

Fig. 4

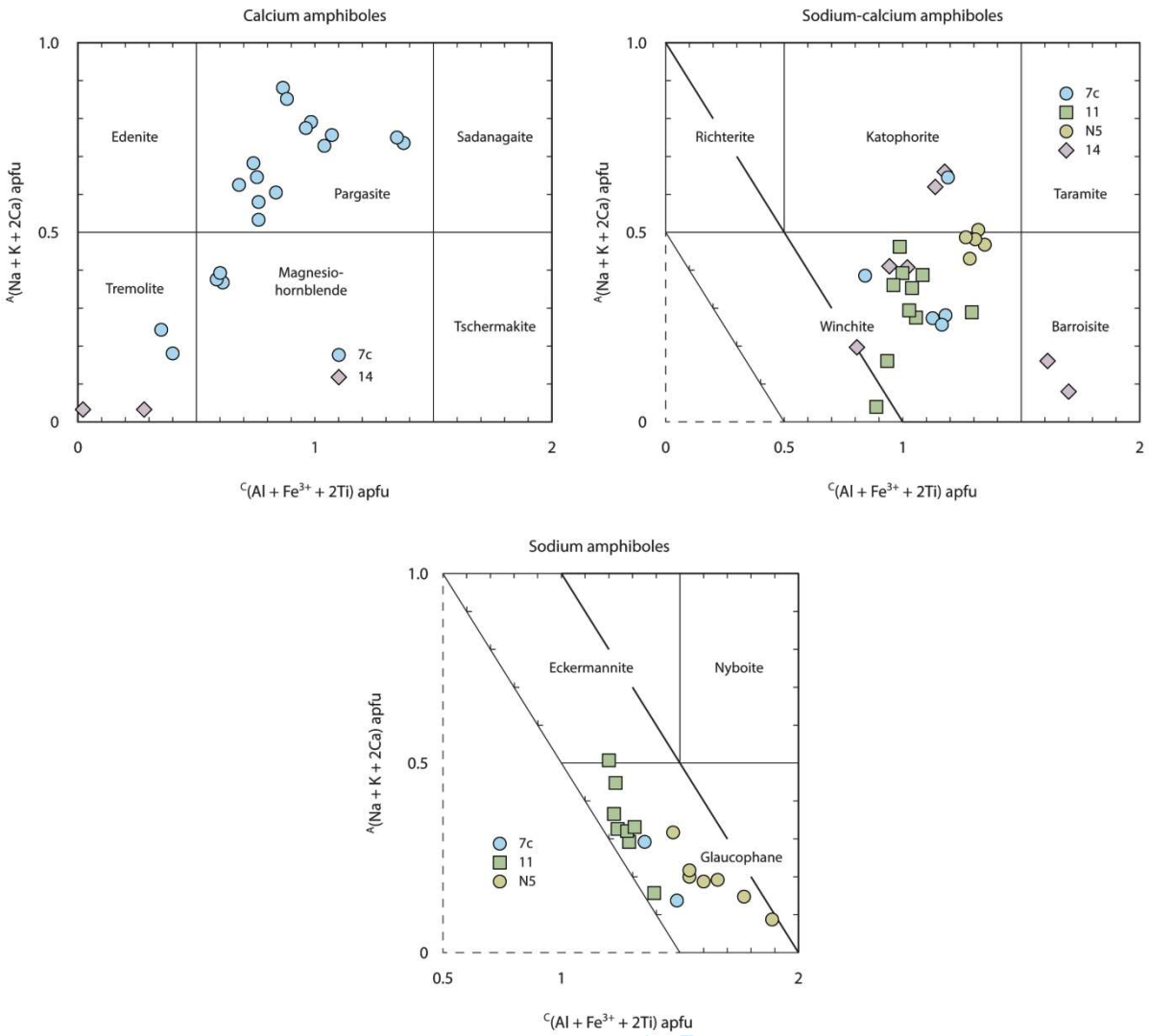
Calcium amphiboles
Edenite
Sadanagaite
Pargasite
Tremolite
Magnesio-hornblende
Tschermakite
7c
14
A(Na + K + 2Ca) apfu
C(Al + Fe3+ + 2Ti) apfu
Sodium-calcium amphiboles
Richterite
Katophorite
Taramite
Winchite
Barroisite
7c
11
N5
14
Sodium amphiboles
Eckermannite
Nyboite
Glaucophane
7c
11
N5

Fig. 5

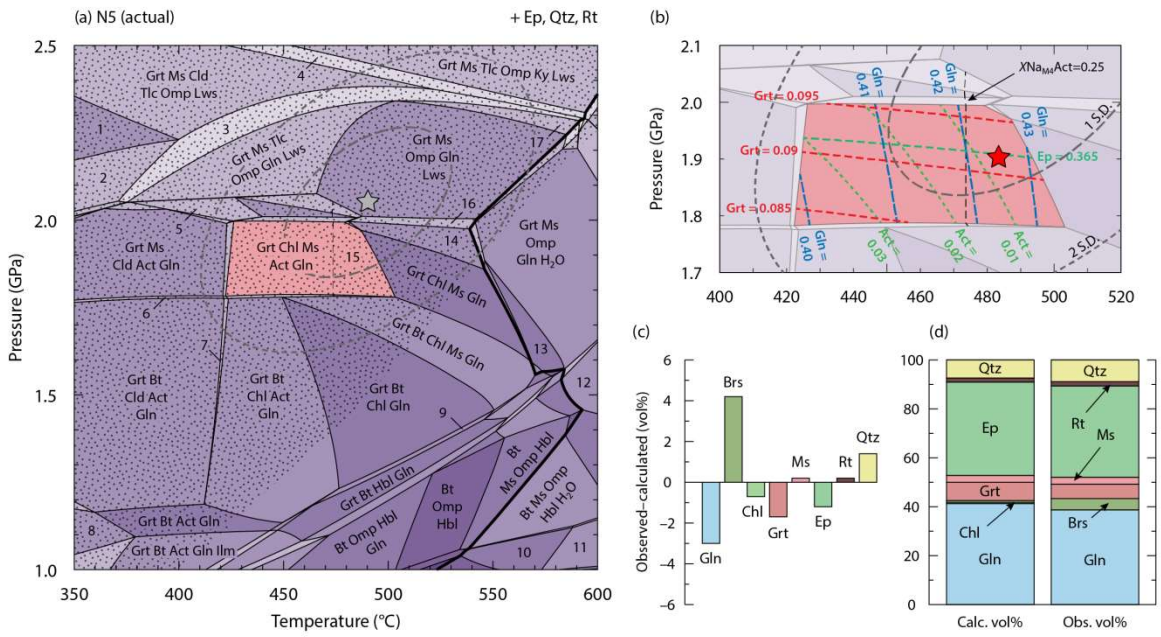
(a) N5 (actual)
+ Ep, Qtz, Rt
Grt Ms Cld Tlc Omp Lws
Grt Ms Tlc Omp Ky Lws
Grt Ms Tlc Omp Gln Lws
Grt Ms Omp Gln Lws
Grt Ms Cld Act Gln
Grt Chl Ms Act Gln
Grt Ms Omp Gln H2O
Grt Chl Ms Gln
Grt Bt Chl Ms Gln
Grt Bt Cld Act Gln
Grt Bt Chl Act Gln
Grt Bt Chl Gln
Grt Bt Hbl Gln
Bt Ms Omp Hbl
Bt Ms Omp Hbl H2O
Bt Omp Hbl
Bt Omp Hbl Gln
Grt Bt Act Gln
Grt Bt Act Gln Ilm
Pressure (GPa)
Temperature (°C)
(b)
XNaMAct=0.25
Grt = 0.095
Grt = 0.09
Grt = 0.085
Ep = 0.365
Gln = 0.41
Gln = 0.42
Gln = 0.43
Gln = 0.40
Act = 0.03
Act = 0.02
Act = 0.01
1 S.D.
2 S.D.
Pressure (GPa)
(c)
Observed–calculated (vol%)
Brs
Qtz
Ms
Rt
Chl
Grt
Ep
Gln
(d)
Qtz
Ep
Grt
Chl
Gln
Rt
Ms
Brs
Gln
Calc. vol%
Obs. vol%

Fig. 6

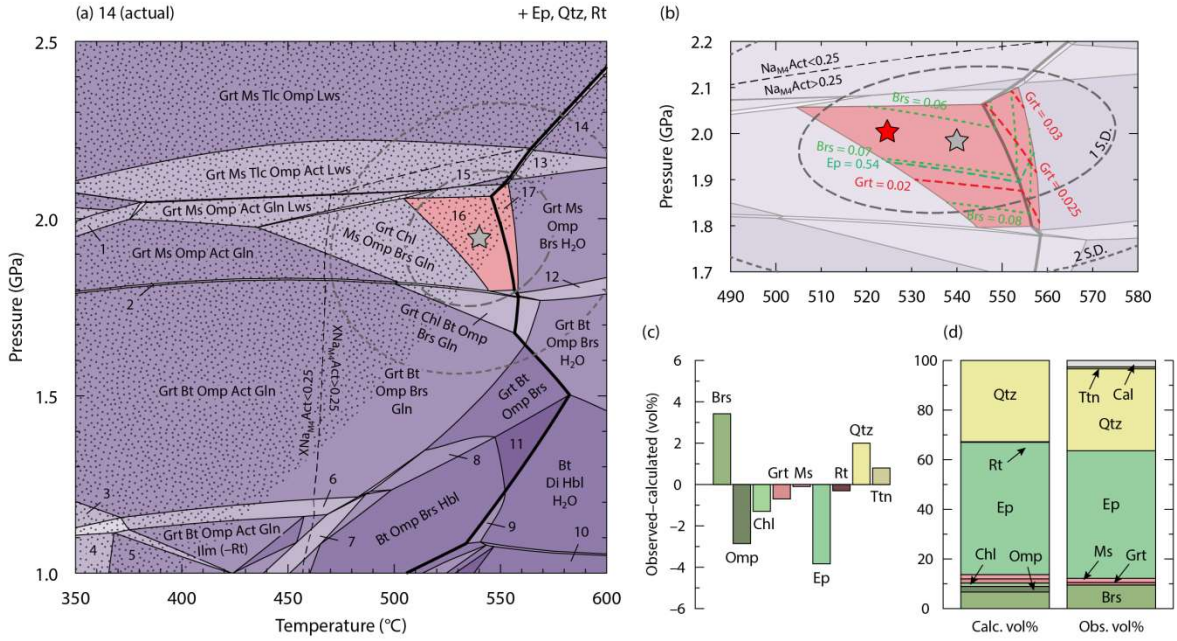
(a) 14 (actual)
+ Ep, Qtz, Rt
Grt Ms Tlc Omp Lws
Grt Ms Tlc Omp Act Lws
Grt Ms Omp Act Gln Lws
Grt Ms Omp Act Gln
Grt Chl Ms Omp Brs Gln
Grt Ms Omp Brs H2O
Grt Chl Bt Omp Brs Gln
Grt Bt Omp Brs H2O
Grt Bt Omp Act Gln
Grt Bt Omp Brs Gln
Grt Bt Omp Brs
XNaMAct<0.25
Bt Di Hbl H2O
Bt Omp Brs Hbl
Grt Bt Omp Act Gln Ilm (–Rt)
Pressure (GPa)
Temperature (°C)
(b)
NaMAct<0.25
NaMAct>0.25
Brs = 0.06
Brs = 0.07
Ep = 0.54
Grt = 0.02
Grt = 0.03
Grt = 0.025
Brs = 0.08
1 S.D.
2 S.D.
Pressure (GPa)
(c)
Observed–calculated (vol%)
Brs
Qtz
Grt Ms
Rt
Ttn
Chl
Omp
Ep
(d)
Qtz
Rt
Ep
Chl Omp
Ttn Cal
Qtz
Ep
Ms Grt
Brs
Calc. vol%
Obs. vol%

Fig. 7

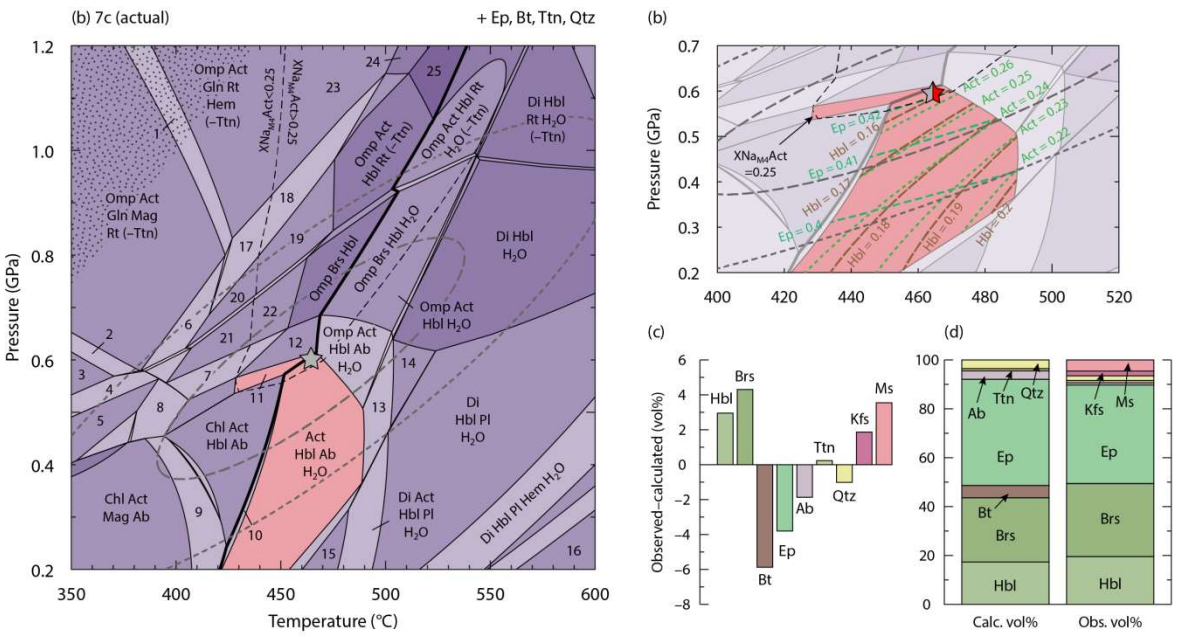
(b) 7c (actual)
+ Ep, Bt, Ttn, Qtz
Pressure (GPa)
Temperature (°C)
Omp Act Gln Rt Hem (–Ttn)
Omp Act Gln Mag Rt (–Ttn)
Omp Act Hbl Rt (–Ttn)
Omp Act Hbl Rt H2O (–Ttn)
Di Hbl Rt H2O (–Ttn)
Omp Brs Hbl
Omp Brs-Hbl H2O
Di Hbl H2O
Omp Act Hbl H2O
Omp Act Hbl Ab H2O
Chl Act Hbl Ab
Act Hbl Ab H2O
Di Hbl Pl H2O
Chl Act Mag Ab
Di Act Hbl Pl H2O
Di Hbl Pl Hem H2O
(b)
(c)
(d)
Observed–calculated (vol%)
Calc. vol%
Obs. vol%

Fig. 8

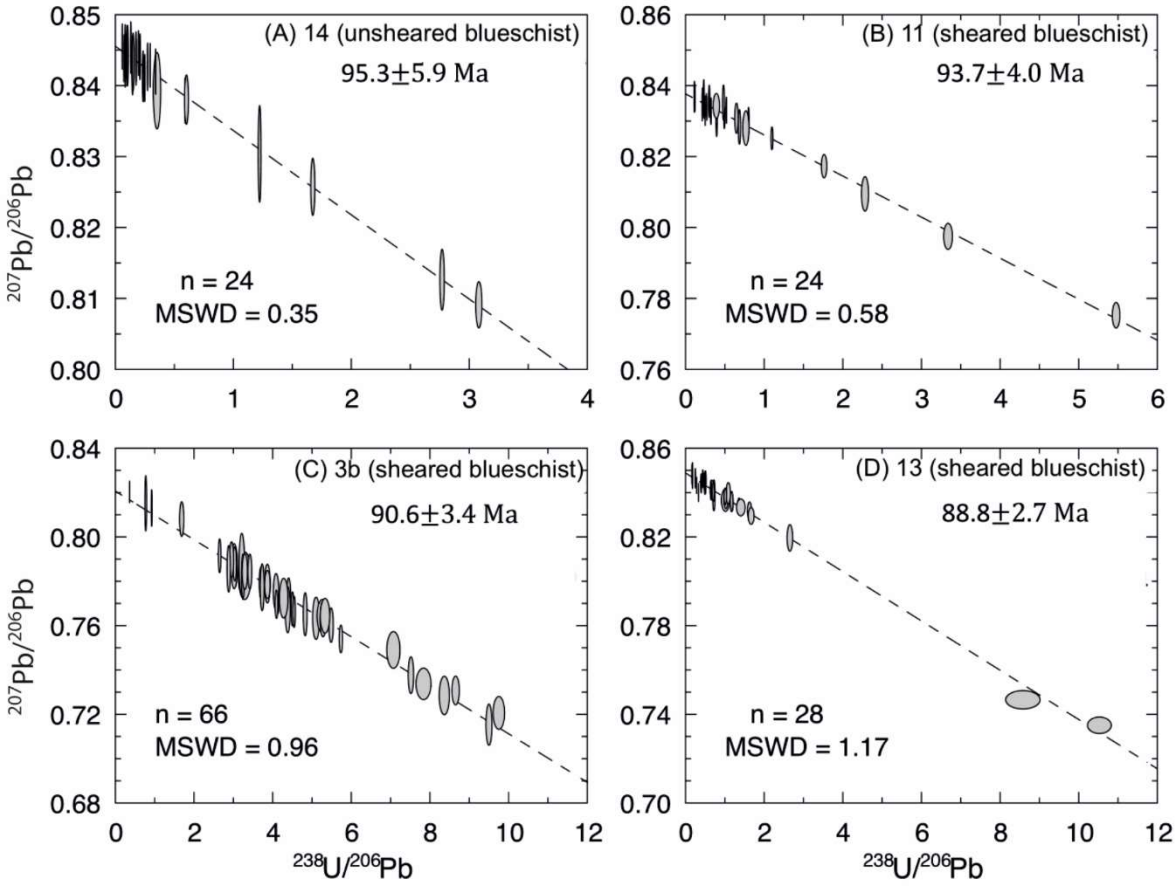
(A) 14 (unsheared blueschist)
95.3±5.9 Ma
n = 24
MSWD = 0.35
(B) 11 (sheared blueschist)
93.7±4.0 Ma
n = 24
MSWD = 0.58
(C) 3b (sheared blueschist)
90.6±3.4 Ma
n = 66
MSWD = 0.96
(D) 13 (sheared blueschist)
88.8±2.7 Ma
n = 28
MSWD = 1.17
207Pb/206Pb
238U/206Pb

Fig. 9

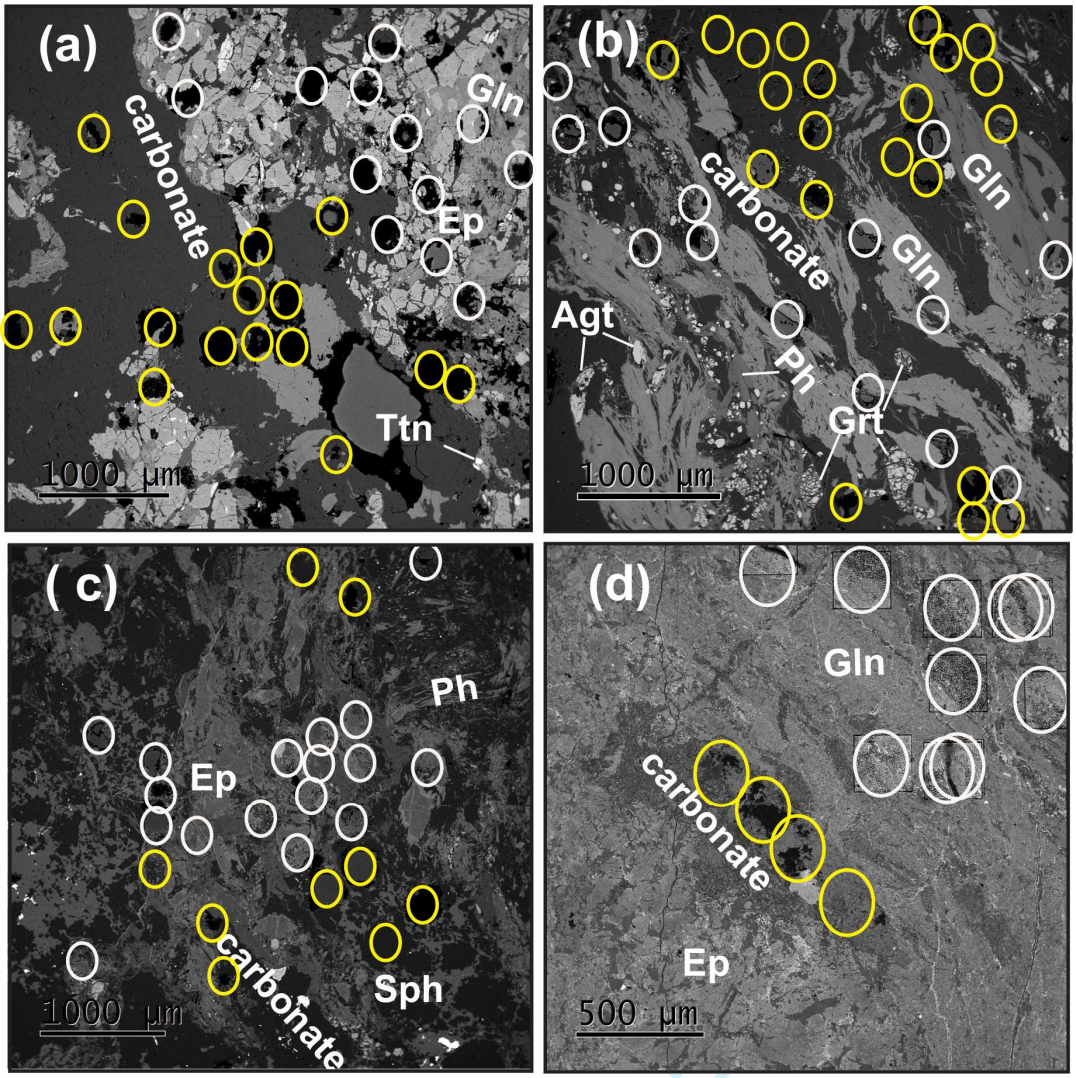

Fig. 10

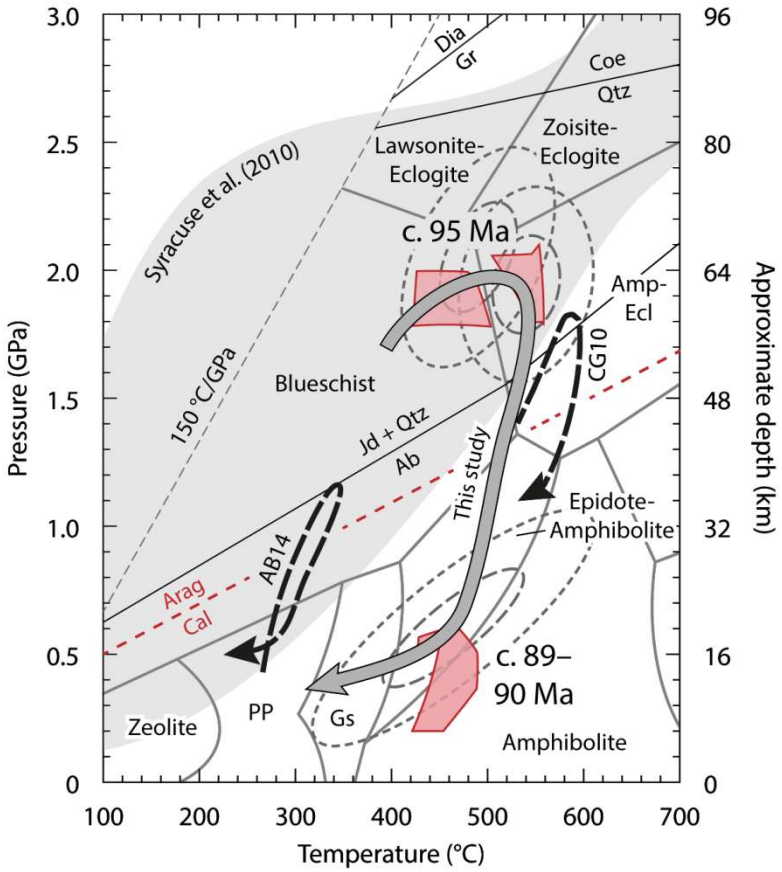

Fig. 11

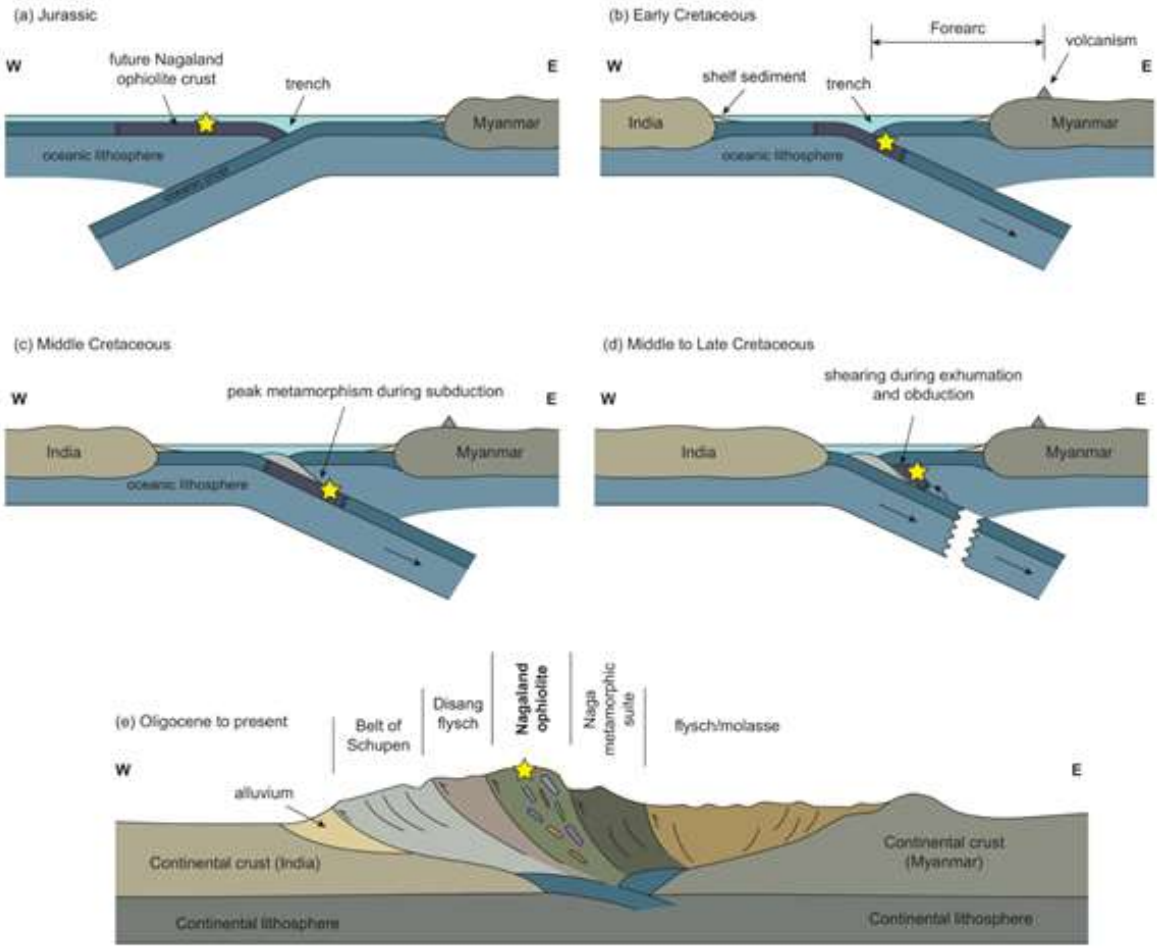

Fig. 12

SUPPLEMENTARY INFORMATION for:

Dating blueschist-facies metamorphism within the Naga ophiolite, Northeast India, using sheared carbonate veins

Bidyananda Maibam*[a], Richard M. Palin[b], Axel Gerdes[c,d], Richard W. White[e], Stephen Foley[f]

[a]*Department of Earth Sciences, Manipur University, Canchipur, Imphal-795003, India*

[b]*Department of Earth Sciences, University of Oxford, Oxford, OX1 3AN, United Kingdom*

[c]*Department of Geosciences, Goethe-University Frankfurt, 60438 Frankfurt, Germany*

[d]*Frankfurt Isotope and Element Research Center (FIERCE), Goethe-University Frankfurt, 60438 Frankfurt, Germany*

[e]*School of Earth and Environmental Sciences, University of St. Andrews, KY16 9AL, UK*

[f]*ARC Centre of Excellence for Core to Crust Fluid Systems, Department of Earth & Planetary Sciences, Macquarie University NSW 2109, Australia*

**corresponding author: bmaibam@yahoo.com*

Contents:

Supplementary Tables 1-5

Extended sample description

GPS coordinates for each sample are given in Supplementary Table 1. These samples can be divided into sheared and unsheared units. Major-element mineral compositional data were obtained on a JEOL JXA-8200 electron microprobe at the Institute of Geosciences, Johannes Gutenberg University of Mainz, Germany. Operating conditions included an acceleration voltage of 15 kV, a beam current of 12 nA, and a 2-μm spot size. A matrix correction for atomic number, absorption, and fluorescence was automatically applied to all analyses. For the data presented below, mineral compositions were recalculated to a standard number of oxygens per formula unit (pfu), with H_2O assumed to be present in stoichiometric amounts. Where stoichiometric criteria could be applied, the proportion of ferric iron was calculated using the software AX (Holland, 2009). Representative compositions of major minerals for all samples are given in Supplementary Table 2. Mineral abbreviations are after Kretz (1983).

Supplementary Table 1. Lithological descriptions and GPS co-ordinates for all studied samples.

Superscript numbers denote whether samples were used for thermobarometry (1) or geochronology (2).

Sample	Lithology	Northing	Easting	Locality
N5[1]	Unsheared blueschist			Near Satuza
14[1,2]	Unsheared blueschist	25°46'02.8"	94°51'03.6"	Moya
7c[1]	Sheared blueschist with cross-cutting carbonate veins	25°36'56.3"	94°51'39.8"	Moya
13[2]	Sheared blueschist	25°46'06.6"	94°51'26.4"	Moya
3b[2]	Sheared blueschist	25°49'19.0"	94°54'58.9"	Luthur-Salomi
11[1,2]	Sheared blueschist with cross-cutting carbonate veins	25°45'25.4"	94°52'16.7"	Salomi-Longkhimong

Supplementary Table 2. Representative mineral compositions.

Sample	N5 (Unsheared)							14 (Unsheared)						
Mineral	Gln	Ep	Brs	Ms	Rt	Grt	Grt	Brs	Cal	Ep	Grt	Ms	Chl	Ttn
Location	Matrix	Matrix	Matrix	Matrix	Matrix	Core	Rim	Matrix	Vein	Matrix	Pblast	Matrix	Matrix	Matrix
Weight %														
SiO_2	56.99	38.32	48.82	50.30	0.03	38.65	38.03	50.55	0.04	38.31	38.44	49.16	28.76	30.67
TiO_2	0.03	0.06	0.31	0.31	99.21	0.10	0.10	0.37	0.00	0.21	0.07	0.48	0.01	37.92
Al_2O_3	7.74	25.28	10.87	27.78	0.03	21.55	21.90	7.58	0.04	25.01	20.89	26.30	17.26	1.16
Fe_2O_3	3.84	9.68	2.30	0.54	0.00	0.03	0.08	2.94	0.00	10.65	1.66	1.51	0.00	0.00
FeO	10.06	0.61	11.27	2.60	0.87	26.63	27.83	11.11	0.09	0.00	17.44	2.11	20.86	0.49
MnO	0.18	0.03	0.15	0.03	0.01	3.62	1.25	0.55	0.67	0.19	7.25	0.02	0.45	0.13
MgO	10.80	0.08	11.76	3.32	0.03	3.17	3.92	12.92	0.03	0.02	3.44	3.56	19.57	0.00
CaO	1.29	23.40	7.72	0.00	0.02	7.88	7.37	8.17	62.13	23.30	11.79	0.00	0.03	28.37
Na_2O	6.89	0.02	4.17	0.68	0.00	0.06	0.00	3.42	0.07	0.03	0.00	0.44	0.00	0.06
K_2O	0.01	0.00	0.37	10.32	0.00	0.00	0.02	0.66	0.00	0.00	0.00	10.38	0.04	0.00
Total	97.85	97.53	97.74	96.05	100.27	101.73	100.52	98.38	63.12	97.79	101.04	94.10	87.07	98.85
Cations per formula unit														
Si	7.95	3.03	7.04	3.35	0.00	3.01	2.98	7.27	0.00	3.03	2.99	3.35	2.98	1.00
Ti	0.00	0.00	0.03	0.02	0.99	0.01	0.01	0.04	0.00	0.01	0.00	0.02	0.00	0.93
Al	1.27	2.36	1.85	2.18	0.00	1.98	2.02	1.29	0.00	2.33	1.92	2.11	2.11	0.04
Fe^{3+}	0.41	0.58	0.25	0.03	0.00	0.00	0.01	0.32	0.00	0.64	0.10	0.08	0.00	0.00
Fe^{2+}	1.17	0.04	1.36	0.14	0.01	1.73	1.82	1.34	0.00	0.00	1.14	0.12	1.81	0.01
Mn	0.02	0.00	0.02	0.00	0.00	0.24	0.08	0.07	0.02	0.01	0.48	0.00	0.04	0.00
Mg	2.25	0.01	2.53	0.33	0.00	0.37	0.46	2.77	0.00	0.00	0.40	0.36	3.02	0.00
Ca	0.19	1.98	1.19	0.00	0.00	0.66	0.62	1.26	1.97	1.97	0.98	0.00	0.00	1.00
Na	1.86	0.00	1.17	0.09	0.00	0.01	0.00	0.95	0.00	0.00	0.00	0.06	0.00	0.00
K	0.00	0.00	0.07	0.88	0.00	0.00	0.00	0.12	0.00	0.00	0.00	0.90	0.01	0.00
Sum	15.14	8.00	15.50	7.01	1.00	8.00	8.00	15.44	2.00	8.00	8.00	7.01	9.97	3.00
Oxygens	23	12.5	23	11	2	12	12	23	3	12.5	12	11	14	5
X_{Mg}	0.66	0.18	0.65	0.70	0.00	0.18	0.20	0.67	0.00	1.00	0.26	0.75	0.63	0.00

Supplementary Table 2 (Continued). Representative mineral compositions.

Sample	7c (sheared)									11						
Mineral	Ab	Mhb	Wnc	Cal	Ep	Ep	Kfs	Ms	Ttn	Agt	Ab	Mrbk	Wnc	Cal	Grt	Ms
Location	Vein	Matrix	Matrix	Vein	Core	Rim	Matrix	Matrix	Matrix	Pblast	Matrix	Core	Rim	Vein	Pblast	Matrix
Weight %																
SiO_2	68.39	51.36	56.25	0.07	37.97	37.28	63.73	51.57	30.24	51.81	67.73	54.78	54.62	0.03	37.75	46.31
TiO_2	0.00	0.07	0.01	0.00	0.26	0.06	0.00	0.27	38.14	0.13	0.00	0.02	0.08	0.00	0.07	0.39
Al_2O_3	19.22	5.07	2.81	0.03	25.84	22.27	18.04	25.08	1.21	4.91	19.61	3.72	5.09	0.01	19.47	25.57
Fe_2O_3	0.00	2.44	8.97	0.00	9.29	14.65	0.31	3.95	0.00	9.64	0.10	10.32	4.41	0.00	2.31	5.66
FeO	0.00	10.50	8.10	0.17	0.00	0.00	0.00	1.52	0.47	3.70	0.00	10.02	13.02	0.04	8.15	2.18
MnO	0.00	0.27	0.19	0.06	0.11	0.29	0.00	0.05	0.09	0.86	0.04	0.42	0.53	0.69	22.88	0.07
MgO	0.00	14.48	12.45	0.01	0.15	0.02	0.02	4.04	0.00	8.49	0.02	9.37	10.42	0.00	2.57	3.13
CaO	0.00	9.48	3.17	63.12	23.38	23.01	0.00	0.03	28.52	15.78	0.02	0.83	2.68	60.75	7.15	0.00
Na_2O	11.71	2.51	5.72	0.01	0.00	0.01	0.20	0.12	0.01	4.76	11.53	6.82	6.15	0.11	0.03	0.49
K_2O	0.02	0.43	0.03	0.02	0.00	0.02	16.02	8.53	0.00	0.03	0.04	0.04	0.05	0.00	0.00	10.36
Total	99.41	96.72	97.73	63.50	97.12	97.68	98.36	95.26	98.68	100.16	99.14	96.37	97.09	61.63	100.48	94.17
Cations per formula unit																
Si	3.00	7.47	7.98	0.00	3.00	2.99	3.00	3.43	0.99	1.93	2.98	7.98	7.90	0.00	3.01	3.22
Ti	0.00	0.01	0.00	0.00	0.02	0.00	0.00	0.01	0.94	0.00	0.00	0.00	0.01	0.00	0.00	0.02
Al	1.00	0.87	0.47	0.00	2.41	2.11	1.00	1.97	0.05	0.22	1.02	0.64	0.87	0.00	1.83	2.09
Fe^{3+}	0.00	0.27	0.96	0.00	0.57	0.89	0.01	0.20	0.00	0.27	0.00	1.07	0.48	0.00	0.14	0.30
Fe^{2+}	0.00	1.28	0.96	0.01	0.00	0.00	0.00	0.09	0.01	0.12	0.00	1.28	1.58	0.00	0.54	0.13
Mn	0.00	0.03	0.02	0.00	0.01	0.02	0.00	0.00	0.00	0.03	0.00	0.05	0.06	0.02	1.55	0.00
Mg	0.00	3.14	2.63	0.00	0.02	0.00	0.00	0.40	0.00	0.47	0.00	2.03	2.25	0.00	0.31	0.32
Ca	0.00	1.48	0.48	1.99	1.98	1.98	0.00	0.00	1.00	0.63	0.00	0.13	0.42	1.97	0.61	0.00
Na	1.00	0.71	1.57	0.00	0.00	0.00	0.02	0.02	0.00	0.34	0.99	1.93	1.72	0.01	0.00	0.07
K	0.00	0.08	0.01	0.00	0.00	0.00	0.97	0.72	0.00	0.00	0.00	0.01	0.01	0.00	0.00	0.92
Sum	5.00	15.34	15.09	2.00	8.00	8.00	5.00	6.84	3.00	4.00	5.00	15.13	15.29	2.00	8.00	7.06
Oxygens	8	23	23	3	12.5	12.5	8	11	5	6	8	23	23	3	12	11
X_{Mg}	0.00	0.71	0.73	0.00	1.00	1.00	1.00	0.82	0.00	0.80	1.00	0.61	0.59	0.00	0.36	0.72

41

Supplementary Table 3. Results of AVPT calculations

Sample	Temperature (°C)*	Pressure (kbar)*	Cor†	Fit§	N#	Excluded end members
N5	489 ± 39	20.5 ± 2.2	0.22	1.53 (1.63)	8	spss, ru, fgl
14	541 ± 34	19.5 ± 1.8	0.15	1.20 (1.49)	7	spss, sph, fgl
7c	464 ± 76	6.0 ± 2.3	0.93	1.18 (1.61)	5	ep, sph, ab,
7c*	476 ± 65	6.2 ± 2.0	0.93	0.90 (1.54)	6	sph, ab, fgl

*Calculated value with associated uncertainty (± 1 S.D.).
†Calculated correlation coefficient for pressure and temperature results, ranging between 0 (wholly uncorrelated) and 1 (perfectly correlated).
§Calculated fit statistic, with sample-specific maximum legal value for 95% confidence given in parentheses.
#Number of independent reactions calculated between end members.

42

Supplementary Table 4. Bulk-rock compositions used for mineral equilibria modelling

Sample	Figures	H_2O	SiO_2	Al_2O_3	CaO	MgO	FeO	K_2O	Na_2O	TiO_2	O
N5	6	5.88	49.66	9.44	11.70	7.41	9.31	0.17	2.64	1.78	2.01
14	7	4.57	59.38	9.56	15.67	2.34	5.56	0.11	0.38	0.29	2.14
7c	8	6.49	45.35	8.11	15.09	10.00	9.93	0.55	1.37	0.39	2.72

43

Supplementary Table 5. U–Pb isotopic data of the studied blueschist samples

Sample No.	grain	$^{206}Pb^{a}$ (cps)	U^{b} (ppb)	Pb^{b} (ppb)	$\frac{Th^{b}}{U}$	$\frac{^{238}U^{d}}{^{206}Pb}$	±2σ (%)	$\frac{^{207}Pb^{d}}{^{206}Pb}$	±2σ (%)	Phase
3b	A06	46683	0.57	0.35	2.574	5.486	0.8	0.7604	0.84	C
3b	A07	45228	0.42	0.34	1.726	4.13	0.6	0.7724	0.74	S
3b	A08	40049	0.41	0.30	1.362	4.504	0.6	0.7678	0.82	S
3b	A09	313580	0.26	2.48	3.194	0.3611	0.5	0.8205	0.5	S
3b	A10	29838	0.21	0.22	1.590	3.238	0.9	0.7891	0.81	C
3b	A11	29405	0.26	0.16	1.744	8.365	1.3	0.7287	0.98	C
3b	A12	30144	0.30	0.23	2.554	4.406	1.0	0.7726	0.97	S
3b	A13	26045	0.56	0.19	2.917	9.752	1.2	0.7208	0.84	S
3b	A14	37615	0.26	0.29	2.114	3.05	1.0	0.7856	0.82	S
3b	A15	30660	0.53	0.21	2.603	9.501	0.7	0.7155	1.1	S
3b	A16	32154	0.12	0.26	2.137	1.686	2.6	0.8082	0.8	S
3b	A17	21010	0.23	0.16	3.933	4.827	0.8	0.7653	1.0	S
3b	A18	24380	0.24	0.19	2.908	4.383	1.2	0.7674	1.1	S
3b	A19	13694	0.11	0.11	2.518	3.288	4.0	0.7827	1.1	C
3b	A20	43860	0.36	0.34	1.454	3.703	1.0	0.7796	0.74	S
3b	A21	41984	0.73	0.32	2.377	7.516	0.7	0.7379	0.92	S
3b	A22	51471	0.54	0.41	2.461	4.544	0.6	0.7664	0.76	S
3b	A23	36041	0.22	0.29	2.390	2.652	1.0	0.7917	0.79	S
3b	A24	27563	0.25	0.22	2.167	3.866	1.5	0.7792	0.92	S
3b	A25	22581	0.16	0.18	1.152	3.022	2.2	0.787	1.1	C
3b	A26	26644	0.27	0.21	2.932	4.28	2.1	0.7726	0.95	S
3b	A27	17740	0.13	0.14	2.387	3.215	1.8	0.7881	1.4	S
3b	A28	44024	0.57	0.34	2.988	5.735	0.6	0.7542	0.68	S
3b	A29	40662	0.27	0.31	3.544	3.036	1.2	0.788	0.8	S
3b	A30	21547	0.19	0.17	1.798	3.733	1.1	0.7775	1.1	S
3b	A31	31724	0.27	0.26	0.712	3.246	0.9	0.7822	1.1	C
3b	A32	65329	0.14	0.54	10.798	0.9236	1.0	0.8133	0.84	C
3b	A38	19073	0.15	0.15	2.008	3.293	1.7	0.7846	0.84	C
3b	A39	48827	0.83	0.36	2.106	8.653	0.9	0.7309	0.73	S
3b	A40	33413	0.41	0.27	2.700	5.103	1.4	0.7635	1.0	S
3b	A41	28942	0.40	0.21	2.739	7.071	1.9	0.7492	0.9	S
3b	A42	34281	0.38	0.26	3.654	5.264	2.1	0.7645	0.8	S
3b	A43	9252	0.02	0.08	5.821	0.7733	2.2	0.8154	1.3	C
3b	A44	42860	0.53	0.34	1.464	5.28	1.2	0.763	0.85	S
3b	A45	39968	0.50	0.32	2.191	5.332	1.8	0.7646	0.84	S
3b	A46	30215	0.25	0.25	1.716	3.421	1.2	0.7846	0.82	S
3b	A165	28595	0.29	0.30	1.800	2.955	1.4	0.79	0.83	S
3b	A166	36178	0.39	0.34	1.537	3.866	1.5	0.7787	0.67	S
3b	A167	6215	0.03	0.06	2.502	1.62	2.3	0.7771	0.84	S
3b	A168	24685	0.25	0.22	1.660	4.086	1.4	0.7754	0.87	S
3b	A169	38043	0.44	0.36	1.698	4.098	0.7	0.7698	0.68	S
3b	A170	18218	0.15	0.17	1.663	2.882	1.2	0.7858	0.76	S

3b	A171	67145	0.82	0.50	2.548	7.836	2.0	0.7339	0.79	S
13	A60	159418	0.42	1.42	8.280	1.016	8.4	0.8368	0.5	C
13	A61	313237	0.05	2.66	5.537	0.06115	2.0	0.8398	0.38	C
13	A62	261899	0.65	2.19	2.420	1.028	4.1	0.8373	0.42	C
13	A63	55562	0.10	0.47	3.605	0.7208	3.4	0.839	0.69	S
13	A64	158085	0.42	1.38	4.167	1.087	4.1	0.8399	0.47	S
13	A65	526092	0.36	4.39	2.059	0.2806	0.4	0.8435	0.37	C
13	A66	191738	1.16	34.10	10.125	2.654	2.2	0.8198	0.6	S
13	A72	388843	1.01	3.06	12.566	1.359	2.1	0.834	0.37	C
13	A73	193233	5.51	1.70	0.169	10.53	2.4	0.7353	0.41	S
13	A74	988575	0.20	8.57	1.319	0.08119	0.7	0.8332	0.32	S
13	A75	527603	1.88	4.67	3.614	1.406	6.4	0.8336	0.37	S
13	A76	283119	0.81	2.45	2.090	1.181	2.3	0.8356	0.35	S
13	A77	427752	0.31	3.41	2.592	0.3309	0.9	0.8403	0.41	S
13	A78	237016	0.15	2.10	5.531	0.2493	2.2	0.8467	0.43	S
13	A79	161435	0.07	1.41	3.403	0.1762	3.5	0.8479	0.57	S
13	A80	240641	0.99	2.16	6.213	1.627	2.6	0.8322	0.38	C
13	A81	213705	0.41	1.99	3.326	0.6789	6.6	0.8414	0.42	S
13	A82	190452	0.21	1.68	9.824	0.4379	1.5	0.8464	0.39	S
13	A83	295855	0.29	2.56	10.553	0.3994	2.8	0.8444	0.42	S
13	A84	211768	0.35	2.12	3.368	0.5029	3.6	0.8455	0.45	S
13	A85	309000	0.37	2.64	7.666	0.4901	2.1	0.844	0.44	S
13	A86	1006451	0.12	9.69	2.300	0.04261	1.6	0.8355	0.38	C
13	A87	472813	0.96	3.48	1.363	1.012	2.6	0.8385	0.37	S
13	A88	294608	0.75	3.29	5.596	0.7062	3.2	0.8405	0.43	C
13	A89	1980020	0.29	17.72	12.090	0.05791	2.9	0.8394	0.33	S
13	A90	214418	0.09	1.86	0.926	0.1674	2.5	0.8485	0.45	C
13	A091	2134501	0.32	18.16	0.600	0.0622	4.4	0.8377	0.32	C
13	A92	314456	1.31	2.71	0.458	1.669	3.7	0.8297	0.37	C
13	A93	580143	0.41	3.95	2.470	0.4795	0.5	0.8455	0.35	C
13	A94	276122	0.42	2.32	18.890	0.6495	1.9	0.8414	0.44	S
13	A95	247814	0.68	2.05	2.381	1.171	2.4	0.8362	0.45	S
13	A96	1268062	0.98	6.95	12.461	0.5039	1.7	0.8431	0.35	S
13	A97	330147	3.14	1.69	1.738	8.582	4.2	0.7468	0.45	S
13	A98	1511920	1.04	13.25	4.565	0.2732	5.1	0.8384	0.31	S
13	A99	585406	0.50	4.90	0.633	0.3547	6.5	0.8384	0.35	S
11	A100	550329	1.62	3.33	0.995	3.338	1.4	0.7978	0.38	C
11	A101	643865	0.43	5.47	2.447	0.2659	0.3	0.8348	0.33	C
11	A107	726889	1.91	6.13	8.982	1.099	1.0	0.8255	0.32	C
11	A108	321175	0.26	2.79	0.137	0.3235	1.1	0.8332	0.38	C
11	A109	895619	6.69	7.54	4.678	3.002	1.3	0.7838	0.34	S
11	A110	427471	0.23	3.70	2.364	0.2135	0.4	0.8343	0.39	C
11	A111	260406	0.53	2.48	45.947	0.8021	0.7	0.8304	0.37	C
11	A112	167449	0.81	1.57	0.194	1.732	1.9	0.7945	0.54	S
11	A113	162814	0.05	1.56	0.227	0.1177	0.9	0.8448	0.49	S

11	A114	129813	0.06	1.28	0.183	0.1681	0.8	0.8405	0.54	S
11	A115	74811	0.08	0.73	0.152	0.3965	1.7	0.8316	0.56	C
11	A116	88180	0.57	0.85	0.271	2.282	1.6	0.8098	0.49	S
11	A117	122657	0.21	1.02	0.226	0.7684	4.2	0.8284	0.48	S
11	A118	365557	0.11	3.10	0.339	0.1198	2.3	0.8369	0.37	C
11	A119	85225	0.15	0.76	7.786	0.6861	1.7	0.8287	0.49	C
11	A120	284139	0.47	2.55	12.306	0.6485	2.7	0.8311	0.42	S
11	A121	432625	0.67	4.94	17.064	0.3922	8.5	0.8346	0.34	S
11	A122	1885183	2.38	17.00	6.513	0.494	0.9	0.8313	0.3	S
11	A123	1437266	3.18	9.84	8.088	1.762	1.6	0.8176	0.33	S
11	A124	481565	0.33	4.17	2.304	0.2727	0.9	0.834	0.34	S
11	A125	185421	0.18	1.68	4.353	0.3782	3.3	0.8421	0.42	S
11	A126	217816	0.06	1.95	0.861	0.1141	3.4	0.8372	0.43	C
11	A127	316865	0.37	2.87	8.533	0.4547	2.6	0.842	0.37	S
11	A128	123976	0.07	1.05	0.224	0.2328	2.0	0.8365	0.54	S
11	A129	224359	0.10	1.98	2.837	0.1777	1.5	0.8427	0.41	C
11	A130	439692	1.44	2.62	10.548	5.474	0.7	0.7756	0.38	C
11	A131	147942	0.16	1.16	2.536	0.4829	2.2	0.8356	0.49	S
11	A132	237211	0.13	2.07	2.142	0.215	0.7	0.8355	0.41	C
11	A133	591044	0.38	5.20	1.967	0.2514	0.3	0.8332	0.42	C
11	A134	192938	0.14	1.62	0.405	0.3029	1.9	0.8359	0.45	C
11	A135	458317	0.61	3.03	2.160	1.097	0.6	0.8233	0.37	C
14	A136	390768	0.65	2.62	0.545	1.672	0.9	0.826	0.4	S
14	A137	688012	0.35	6.94	1.298	0.1749	1.6	0.8443	0.35	S
14	A138	1170631	0.83	11.88	2.712	0.2475	1.2	0.8413	0.33	C
14	A139	1931275	0.99	16.01	0.699	0.2946	0.5	0.8431	0.3	S
14	A140	817585	1.01	4.77	4.519	3.079	0.7	0.8094	0.33	C
14	A141	1377486	0.67	11.55	0.789	0.2726	0.9	0.8429	0.33	S
14	A142	102777	0.65	1.51	1.546	1.222	0.8	0.8306	0.68	S
14	A143	1889857	2.33	16.77	5.000	0.5913	0.2	0.8381	0.32	C
14	A144	181455	0.08	1.33	2.755	0.3524	7.3	0.8395	0.53	S
14	A145	2133448	0.73	17.86	0.535	0.1957	0.6	0.8448	0.31	S
14	A151	1728879	0.79	13.25	1.646	0.3401	0.3	0.8422	0.31	S
14	A152	732208	0.40	5.15	7.157	0.6019	2.3	0.8383	0.34	S
14	A153	1122112	0.20	7.77	0.182	0.208	1.4	0.8443	0.32	S
14	A154	634125	0.25	6.79	0.425	0.1307	1.8	0.8456	0.35	S
14	A155	247895	0.06	2.65	1.102	0.08261	4.5	0.8444	0.43	S
14	A156	508240	0.23	5.36	1.686	0.1454	3.5	0.8431	0.41	S
14	A157	1049201	0.18	11.18	0.479	0.05772	1.5	0.8457	0.31	S
14	A158	369712	0.13	4.23	1.415	0.1012	7.2	0.8445	0.42	S
14	A159	1040233	0.22	11.17	0.464	0.07095	0.9	0.8441	0.32	C
14	A160	498591	0.30	2.82	2.304	2.768	0.6	0.8129	0.43	C
14	A161	1012897	0.47	13.87	0.378	0.09687	3.6	0.8444	0.32	S
14	A162	460864	0.21	4.94	1.221	0.1502	4.3	0.8436	0.4	S
14	A163	1508708	0.80	16.24	0.341	0.1755	0.2	0.8435	0.32	S
14	A164	606128	0.43	6.57	5.745	0.2345	1.9	0.8416	0.35	S

Spot size = 235 μm; depth of crater ~20μm. $^{238}U/^{206}Pb$ error is the quadratic additions of the within run precision (2 SE) and the external reproducibility (2 SD) of the NIST 614. $^{207}Pb/^{206}Pb$ error propagation (^{207}Pb signal dependent) following Gerdes and Zeh (2009).

[a]Within run background-corrected mean ^{207}Pb signal in cps (counts per second).

[b]U and Pb content and Th/U ratio were calculated relative to NIST SRM-614.

[c] percentage of the common Pb on the ^{206}Pb. b.d. = below detection limit.

[d] Corrected for background, within-run Pb/U fractionation (in case of $^{206}Pb/^{238}U$) and subsequently normalized to NIST 614 (ID-ICPMS value/measured value).

S – Amphibole/Epidote
C – Calcite

Highlights

(a) Naga ophiolite has undergone polymetamorphic events.

(b) Unsheared samples peak *P–T* conditions of ~1.9 GPa and ~480–520 °C.

(c) Sheared sample stable at lower *P–T* conditions of ~0.6 GPa and ~470 °C

(d) U–Pb ages of the Nagaland blueschist underwent peak and retrograde metamorphism c. 95 Ma and c. 90 Ma.

(e) Combined U–Pb age and calculated *P–T* that Nagaland blueschist rocks exhumed at a rate of ~1 cm/year

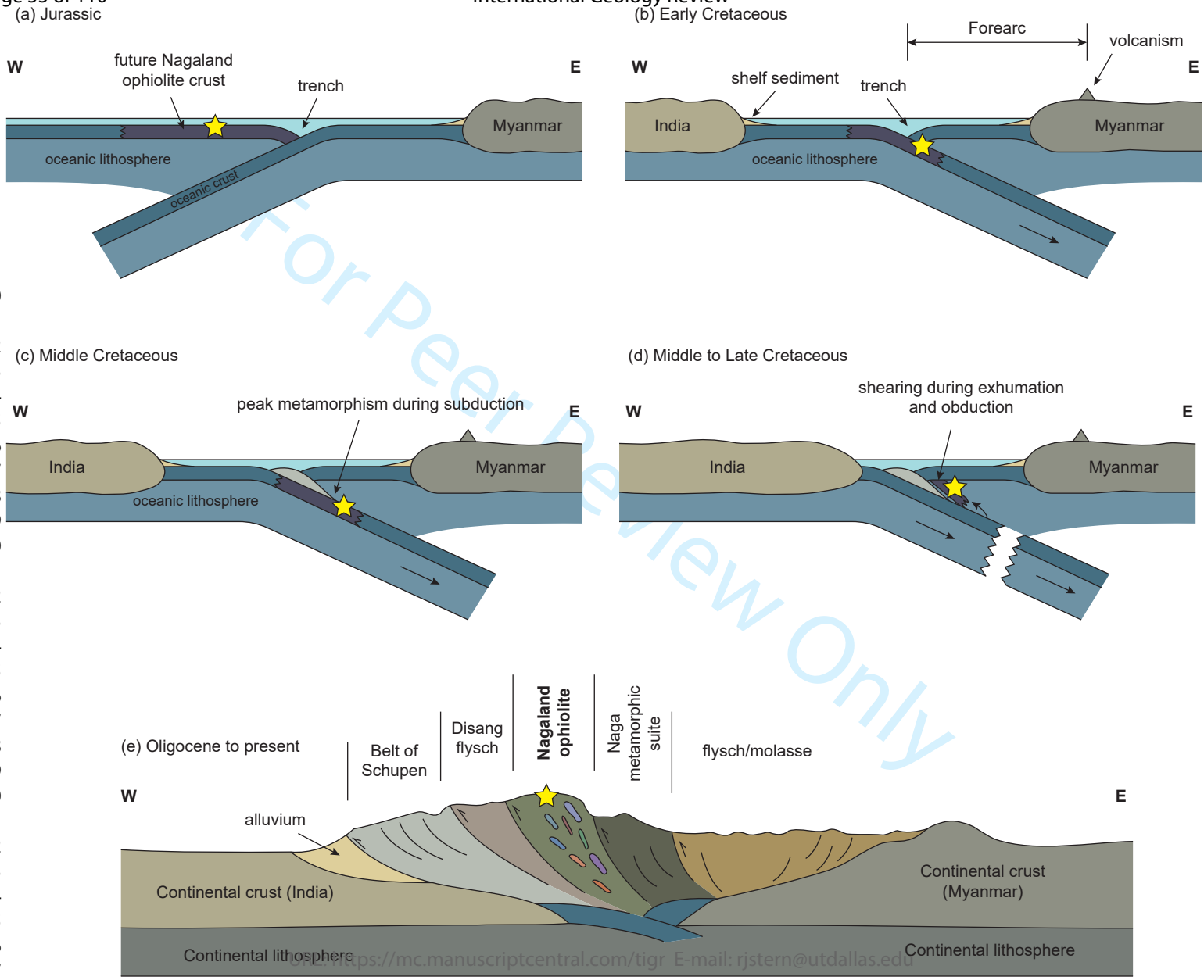

Fig. 11

Reviewer: 1

Comments to the Author
Review of “Dating blueschist-facies metamorphism within the Naga ophiolite, Northeast India, using sheared carbonate veins” by Maibam et al., submitted to International Geology Review.

This is a quite interesting and concisely written paper that presents the results of a classical tectonometamorphic study combined with a novel approach to absolute dating. Overall, the conclusions drawn sound convincing and well supported by the provided data, which are undoubtedly of high quality. However, I have made some remarks about some aspects that in my opinion need to be carefully elucidated and/or better presented before the article can be considered ready for publication. In the following lines I am summarising the main points of my criticism, but the authors are referred to the attached pdf file for more detailed comments and specific suggestions.

My first concern regards the “Geological background” section, which is too brief and general in my opinion (please refer to the attached comments). I think the authors should spend some additional effort into providing more detailed information about the geology of the investigated area, so that a reader that is not familiar with such topics (like I am) can easily understand what is the general context and what are the main points of debate in the scientific literature. In this way, the authors will not only help the reader to get into the presented topics, but also, and most importantly, to get convinced about the significance of their study, explaining what is the great contribution they are giving in order to resolve those issues that are still a matter of debate. In the present version of the manuscript I am not sure this is completely clear, especially as regards the geochronological issues. The authors mention numerous age data from the existing literature and then conclude that there is “a paucity of reliable geochronological age data” (lines 151-152), although they actually do not explain on what basis they can say this. I think they should definitely add some more specific information and comments about this, in order to sound completely convincing and to give further strength to their novel approach.

As regards the “Analytical methods” and “Sample petrology” sections, I have found a number of controversial points that need to be elucidated.
- first of all, I think that the section on the analytical techniques should include also some information about the investigated samples, before describing what was done. Few notes on sampling activities, including locations, stratigraphic positions, lithotypes, number of collected samples etc., would be sufficient (and absolutely necessary, in my opinion).
- mineral abundances are said to have been calculated (“Calculated volume proportions of minerals in each sample are given below”, lines 164-165), but in the following sections of the manuscript these are said to have been determined via point counting (“Mineral proportions for each sample were

determined using the software JMicroVision", lines 308-309). This needs to be clarified. I do not think that these were calculated, but if so, the authors should explain how this was made. In addition, where they mention that mineral abundances were obtained by point counting, the authors say that this was made on a total of 500 points for each of the analysed samples in thin section. I am not sure this can be considered sufficient to yield statistically reliable modal proportions. To my knowledge, point counting is generally made on at least 3000-4000 points per sample. Please also consider that the investigated samples include a relatively large number of different mineral phases (7 major phases plus 3 accessory phases for sample N5; 8 plus 3 for sample 14; 8 plus 2 for sample 7c; 8 plus 4 for sample 11), so counting only 500 randomly chosen points throughout the entire thin section can very likely bias the final results.

- bulk rock samples are said to have been analysed by XRF (lines 168-177), but the results are not reported neither in the main manuscript, nor in the Supplementary Files. But what is more important, later in the text, in the "Thermobarometry" section, rock compositions are said to have been calculated using mineral modes and compositions (lines 306-307). I warmly invite the authors to clarify this.
- the analysed samples are said to be six, but those that are described are just 4: the sheared N5 and 14 and the unsheared 7c and 11. Two additional sheared samples, 3b and 13, are in some instances mentioned, but nothing is reported about their petrography, mineral chemistry or bulk rock composition. I think this should be amended, providing a description of the general petrographic and mineral chemistry features of these samples, exactly the same way this is done for the other 4 samples. If for some reason, this is not possible, I think the authors should explicitly mention it and provide full explanations.
- the unsheared sample 14 is said to be a blueschist (or a metabasite) sample like all the other investigated samples, but I have to say that I find it hard to agree with that. Its mineral composition is dominated by epidote (50%) and quartz (35%), with only 10% Na-Ca amphibole (i.e., the "blue" or "glaucophane" amphibole; see lines 236-238). In addition, the bulk composition reported in the Supplementary Table 3 is much richer in SiO_2 and poorer in MgO and FeO with respect to the other samples. I think this requires to be taken into account by the authors.
- since bulk rock compositions have been obtained for the investigated samples (whether directly, through XRF analyses, or indirectly, calculated using mineral modes and compositions – see previous point), I expect that a paragraph of the "Sample petrology" section is devoted to a brief description of these. I think this would be absolutely necessary, also considering that these compositions are then used for phase equilibria modeling, so that the reader can understand why the authors chose the specific model system they employed for such calculations.

As regards the "Thermobarometry" (which I think should be renamed more properly as, e.g., "Phase equilibria modeling") and the "Discussion and implications" sections I have a few smaller remarks:

- only one of the 4 unsheared samples was used for calculating bulk rock pseudosections (i.e., sample 7c), but the authors do not provide any explanation about their choice to focus on this sample only. I think at least a few notes on this should be added.

- the authors did not explain why they assumed that some phases are in excess, which I think needs to be adequately elucidated.
- in constraining peak P-T conditions for unsheared samples, the authors use together the results for the two investigated samples N5 and 14. I think it would be much better if they present the results for these two samples separately, and then they propose a single P-T range by comparing them and see where the best matches for both samples overlap.
- the authors usually refer to the “best matching assemblages” but to me this sounds like a very vague concept, if they do not explain what was the strategy they employed in order to identify such best matches. I guess these are defined as those minimizing the differences between observed and calculated mineral abundances, but maybe this can be done in more than just one single way, e.g., not only by minimizing the differences of mineral abundances, but maybe also by minimizing the squared residuals of the differences, or maybe even in some other way.
- in the conclusive section, when presenting the results of their estimates for P-T conditions, I think the authors can simply refer to the conditions obtained for the best matching assemblages, rather than repeating again what is the total range for the peak and retrograde assemblages (which were already discussed in the “Thermobarometry” section). I think they should report such tighter ranges also in the other sections of the paper (e.g., abstract, conclusions) where they mention the results of their models.
- since the proposed P-T-t path (Fig. 10) is quite different from those from the available literature reported for comparison, I would expect that this was discussed a little bit, trying to provide some explanations for such mismatches [which are particularly evident for the path from Ao and Bhowmik (2014)]. On the other hand, the authors simply present the proposed P-T-t path in just three lines (400-402), completely avoiding any comment on the compared models. I think this issue needs to be addressed.

Finally, as regards the Supplementary Files (i.e., Electronic Appendix), I have to say that most of the contents that are presented are actually just a repetition of what was already reported in the main text. The authors should report in this section only additional material that was not previously included in any parts of the manuscript, like their Supplementary Tables and Supplementary Figure 5 (which thus should be renamed to “Supplementary Figure 1”). In addition, as regards mineral analyses reported in Supplementary Table 2, I think these should include not only a selection of some representative ones, but the entire dataset available to the authors, not only because there are no space limitations for electronic supplementary materials, but also because providing a large dataset surely adds robustness and value to their work.

Lorenzo Fedele

Dipartimento di Scienze della Terra,
dell’Ambiente e delle Risorse (DiSTAR)

Università degli Studi di Napoli Federico II
Complesso Universitario di
Monte Sant'Angelo, Edificio 10 - L1
Via Cintia 21,
80126 Napoli
e-mail: lofedele@unina.it
tel.: +390812538114

Reviewer: 2

Comments to the Author
This manuscript presents petrological and geochronological data for blueschist facies rocks from the Nagaland ophiolite. The paper connects pressure-temperature conditions for two distinctly different types of samples – one unsheared and one sheared - with geochronology to interpret the timing of metamorphism and rate of exhumation for these samples. The paper will be of interest primarily to structural and metamorphic geologists, and those interested in the tectonics of exhumation.

I found the paper to be well-written and the concepts were clearly and concisely described. The P-T conditions are clearly quite different for the two suites of mineral assemblages and the textural differences are clearly shown in the figures. The interpretation, if is supported fully, could be an interesting and exciting contribution. However, I think that more attention needs to be paid to providing the context for the analytical spots and a fuller discussion of recrystallization in the context of the spots analyzed could be provided.

Analytical spot context: The context for the spots analyzed needs to be better documented. The text in the abstract for the manuscript states that the geochronology is "U-Pb in situ analysis of carbonate grains (aragonite-calcite)". However in line 90-91 this is now described as "millimetre-sized minerals and mineral assemblages (e.g., carbonate, epidote, amphibole, etc.)." A look through the data table indicates that <25% of the analyses for sample 3b are carbonate. The other samples also have fewer than 50% carbonate analyses. This raises a number of questions. A look at supplemental Figure 5 shows back-scattered electron imaging of the samples with white circles on the analytical spots. This figure is incredibly important as it provides context for the analyses. It might be worth incorporating this as a regular figure of the paper. However, looking at this figure it is still not clear from the figure which spots are on which mineral(s), and whether the placement of the spots on carbonate are indeed in recrystallized veins as is described in the text. The vein-like regions labeled "carbonate" are remarkably devoid of analytical spots. This may be a simple issue solved by better labeling. One way to improve this would include to color code the spots on the diagram to highlight the carbonate analyses, in particular those that are recrystallized carbonate. As it looks right now, many of the spots fall on black parts of the image (are those minerals or holes in the section?), and it looks like the minority are on carbonate. The inset figures do not provide much useful information because their

position on the larger scale image is not marked and there are no analytical spots located on those images. The text of the abstract should be changed to reflect that these analyses are of both silicate minerals and carbonates. Would the data interpretation change if only carbonate data were evaluated? If so, it would strengthen the interpretation to demonstrate that.

Thanks for the comment on the documentation of the analysed spots. We would like to share the presented BSE images and the analysed spots are representative. We do not present the full thin sections. As suggested, we have increased the labelling of the spots. Reviewer has rightly pointed out the black parts in the images are laser holes, where the laser spot has penetrated the phases.

The inset images have deleted. The abstract has been modified with the insertion of silicate phase analysis. Geochronology data is improved when we consider the carbonate and cogenetic silicate phases, compared to the carbonate data only.

Additionally, a more in-depth discussion of the likely recrystallization of the various minerals analyzed would be helpful in supporting the conclusions of the study. It is stated that the carbonate is selected from recrystallized veins. Is the carbonate in the unsheared sample still aragonite or might it be calcite? If it has reverted, did it recrystallize upon reversion and thus is the age for the unsheared sample possibly not a peak age? Are the other minerals dated in the sheared samples (epidote, amphibole) likely to recrystallize during exhumation or might they simply be reoriented and not recrystallized?

Thanks for the comment but we cannot comment much on the likely crystallisation of the various minerals. We have inferred the carbonates in the sheared and unsheared samples as calcite and aragonite on the basis of the estimated P-T range and well-established aragonite-calcite stability curve.
We cannot comment on the recrystallisation affecting the isotopic values. As presented in the text, in the present study instead of dating single accessory mineral domains, millimetre - sized minerals and mineral assemblages (e.g., carbonate, epidote, amphibole etc.) that recrystallised and equilibrated during a single tectonic event and which contain measurable amounts of U and Pb can be used to determine crystallization ages. Here we apply this method to dynamically recrystallised carbonate veins and selected mineral assemblages (amphibole, epidote) in blueschists within the Kiphiere District of the Nagaland ophiolite belt and integrate these ages with thermobarometric data to produce new constraints on the timing and rates of subduction and exhumation cycle of Neo -Tethyan crust in the Indo - Myanmar region.

Below I discuss specific comments keyed to section and line numbers in the manuscript draft.

Specific comments

Abstract, line 39 – This should be reworded to indicate that other minerals were included in the analytical data set.

Done

Line 50 – “HT-LP” here should be “HP-LT”

Done

Lines 94-101 – This section seems like it would be more appropriate in the Methods section.

Done

Geological Background – There are a lot of names here, some of which need to be more clearly defined/stated near the beginning of the section. In particular the Manipur ophiolitic nappe isn’t defined, it is just part of a description in line 136, so it needs to be clearly stated what/where it is before that. Also it should be made clear in the first paragraph of this section which ophiolite is the Naga ophiolite. It appears first on line 130 as “Nagaland ophiolite belt” without a clear introduction. As it is the fiocus of the paper, it would be helpful to more clearly define it early on.

The geological has improved with additional information taking account of the suggestions.

Lines 164-165 – How are the volume proportions described here calculated? This needs to be explained.

It has been explained.

Line 210 – “sheared OR unsheared” rather than “and”

Done

Line 308-311 – This information seems more appropriate for the Methods section. Perhaps this addresses the question I had in lines 164-165? Also it is worth considering putting the information about how phase diagrams were calculated in the Methods section (lines 293-304).

Have transferred to the Method section.

Lines 353+ U-Pb geochronology - It is difficult to see clearly that recrystallized calcite was chosen for analysis, based on the images in the supplementary file. This raises the question of whether minerals recrystallized during deformation or not. Discussion of whether older ages could be preserved during

shearing would be important. Would resetting be expected during shearing of these minerals? Preferred orientation, bending and curving (lines 390-391) do not require recrystallization.

Thanks for the comment but the represented figures are for representative purpose only and do not reflect the overall feature.

As given above we cannot comment on the recrystallisation affecting the isotopic values. In the present study instead of dating single accessory mineral domains, millimetre -sized minerals and mineral assemblages (e.g., carbonate, epidote, amphibole etc.) that recrystallised and equilibrated during a single tectonic event and which contain measurable amounts of U and Pb can be used to determine crystallization ages.

Line 401 – If these are slab-top temperatures from Syracuse et al., 2010 that should be indicated here.

Indicated

Line 405 – Change “out” to “our”

Done

Lines 435-437 – The uplift rate calculated here would be vertical uplift since the distance is based on changes in pressure. However, as indicated in Figure 11, some or all of the exhumation may not be 100% vertical, and there may be some component along the subduction plate interface. This possibility should be discussed and included in estimates.

Possibility is discussed with additional info.

Reviewer: 3

Comments to the Author
Comments:

1. Pseudosections/Phase equilibria modeling. MnO is critical to control the garnet stability. It is OK to omit the modeling, but reasonable explanations are necessary. Naturally, pseudosections in the Mn-free system have a risk of explaining observed mineral assemblages.

There are no manganese bearing activity composition models available for either the amphiboles or clinopyroxene, it is not currently possible to consider manganese in any confident way in meta basic systems.

In Supplementary Figures 6 and 7, please illustrate isopleths of garnet end-member compositions and phengite Si apfu.

We have not contoured these isopleths as we don't believe this is necessary for the overall interpretation of the rocks in question. it is unclear from the comment why the reviewer wants these isopleths calculated and for what purpose.

In the Supplementary Figures, I'm curious about the assumption (?) of excess Ep (and also Rt) in the whole P-T range (1.0–2.5 GPa and 350–600°C). The stability of biotite also loos strange to me.

In these calculations epidote and rutile are found to be in excess (stable in all fields) rather than assumed to be in excess. Therefore, the in excess notation is simply to simplify the labelling of diagrams. In addition, without clarification of what is considered to be odd will strange in the stability biotite it's difficult to comment on this. the stability biotype in the diagram is what is predicted by the thermodynamic modelling.

2. Sodic amphibole compositions. In Figure 5, please add Fe3+/(Fe3+/Al) versus Mg# diagram for analyzed sodic amphibole. Also, please discuss the consistency of the composition of sodic amphibole and the modeled amphibole composition, especially Fe3+.

We don’t feel the suggested plot would be particularly informative. Furthermore, given that the Mg# is somewhat dependent on the estimation of ferrous vs ferric iron from the probe analyses there is a danger of there being a correlation of errors or co-dependent variables in such a plot. Further, a direct comparison between the model compositions and the probe analyses would involve considerable new calculation to extract this information from the model results.

3. Sonic pyroxene (aegirine-augite). Sample 11 contains aegirine-augite + quartz + albite. This mineral association is helpful to constrain P-T.

Thanks for the comment. Preliminary investigation of phase equilibria stability in sample 11 did not allow for reliable thermobarometry to be performed due to the high variance of the interpreted peak mineral assemblage

4. In general, vein formation requires brittle deformation.

While classic straight sharp-edged veins require brittle deformation many other vein-like structures do not (for example in migmatites where a ductile parting process may operate, see papers by Brown, Sawyer etc.)

5. Rutile. Why don't you try rutile U-Pb dating to compare the results? I think dating is more straightforward than carbonate dating.

We have tried to analyse rutile but because of low U concentration, could not yield a producible age.

6. Occurrence of carbonate in unreformed samples. Petrographic information on sample 14 is weak. Please describe more about the dated carbonate mineral. The authors considered the calcite in unreformed samples was aragonite. Do you see any topotactic pseudomorphs after aragonite? For example, see Bradt et al. (2004) https://doi.org/10.1016/S0191-8141(03)00099-3

We have inferred the carbonates in the sheared and unsheared samples as calcite and aragonite on the basis of the estimated P-T range and well-established aragonite-calcite stability curve.

7. Others

Line 144. 1 kbar ==> 0.1 GPa

Done

Line 150-151. ~11.5 kbar ==> 1.15 GPa; 6 kbar ==> 0.6 GPa

Done

Line 230. Si = 3.34–3.38 pfu ==> Si = 3.34–3.38 pfu for O = 11

Done

Line 237. sphene ==> titanite

Done

Lines 269, 273, 278. muscovite ==> phengite

Done

Line 287. Please add the jadeitite component of the aegirine-augite.

Done

Line 326. 1 kbar ==> 0.1 GPa

Done

Line 384. I think better to say "metamorphic recrystallizations"

Done

Supplementary Table 4.

- Please use "GPa" instead of "kbar"

Done

Supplementary Figure 5.

Ms ==> Ph

Sph ==> Ttn

Done

Dating blueschist-facies metamorphism within the Naga ophiolite, Northeast India, using sheared carbonate veins

Bidyananda Maibam[a]*, Richard M. Palin[b], Axel Gerdes[c,d], Richard W. White[e], Stephen Foley[f]

[a]*Department of Earth Sciences, Manipur University, Canchipur, Imphal-795003, India*

[b]*Department of Earth Sciences, University of Oxford, Oxford, OX1 3AN, United Kingdom*

[c]*Department of Geosciences, Goethe-University Frankfurt, 60438 Frankfurt, Germany*

[d]*Frankfurt Isotope and Element Research Center (FIERCE), Goethe-University Frankfurt, 60438 Frankfurt, Germany*

[e]*School of Earth and Environmental Sciences, University of St. Andrews, KY16 9AL, United Kingdom*

[f]*ARC Centre of Excellence for Core to Crust Fluid Systems, Department of Earth & Environmental Sciences, Macquarie University NSW 2109, Australia*

**corresponding author: bmaibam@yahoo.com*

Keywords: blueschist; dynamic recrystallisation; exhumation; petrological modelling; U–Pb carbonate geochronology

ABSTRACT

The tectonic significance of blueschist-facies rocks associated with the Indo-Myanmar ophiolite belt is uncertain, given ~~their~~ lack of detailed petrological study and the paucity of

reliable age data for different stages in their geological evolution. Here, we present new integrated petrological and geochronological data for samples from the Nagaland complex of the Indo-Myanmar ophiolite belt, northeastern India, which constrains the pressure–temperature conditions and absolute ages of peak and retrograde metamorphism. Several samples of blueschist were collected from the region, which have been variably deformed and subjected to shear recrystallization. Based on microstructural constraints and mineral geochemistry, garnet, omphacite, barroisite, chlorite and muscovite are interpreted to represent a high-pressure prograde-to-peak metamorphic assemblage, and omphacite, actinolite, hornblende and albite represent a lower-pressure retrograde metamorphic assemblage that formed during shear-related exhumation. Petrological modelling and thermobarometry indicates that unsheared samples equilibrated at ~1.9 GPa and ~~**420–560 °C**~~ ~480–520 °C **(LARGE T RANGE AT FIXED P EXPLAINED IN THE TEXT)** at peak metamorphism, indicating subduction to ~60 km depth, whereas sheared and recrystallised samples re-equilibrated at ~0.6 GPa and ~470 °C **(EXTREMELY PRECISE P-T RANGE INSTEAD)** during retrograde metamorphism associated with obduction of the Naga ophiolite onto the Indian foreland. U–Pb *in-situ* analysis of carbonate grains (aragonite–calcite) and associated silicate phases (epidote, prehnite, amphibole etc.) in different microstructural positions, including within dynamically recrystallised shear bands that cross-cut older metamorphic fabrics and cogenetic silicate phases, constrains the age of peak metamorphism to be c. 95 Ma and retrograde metamorphism to be c. 90 Ma. Based on the overall progression of ages in the sheared and unsheared samples, we interpret that the area experienced ~~atypically slow~~ exhumation at a time-averaged rate of ~1 cm/year in the order of Phanerozoic period plate tectonic rate **(ARE YOU SURE THIS CAN BE CONSIDERED A SLOW EXHUMATION RATE? TO MY KNOWLEDGE, RATES IN THE ORDER OF MM/YR ARE ALSO COMMON, SEE E.G., MANZOTTI ET AL., 2008,**

CORRECTED**).** which is in the order of rates of plate tectonic processes on the Phanerozoic Earth

1. Introduction

High-pressure metamorphic belts provide a critical record of the geological evolution of paleo-plate boundaries, and provide valuable constraints on tectonothermal models of both modern and ancient ~~orogenesis~~ orogeneses (e.g. Ernst 1973; Carswell 1990). Blueschist-facies rocks form at high-pressure–low-temperature (H~~*T*~~***P***–L~~*P*~~***T***) metamorphic conditions characteristic of subduction zones (Miyashiro 1961; Cloos 1985; Palin and White 2016) or ephemerally in the embryonic stages of collisional orogeny (Wang and Foley, 2020), where they may subsequently recrystallize to greenschists or amphibolites under higher temperatures and/or lower pressures (Ernst 1973). Combining mineral equilibria constraints on the thermobarometric conditions under which sequential assemblages formed with absolute ages obtained via *in-situ* geochronology**,** can elucidate the timing and timescales of geodynamic processes that control the subduction–exhumation cycle (e.g. Terry *et al*. 2000; Rubatto and Hermann 2001; St-Onge *et al*. 2013).

The power of this integrated technique is demonstrated here ~~using the example of~~ in the case of the Indo-Myanmar ophiolite belt, a part of the Indo-Myanmar Range that extends to the east and southeast of the Himalayan orogen. The geological history and tectonic evolution of this belt is currently poorly understood, such that more precise constraints on the pressure–temperature–time (*P*–*T*–*t*) path of key lithologies ~~from the complex~~ are necessary to improving our geological understanding of this part of southeast Asia. Much of the current uncertainty concerning the tectonic evolution and significance of these Indian-plate ophiolitic rocks stems from a lack of reliable petrochronological data. In particular, the timing and *P*–*T* conditions of high-pressure metamorphism in the Indo-Myanmar belt is poorly constrained

due to the general absence of datable mineral phases in mafic igneous rocks that are reactive at subsolidus subduction-zone H*P*–L*T* metamorphic conditions. Zircon from jadeitites in this region have previously ~~produced~~ yielded U–Pb ages ranging from Late Jurassic (c. 147 Ma: Shi *et al*. 2008) to Late Cretaceous (c. 77 Ma: Yui *et al*. 2013), although all of these data show significant scatter due to incomplete recrystallization of magmatic grains and metasomatic/hydrothermal activity during subduction and exhumation, which can partially reset isotope systems (Wang and Griffin 2004). Furthermore, these former studies performed geochronology on zircon grains separated from the host rocks, which ~~prohibits~~ inhibits direct correlation of age data with *P*–*T* conditions derived from metamorphic assemblages and microstructures, leading to potentially unreliable geological interpretations.

The zircon U–Pb isotope system is widely applied for dating the crystallization and re-crystallization of mineral assemblages during high-temperature metamorphic events (e.g. Williams and Claesson, 1987; Parrish, 1990; Robb *et al*. 1999, Rubatto et al., 2001). However, some lithologies and/or geological processes often cannot be dated directly by this technique due to the absence of appropriate minerals that incorporate measurable amounts of radiogenic nuclides. Examples of such rocks can be found in shear zones, ~~such as mylonites and tectonic carbonates,~~ but this issue also extends to H*P*–L*T* metamorphic rocks, ore mineralisation**s**, diagenetic minerals and cement**s**, some sedimentary rocks, and some alteration assemblages (e.g. Gilley *et al*. 2003). Recent studies have focused on the application of *in-situ* U–Pb isotope analyses of low-U minerals ~~(e.g., carbonate**s**, epidote**s**, amphibole**s** etc.)~~ in thin section by laser ablation inductively coupled plasma mass spectrometry (LA-ICP-MS) for geochronological study (Millonig *et al*. 2012; Coogan *et al*. 2016; Ring and Gerdes 2016; Roberts and Walker 2016; Li *et al*. 2014). Thus, instead of dating single accessory mineral domains, millimetre-sized minerals and mineral assemblages (e.g., carbonate, epidote, amphibole etc.) that recrystallised and equilibrated during a single tectonic event and which contain measurable

amounts of U and Pb can be used to determine crystallization ages (e.g. Burisch *et al*. 2017; Ring and Gerdes 2016).

~~According to Rasbury and Cole (2009), a linear regression taken through a group of samples from the same system produces a slope from which an age can be calculated using the accepted decay rate for the parent isotope. If the system being analysed has no initial heterogeneity, and it remained closed throughout the duration of the decay process, all scatter of data points about the isochron can be explained by analytical uncertainties. A statistical test of this is the mean squared weighted deviate (MSWD). Closed isotopic systems will plot as a line, giving a precise age and low **mean squared weighted deviate (MSWD) of** ~1, while systems that have not remained closed will show scatter and have a high MSWD (>>1).~~ Here we apply ~~this~~ the isochron method to dynamically recrystallised carbonate veins and selected mineral assemblages ~~(amphibole, epidote)~~ in blueschists within the Kiphiere District of the Nagaland ophiolite belt and integrate these ages with thermobarometric data to produce new constraints on the timing and rates of subduction and exhumation of Neo-Tethyan crust in the Indo-Myanmar region.

2. Geological background

The Indo-Myanmar Range is thought to represent a relict eastward-dipping subduction zone that runs from the eastern edge of the Himalayan Range in southeast Tibet to the island of Sumatra in the south (Allen *et al*. 2008**; Fig. 1**). The Eastern Himalayas, about 700 km long, trends ENE-WSW. Broadly N-S trending to sigmoid IMR has subdivided into three sectors from north to south of about 400 km length each e.g., Naga Hills, Chin Hills and Arakan Yoma (Acharyya 2015). The belt continues as the Anadaman Nicobar island arc in the south. Belts of narrow tectonised but nearly continues, late Mesozoic-Eocene ophiolite and associated sediments skirt along the northern margin of the Himalayas (Indus-Tsangpo

Ophiolite-ITO) and the eastern margin of the Himalayas IMR. Structural relationships show that Indian-plate oceanic crust was overridden by units of the **West Burma Block (ANY INFORMATION ABOUT THESE? JUST A FEW NOTES ABOUT E.G., LITHOLOGY, TECTONIC SIGNIFICANCE ETC. WOULD BE USEFUL)** (e.g. Holt *et al*. 1991; Mitchell *et al*. 2007; Searle *et al*. 2007), although its age of formation and the timing of its obduction are poorly known. The Indo-Myanmar ophiolite belt separates subducted Indian-plate oceanic lithosphere to the west from a closely associated high-pressure metamorphic belt and Jurassic to Cretaceous magmatic arc–forearc complex of the Burmese plate to the east (Mitchell *et al*. 2012). The Naga Hills ophiolite is represented by peridotite, cumulate mafic-ultramafic, mafic volcanics, eclogite, glaucophane schist, amphibolite and late felsic intrusives. The ophiolite sequence has an east-dipping thrust contact with the underlying flysch-like sediments of the Disang and Barail Formations exposed to the west, and are overthrust from the east by continental metamorphic rocks of the Naga Metamorphics consisting of quartz mica-schist, garnet mica-schist, quartzite, and granitic gneiss (Brunnschweiler, 1966). The mid-Cretaceous, fossil-bearing Nimi Formation occurs at the contact between the ophiolite and the Naga Metamorphics (Chatterjee and Ghose, 2010). Within this belt, blueschist- and eclogite-facies mafic rocks (SOME INFORMATION ABOUT THESE ROCKS, ARE THESE MAFIC? CARBONATIC?) occur as tectonic slices (or detached layers and lenses) intercalated with unmetamorphosed **(MAYBE YOU SHOULD explicitly mention THIS, OTHERWISE IT MIGHT SOUND A LITTLE BIT ODD, SINCE ALSO BLUESCHISTS AND ECLOGITES ARE MAFIC ROCKS, DONE)** mafic and ultramafic units. Basement lithologies underlie Palaeogene sediments in the ophiolite belt, although their geological history and lithological constitution are uncertain (Acharyya 2015). Ophiolitic rocks within the Indo-Myanmar belt have been subdivided into two parallel groups: the **(I AM NOT SURE THEY DISPLAYED IN FIG.**

1, AS I THINK THEY SHOULD) 'Eastern' and 'Western' belts (Mitchell 1993), although both show similar structural and petrological characteristics. Accretion of the Eastern Belt, which contains metamorphosed ultramafic rocks in northern Myanmar that host world-famous jadeitites, is thought to have occurred sometime after the Mesozoic (Gansser 1980; Mitchell 1993; Shi *et al*. 2008). The Western Belt along the Naga and Manipur hills, which forms part of the Indo-Myanmar Range, formed due to collision between India and the Burmese microplate during the late Oligocene (Sengupta *et al*. 1990).

There is still controversy about emplacement ages of ophiolites in these two belts: the 'Eastern Belt' is inferred to mark the locus of the subduction zone into which the ophiolites were accreted since Mesozoic, whilst the 'Western Belt' was inferred to have been caused by a late Oligocene terminal collision between the Indian and the Burmese continental blocks (Shit et al., 2014 and references therein). In the 'Western Belt' a combination of radiolarian biostratigraphy and whole-rock K–Ar geochronology suggests an Upper Jurassic age (Kimmeridgian–Lower Tithonian) for marine sedimentation and volcanism in the (**YOU DID NOT MENTION WHETHER THIS BELONGS TO WESTERN OR EASTERN BELT** DONE – NOW MENTIONED AT THE START OF THE SENTENCE**)** Nagaland ophiolite belt (Sarkar *et al*. 1996; Baxter *et al*. 2011). The mid-Cretaceous, fossiliferous Nimi Formation occurs at the contact between the ophiolite and the Naga metamorphic units, and so gives a maximum age constraint on the initiation of obduction. Recently, Singh et al. (2017) reported U–Pb zircon ages ranging between 116 and 119 Ma from the plagiogranite **(YOU DID NOT MENTION THE OPHIOLITE SEQUENCE EARLIER, THIS IS THE FIRST TIME ONE READ ABOUT THIS PLAGIOGRANITE UNITS? WHICH I THINK IT IS NOT A GOOD IDEA. MAYBE YOU MIGHT WANT TO INCLUDE FEW NOTES ABOUT THE STRUCTURE OF THE NAGALAND OPHIOLITE BEFORE THIS DESCRIPTION OF THE AVAILABLE GEOCHRONOLOGICAL**

DATA? DONE**)** of the studied ophiolite. In the 'Eastern Belt' falling in the Mynamar Shi *et al*. (2008) reported a sensitive high-resolution ion microprobe (SHRIMP) U–Pb zircon age of 146.5 ± 3.4 Ma ~~from~~ for jadeitites of the Jade Mines area, Myanmar, and ~~suggested~~ proposed that subduction may have begun during the Late Jurassic. Mitchell (1993) suggested that the Manipur ophiolitic nappe was emplaced along the Indo-Myanmar ranges during the Mid-Eocene and was followed by a switch to east-dipping subduction from the mid-Miocene onwards. Recently, Liu *et al*. (2016) reported a c. 125 Ma U–Pb zircon crystallisation age for rodingite associated with formation of the ophiolite, and a c. 115 Ma age ~~from~~ **for** garnet amphibolites ~~that may date metamorphism~~ within the Kalaymo ophiolite belt, which lies adjacent to the Indo-Myanmar ophiolite belt. Shi et al. (2014) reported superimposed tectono-metamorphic ages **(NOT SURE ABOUT BY THESE SUPERIMPOSED TECTONOMETAMORPHIC AGES, MAYBE YOU SHOULD ELUCIDATE A LITTLE,** we are reporting the ages as interpreted by Shi et al., 2014 and cannot elucidate any further than the conclusions provided in that work**)** of phengitic mica Ar-Ar ages from blueschist-facies rocks in the Tagaung-Myitkyina Belt. They interpreted a Jurassic age (152.4 ± 1.5 Ma) obtained from glaucophane (**DID YOU MENTION THAT THEY DATED PHENGITIC MICA,** they have analysed both the phengite and glaucophane**)** as the lower limit of the subduction age and suggested that Eocene (45.0 ± 1.3 Ma) (OBTAINED IN WHAT KIND OR MINERAL PHASE, DONE**)** ages recorded an intra-continental shearing deformation event.

Chatterjee and Ghose (2010) documented eclogite- and blueschist-facies **(AGAIN ANY INFORMATION ABOUT THE LITHO-TYPE,** DONE**)** rocks present as thrust slices and lenses within the volcanic and ultramafic rocks of the Naga ophiolite belt ~~complexes~~ **(IS THIS THE SAME AS NAGALAND OPHIOLITE BELT? PLEASE NOTE THAT EVEN THOUGH THIS MIGHT SOUND ABSOLUTELY OBVIOUS TO**

YOU, THIS IS NOT THE CASE FOR A READER WHO IS NOT FAMILIAR WITH THE LOCAL GEOLOGY (AS I AM), TO WHICH ALL THESE FOREIGN NAMES SOUND NEW AND POSSIBLY CONFUSING, DONE**).** Ao and Bhowmik (2014) deduced the thermal history of the eclogite and blueschist rocks ranging from ~~11.5 kbar~~ 1.15 GPa and ~340 °C to ~~6 kbar~~ 0.6 GPa and 335 °C. Despite an improved understanding of the tectonic evolution of the Indian ophiolite belt, a paucity of reliable geochronological age data **(I AM NOT SURE ABOUT THIS IS EVIDENT FROM WHAT YOU REPORTED ABOVE, YOU MENTION NUMEROUS AGE DATA, WHICH MIGHT SOUND PERFECTLY RELIABLE IF YOU DO NOT EXPLAIN WHY DO NOT CONSIDER THEM SO. MAY BE YOU MIGHT ADD SOME MORE SPECIFIC COMMENTS ABOUT THIS, EXPLAINING WHY THE DATA IS AT LEAST QUESTIONALBE. I AM SURE THIS WILL HELP THE READER (ESPECIALLY THE non-expert ONE) TO UNDERSTAND WHAT IS THE POINT OF STRENGTH OF YOUR NOVEL APPROACH TO SUCH TOPICS,** DONE**)** has hindered the correlation of sutures and collisional deformation episodes within the region (**AGAIN I AM AFRAID THAT IF YOU DO NOT PROVIDE SOME ADDITIONAL DETAILS (POSSIBLE WITH SOME EXAMPLES), IT IS NOT COMPLETELY CLEAR WHAT ARE THE PROBLEMS HERE. PLEASE NOTE THAT IS A RATHER GENERAL STATEMENT THAT MIGHT APPLY VIRTUALLY TO ANY CASE STUDY. SO I WARMLY INVITE YOU TO INCLUDE SOME ADDITIONAL DETAIL. I AM NOT SAYING YOU SHOULD MAKE A THOROUGH REVIEW ABOUT THESE ISSUES BUT SIMPLY ADD SOME INFORMATION ABOUT E.G., THE MOST PROBLEMATIC POINTS OF DEBATE THAT MIGHT BENEFIT FROM THE RESULTS OF YOUR WORK)**

3. Analytical methods

The eclogites and blueschists rocks of Naga Hills occur as NE–SW to N–S oriented, steeply east-dipping shear fault-bound tectonic slices or detached layers and lenses intercalated with basaltic and ultramafic units parallel to the shear faults in the Naga Hills ophiolite of Phek district, Nagaland (Chatterjee and Ghose, 2010). In the area eclogite constitutes the core of some lenses, which are surrounded by successive layers of garnet-blueschist, glaucophanite and greenschist. Twenty metamorphosed samples were collected between Longkhimong and Moya villages, after systematic petrographic study six samples were selected for detailed study. Mineral compositional data for all samples (**YOU NEVER DESCRIBED THESE EARLIER IN THE TEXT. I THINK IT WOULD BE BETTER TO FIRST EXPLAIN WHAT KIND OF SAMPLES WERE INVESTIGATED, AND THEN HOW. MAYBE YOU CAN ADD SOME NOTES ABOUT THE SAMPLING ACTIVITIES, INCLUDING LOCATIONS, STRATIGRAPHIC POSITIONS, LITHOTYPES, NUMBER OF COLLECTED SAMPLES ETC.** DONE**)** were obtained on a JEOL JXA-8200 electron microprobe housed at the Institute of Geosciences, Johannes-Gutenberg University of Mainz, Germany. Operating conditions included an acceleration voltage of 15 kV, a beam current of 12 nA, and a 2 μm spot size. A matrix correction for atomic number (Z), absorption (A), and fluorescence (F) was automatically applied to all analyses. For the data presented below, mineral compositions were recalculated to standard numbers of oxygens per formula unit (pfu) using the software AX (Holland 2009), with OH assumed to be present in stoichiometric amounts. The proportion of ferric iron in different mineral species was also calculated using ~~the software~~ AX ~~(Holland 2009)~~. Mineral proportions for each sample were determined using the software JmicroVision (Roduit 2010), with each individual count consisting of five hundred points randomly distributed over a digitally scanned thin-section image. Calculated volume proportions (**HOW HAVE THIS BEEN CALCULATED? I THINK YOU SHOULD SPECIFY THIS, ALSO CONSIDERING**

THAT YOU DID NOT JUST MAKE A MODAL BY SIMPLE POINT COUNTING. THEREFORE, I THINK IT IS ABLUTELY NEVESSARY TO EXPLAIN HOW DID YOU MAKE THIS KIND OF CALCULATION) of minerals in each sample are given below. These bulk compositions are given in Supplementary Table 3. ~~Mineral proportions for each sample were determined using the software JmicroVision (Roduit 2010), with each individual count consisting of five hundred points randomly distributed over a digitally scanned thin-section image.~~ Mineral abbreviations are after Kretz (1983). Representative **(WHY ONLY SOME REPRESENTATIVES? YOU CAN INCLUDE ALL YOUR DATASET IN THE ESM** – we believe that providing all data in electronic appendices offers no significant benefit from providing representative examples. This is our preferred style for data presentation and indeed it is commonplace in petrological studies to only show representative examples.**)** compositions of major minerals for all samples are given in Supplementary Table 2 and photomicrographs of microstructural features and assemblages are shown in Figures 2 and 3.

Bulk-rock compositions for use in petrological modelling were obtained from X-ray fluorescence (XRF) via the production of glass ~~pellets~~ beads **(IS THIS CORRECT? TO MY KNOWLEDGE, YOU CAN HAVE "PRESSED POWDER PELLETS", BUT FUSED SAMPLES ARE REFERRED TO AS 'GLASS BEADS' PLEASE CHECK** DONE**)** in order to guarantee standardised and reproducible analyses. Powdered rock samples were initially dried overnight at 105 °C. Approximately 5.2 g of lithium tetraborate ($Li_2B_4O_7$) flux and 0.4 g of powdered rock sample were then weighed, homogenized, and melted in a Vulcan AMA melting device to produce each glass ~~pellet~~ beads **(HERE AND IN THE FOLLOWING: AS IN THE PREVIOUS COMMENT, PLEASE CHECK IF 'PELLET' IS APPROPRIATE)**. These ~~pellets~~ beads were then analyzed in a Philips MagXPRO spectrometer with a rhenium X-ray tube housed in the Institute of Geoscience, Johannes

Gutenberg University of Mainz, Germany. Detection limits are estimated to be 100 µg g^{-1} for light elements (Na, Mg, Al) and 10 µg g^{-1} for heavy elements (K to U). Analysed major oxides comprised SiO_2, Al_2O_3, total Fe_2O_3, MnO, MgO, CaO, Na_2O, K_2O, TiO_2, P_2O_5, SO_3, Cr_2O_3, and NiO.

All U–Pb ages for the analysed carbonate grains and silicate phases were acquired *in situ* from polished thin sections by laser ablation-inductively coupled plasma-mass spectrometry (LA-ICP-MS) at the Goethe University Frankfurt (GUF), using a Element2 (Thermo-Scientific) sector field ICP-MS coupled to a RESOlution ArF Excimer laser (Compex Pro 102). The applied method was similar as described in Ring and Gerdes (2016), Burisch *et al*. (2017), Hansman *et al*. (2018) and Salih *et al*. (2019). Ablation spot size was 213 µm and crater depth was ~20 µm. Samples were screened by LA-ICP-MS for suitable Pb and U concentration and variability, and selected spots were subsequently analysed in fully automated mode. Spot analyses consisted of 20 s background acquisition followed by 20 s sample ablation. Surface contamination was removed prior to each spot analysis via a 3-s pre-ablation. Soda-lime glass SRM-NIST 614 was used as a reference material together with two carbonate reference materials – WC-1 and a Zechstein dolomite – to bracket sample analysis. SRM-NIST 614 yielded a depth penetration of about 0.5 µm s^{-1} and an average sensitivity of 280,000 cps/µg g^{-1} for ^{238}U. The detection limits for ^{206}Pb and ^{238}U were ~0.1 and 0.05 ng g^{-1}, respectively. All data were corrected using an MS Excel spreadsheet program (Gerdes and Zeh, 2006, 2009). NIST 614 was used as a standard for the analysis of silicate phases (**SO YOU ANALYSED SILICATE PHASES ALSO? THIS IS NOT WHAT IS REPORTED IN THE ABSTRACT. PLEASE ELUCIDATE,** DONE**)**. The possible offset related to sample matrix is within the analytical uncertainty of the quoted ages.

The $^{207}Pb/^{206}Pb$ ratio was corrected for mass bias (0.3%) and the $^{206}Pb/^{238}U$ ratio for inter-element fraction (ca. 5%) using SRM-NIST 614. An additional correction of 4% was

applied on the $^{206}Pb/^{238}U$ to correct for difference in the fractionation due to the carbonate matrix. This resulted in a lower intercept age of 23 WC-1 spot analyses of 254.1 ± 1.5 (MSWD = 1.5; anchored at $^{207}Pb/^{206}Pb$ of 0.851) and 253.9 ± 3.4 (MSWD = 1.5; n = 17) for the Zechstein dolomite used as an in-house reference material in Frankfurt. Data were plotted on a Tera-Wasserburg diagram and ages calculated as lower intercepts using Isoplot 3.71 (Ludwig 2007). All uncertainties are reported at the 2 sigma level.

According to Rasbury and Cole (2009), a linear regression taken through a group of samples from the same system produces a slope from which an age can be calculated using the accepted decay rate for the parent isotope. If the system being analysed has no initial heterogeneity, and it remained closed throughout the duration of the decay process, all scatter of data points about the isochron can be explained by analytical uncertainties. ~~A statistical test of this is the mean squared weighted deviate (MSWD).~~ Closed isotopic systems will plot as a line, giving a precise age and low **mean squared weighted deviate (MSWD) of** ~1, while systems that have not remained closed will show scatter and have a high MSWD (>>1).

4. Sample petrology

Out of the twenty collected samples we have selected four metabasite samples for systematic study and ~~well constrained P-T conditions could derived from four samples only~~thermobarometry Six metabasite samples were collected from (**AS SAID IN A PREVIOUS COMMENT, I THINK THAT GENERAL INFORMATION ABOUT THE INVESTIGATE SAMPLES SHOULD BE REPORTED IN THE TEXT. ALSO YOU SAY THAT YOU COLLECTED 6 SAMPLES, BUT IN THE FOLLOWING SECTION IT SEEMS TO ME THAT YOU ARE DESCRIBING ONLY 4 OF THEM: THE UNSHEARED N5 AND 14 AND THE SHEARED 7C AND 11. PLEASE ELUCIDATE)** ~~around Moya and Longkhimong (Fig. 1C) to place constraints on the metamorphic and~~

~~deformational history of the Nagaland ophiolite belt.~~ Locality information and GPS co-ordinates for each outcrop are given in Supplementary Table 1 and location map is presented in Figure 1C. Field photographs of the studied samples are presented in Figure 1D. The samples occur as meter-sized boulder blocks, which occur individually and in clusters (Fig. 1 D1, D3) within serpentinites. Samples are thus classified as either sheared ~~and~~ or unsheared based on the occurrence of key deformational features present at the field, hand sample, and microscopic scale. Samples N5 and 14 lack evidence of post-peak shear-driven recrystallization and likely represent relics of undeformed, peak metamorphic blueschists. By contrast, samples 7c, 13, 3b, and 11 are strongly sheared and represent subsequently deformed equivalents of these older units.

4.1. Sample description

4.1.1. Unsheared samples N5 and 14

Unsheared samples N5 and 14 exhibit a largely unfoliated microstructure and show no evidence of pervasive retrogression following peak blueschist-facies metamorphism during subduction, though localised retrogression does occur. Sample N5 is a blueschist that contains abundant sodic amphibole (38%) and epidote (37%), with minor quartz (9%), garnet (6%), sodic–calcic amphibole (4%), phengite (3%), and rutile (2%). Accessory pyrite, zircon, and apatite ~~(all <<1%)~~ also occur. Garnet porphyroblasts are between 0.5 and 2 mm in diameter (Figures 2a–b) and exhibit no substantial major element compositional zoning, with core compositions of $Alm_{56–58}Prp_{12–14}Grs_{21–22}Sps_{7–8}$ and rim compositions of $Alm_{60–61}Prp_{15–16}Grs_{22–23}Sps_{3–4}$ (Supplementary Table 2 and Fig. 4). Core regions contain inclusions of pumpellyite, phengite, epidote, barroisite, actinolite, and quartz, and rims contain inclusions of phengite, epidote, actinolite, rutile, and quartz. Some grains show replacement by chlorite at their outermost rims. Matrix phengite ~~contains~~ has Si = 3.34–3.38 pfu (on a 11 O basis;

Supplementary Table 2) and grains included in the outer rims of garnet ~~contain~~ has Si = 3.32–3.35 pfu. Epidote shows no significant compositional zoning from core to rim, with a minor range in pistacite content ~~([~~XPs = $Fe^{3+}/(Al^{3+}+Fe^{3+})$~~])~~ of 0.18–0.21 (Supplementary Table 2). According to the classification scheme of Hawthorne *et al*. (2012), sodic and sodic-calcic amphiboles in the matrix are glaucophane and winchite–katophorite, respectively (Figure 5).

Sample 14 is modally dominated by epidote (50%) and quartz (35%), with lesser garnet (1%), sodic-calcic amphibole (10%), phengite (2%), rutile (0.5%), ~~sphene~~ titanite (0.5%), and carbonate (~~2~~1%) (**BASED ON SUCH MINERALOGY, HOW CAN YOU CONSIDER THIS TO BE A BLUESCHIST (METABASIC) ROCK? ALSO PLEASE NOTE THAT SUM OF THE LISTED MINERALS IS 101%** We follow the definition of Ernst (1963) in that a blueschist defined by the presence of the minerals glaucophane + (lawsonite or epidote) +/- jadeite +/- albite or chlorite +/- garnet +/- muscovite in a rock of roughly basaltic composition**)**. Accessory minerals include chlorite, apatite, and zircon (all <<1%). Although sample 14 ~~contains~~ **displays** no foliation, it is mildly anisotropic, with alternating centimetre-scale quartz- and epidote-rich domains. In contrast to the large porphyroblasts present in sample N5, garnet forms <0.1 mm diameter grains that are restricted to quartz-rich regions (Figure 2). These garnet grains have no inclusions and are compositionally homogeneous ($Alm_{36–39}Prp_{10–13}Grs_{31–36}Sps_{36–39}$) (**VERY DIFFERENT FROM SAMPLE N5, FURTHER HIGHLIGHTING THAT THIS CANNOT BE CONSIDERED SAME ROCK TYPE AS THE REPIUOS, IN MY OPINION** we do not consider this the same rock type. it is simply grouped here with 14 due to it being unsheared. the degree of deformation is the primary discriminator in this work.**)**. Epidote shows no significant zoning, with core and rim compositions both having similar pistacite contents of 0.20–0.24 (Supplementary Table 2). Matrix rutile is partially or fully replaced by titanite (Figure 2), though rare inclusions in sodic-calcic amphibole lack such pseudomorph textures.

Phengite contains Si = 3.34–3.35 pfu (~~for 11 oxygens;~~ Supplementary Table 2) and in places is intimately intergrown with chlorite, though the extremely fine-grained nature of these intergrowths prohibited reliable compositional analysis of either phase. Sodic-calcic amphibole in the matrix is barroisite–winchite–katophorite (Hawthorne *et al*. 2012; Figure 5), with rare tremolite**,** likely representing minor post-peak retrograde mineralogical transformation.

~~Most natural carbonate occurs in the form of calcite and can be transported to the Earth's interior via subduction of carbonate-rich sediments or metasomatized oceanic crust (Zhang *et al*. 2018). Calcite transforms to aragonite at high pressure. Although may revert back to calcite during exhumation if there are no kinetic limitations. At the *P–T* conditions of peak metamorphism for samples N5 and 14 (see below), the carbonate likely stabilised in the form of aragonite, whereas carbonate in sheared samples 11 and 7c is calcite, which indicates polymorphic transformation following exhumation from peak depths (**IN MY OPINION, THIS IS NOT APPROPRIATE FOR A SAMPLE DESCRIPTION SECTION LIKE THIS IS. I THINK IT SHOULD BE MOVED TO THE DISCUSSION SECTION. ALSO, I WOULD SUGGEST ADDING A FEW REFERENCES FOR THE GENERAL STATEMENT ABOUT CARBONATE MINERALS AND ON CALCITE/ARAGONITE TRANSITIONS AT THE BEIGINNING OF THIS PIECE OF TEXT.**) Analysed spots are presented in Supplementary Figure 5.~~

4.1.2. Sheared samples 11 and 7c

In contrast to N5 and 14, **(SO YOU THINK THAT SAMPLES N5 AND 14 ARE MINERALOGICALLY HOMOGENEOUS? I FRANKLY CANNOT AGREE WITH IT, SINCE ONE IS BASICALLY GLN+EP, THE OTHER IS EP+WTZ. I THINK YOU SHOULD CAREFULLY RE-CONSIDER THIS** The confusion here emanates from

poor wording, which we have corrected. We do not think that both samples are similar (mineralogically) or homogenous – just that they are unsheared. The text has been modified accordingly.) sheared samples 11 and 7c ~~are mineralogically heterogeneous,~~ contain~~ing~~ distinct spaced foliations that are truncated by carbonate- and quartz-filled veins. These crosscutting veins commonly form shear bands (Figures 3e–f) and locally deflect the main metamorphic foliations at their boundaries (Figure 3b), indicating that shearing and vein formation post-dated subduction metamorphism. The host rock domains in sample 7c are dominated by epidote (39%), calcic amphibole (32%), and sodic–calcic amphibole (18%), with minor phengite ~~muscovite~~ (4%), albite (2%), K-feldspar (2%), titanite (1%), and quartz (2%). Apatite and zircon occur as accessory phases (**PLEASE NOTE THAT SUM OF THE PHASES LISTED ABOVE IS ALREADY 100%** these are simply rounding issues and accessory phases, by definition, have very minor volumetric proportions. if we are to round the volume of the accessories to the nearest integer, they would have 0% volume anyway, leaving a total of 100%.). The main metamorphic foliation is defined by elongate and aligned crystals of epidote and amphibole (Figure 3a). Large green calcic amphibole is mostly pargasite with thin magnesiohornblende outer rims, and sodic-calcic amphibole is winchite (Figure 5). Matrix ~~muscovite~~ phengite has Si = 3.39–3.43 pfu and epidote cores have *X*Ps = 0.19–0.25 and rims have *X*Ps = 0.26–0.33 (Supplementary Table 2). Quartz- and carbonate -filled veins crosscut and offset this epidote- and amphibole-defined metamorphic foliation (Fig. 3b).

Sample 11 contains abundant sodic amphibole (33%), quartz (34%), carbonate (14%), and sodic pyroxene (11%), with subsidiary sodic–calcic amphibole (2%), ~~muscovite~~ phengite (1%), garnet (2%), and albite (1%). Accessory pyrite, titanite, apatite, and zircon (all <<1%) also occur. Alternating sodic amphibole (glaucophane) and quartz-rich bands define a spaced foliation that wraps around porphyroblasts of pyroxene and garnet (Figure 3c). Grains of the

latter are commonly less than 1 mm in diameter and are variably replaced by aggregates of carbonate, albite and/or quartz (Figure 3d). Though individual grains lack any significant major-element compositional zoning from core to rim, compositions vary significantly between grains; the majority are spessartine-rich ($Alm_{19–24}Prp_{10–14}Grs_{17–20}Sps_{45–51}$), while others are richer in almandine and grossular ($Alm_{26–29}Prp_{12}Grs_{23–32}Sps_{28–37}$). Minor sodic-calcic amphibole in the matrix is winchite, and sodic pyroxene porphyroblasts are compositionally classified as aegirine–augite (X_{Jd} = 0.04-0.23) **(GIVE JADEITITE COMPONENT)** (Morimoto *et al*. 1988).

5. Thermobarometry/Phase equilibria modelling (MAY BE A DIFFERENT NAME LIKE E.G., "PHASE EQUILIBRIA MODELLING" WOULD BE MORE APPROPRIATE, DONE)

Constraints on the *P–T* conditions of peak subduction-zone metamorphism were obtained from unsheared samples N5 and 14, whereas constraints on the *P–T* conditions of subsequent ductile shearing were obtained from **sheared** sample 7c (**WHAT ABOUT THE OTHER SHEARED SAMPLE 11? WHY YOU DID NOT USE THIS HERE? I THINK YOU SHOULD ADD SOME EXPLAINATION**). Preliminary investigation of phase equilibria stability in sample 11 did not allow for reliable thermobarometry to be performed due to the high variance of the interpreted peak mineral assemblage. Phase diagrams showing the *P–T* conditions over which equilibrium mineral assemblages are calculated to occur in a specific bulk-rock composition (pseudosections) (**SINCE YOU ARE USING BULK ROCK COMPOSITIONS HERE I THINK YOU SHOULD ADD A SECTION ABOVE IN WHICH ROCK COMPOSITIONS ARE PRESENTED AND DESCRIBED, AT LEAST A LITTLE BIT. THIS IS NECESSARY ALSO TO UNDERSTAND WHY DID YOU CHOOSE THAT SPECIFIC MODEL SYSTEM.** This is unnecessary – the petrological

modelling community has well-defined compositional systems for use in modelling particular protoliths (e.g. metabasalts). These are constrained by the available a-x relations rather than the mineralogy of the rocks themselves.) were constructed using THERMOCALC v3.40i and the internally consistent thermodynamic data set ds55 (Powell and Holland 1988; Holland and Powell 1998; updated to August 2004) in the Na_2O–CaO–K_2O–FeO–MgO–Al_2O_3–SiO_2–H_2O–TiO_2–O (NCKFMASHTO) compositional system. The following activity–composition relations for solid-solution phases were used: clinoamphibole (**WHAT IS THE SOURCE FOR THIS**) (calcic, sodic-calcic, and sodic amphibole; Diener and Powell 2012), clinopyroxene (diopside and omphacite, Diener and Powell 2012), muscovite and paragonite (Coggon and Holland 2002), talc and epidote (Holland and Powell 1998), chlorite (Holland *et al*. 1998), biotite and garnet (White *et al*. 2007), plagioclase and K-feldspar (Holland and Powell 2003), ilmenite and hematite (White *et al*. 2000). Albite, lawsonite, rutile, titanite, quartz, kyanite, and H_2O were treated as pure phases.

5.1. Metamorphic mineral equilibria modelling parameters

Bulk-rock compositions used for modelling were obtained via XRF analysis, as discussed previously (Supplementary Table 2) (**THIS IS GETTING TORTOUS. IN THE ANALYTICAL TECHNIQUES SECTIONS YOU SAID YOU ACTUALLY DETERMINED BULK ROCK COMPOSITIONS VIS XRF ANALYSES. SO WHY YOU DID NOT USE THEM? NOT EVEN MENTIONING THAT IN THE 'ANALYTICAL METHOD' SECTION YOU EXPLICITLY REPORTED THAT 'BULK-ROCK' COMPOSITION FOR USE IN PETROLOGICAL MODELLING WERE OBTAINED FROM X-RAY FLOURESCENCE (XRF)' (LINES 168-169). IN ADDITION, YOU REFER TO SOME SORT OF CALCULATION FOR OBTAINING MINERAL ABUNDANCES, SO I AM WONDERING IF THE 'MINERAL PROPORTIONS' INDICATED HERE ARE ACTUALLY MODAL PROPORTIONS**

(I.E., DETERMINED DIRECTLY, VIA POINT COUTING) OR RATHER WERE CALCULATED IN SOME SORT OF WAY (WHICH NEEDS TO BE SPECIFIED). PLEASE CAREFULLY ELUCIDATE ALL THIS. AFTER GOING THROUGH THE MANUSCRIPT, I'VE NOTICED THAT THE RESULTS OF XRF ANALYSES ARE NEVER EVEN REPORTED IN THE ELECTRONIC APPENDIX. ALL THIS IS DEFINITELY NEEDS TO BE CLARIFID – this was an unfortunate typo; we apologize for the confusion. XRF data were used.). ~~These bulk compositions are given in Supplementary Table 3. Mineral proportions for each sample were determined using the software JMicroVision (**SO FINALLY, THE MODAL PROPORTIONS TURN OUT TO BE DETERMINED (NOT CALCULATED) VIA POINT COUNTING. I THINK THIS SHOULD BE SAID MUCH EARLIER, IN THE ANALYTICAL TECHNIQUES SECTION.**) (Roduit 2010), with each individual count consisting of five hundred points (**ARE YOU SURE THESE ARE SUFFICIENT? TO MY KNOWLEDGE, YOU NEED TO HAVE MUCH MORE OINTS (3-4 THOUSANDS) IN ORDER TO CONSIDER YOUR MODAL ANALYSIS STATISTISCALLY RELIABLE**.) randomly distributed over a digitally scanned thin-section image~~ **(NOT CLEAR TO ME: IS THIS IMAGE COVERING THE ENTIRE THIN SECTION AREA, OR JUST A PART OF IT? I GUESS (AND HOPE) THE SECOND, BUT MAY BE IT WOULD BE USEFUL TO EXPLICITLY MENTION THIS** – point counting was applied to the entire thin section image, aside from areas that do not actually contain pieces of the rock (e.g. as it is not a perfect rectangle). 500 points were sufficient in this case, as we kept track of the evolving proportions during analyses and the values converged on final results after ~300 points or so; thus, adding an extra 500 or 1000 points onto this initial 500 will produce no better precision.). For sample 7c, areas adjacent to shear bands were excluded from consideration

during point counting such that the proportions obtained represent unsheared portions of the sample that equilibrated prior to deformation.

~~Although Schmidt and Poli (1998) suggest that seafloor-hydrated metabasites can contain up to 5–6 wt.% H_2O, prograde metamorphism during subduction results in the breakdown of hydrous phases such as chlorite, epidote, and amphibole, leading to progressive dehydration and fluid loss from the local environment (e.g. Guiraud *et al.*, 2007, Hernandez-Uribe *et al.*, 2020)~~ **(THIS IS COMMON KNOWLEDGE. I DO NOT THINK IT IS NECESSARY TO REPORT IT. MOREOVER, I DO NOT THINK IT APPROPRIATE IN THIS SECTION, WHERE I EXPECT TO SEE ONLY INFORMATION ABOUT HOW YOU PERFORMED YOUR MODELS - deleted**). The ~~effective~~ fluid contents ~~of~~ for each bulk rock composition during metamorphism were calculated using the proportions of hydrous phases present in each equilibrium mineral assemblage, assuming H_2O was present in stoichiometric amounts. Mixed-component fluids were not considered due to the lack of reliable a-x relations for C–O–H fluids at elevated pressures (**NOT SURE ABOUT WHAT YOU MEAN WITH THIS. WHAT ARE THESE 'RELIABLE C-O-H FLUIDS' THAT LACK AT ELEVANTED PRESSURES? DO YOU MEAN MODELS FOR SUCH KIND OF FLUIDS" PLEASE ELUCIDATE**. done); nonetheless, however, this should not have any significant effects on our calculated diagrams, as unsheared sample N5 does not contain carbonate, unsheared sample 14 contains only a minor proportion (2.2 vol. %), and carbonate veins in sheared sample 7c are interpreted from microstructural constraints to post-date final metamorphism and textural equilibration. Pressure uncertainties for assemblage field boundaries are approximately ~~±1 kbar~~ 0.1 GPa (Powell and Holland 2008; Palin *et al*. 2016). ~~Calculated *P–T* pseudosections for each sample are given below.~~

5.1.1. Unsheared samples

~~The range of mineral parageneses and microstructural features in each sample allows *P–T* constraints to be placed on peak metamorphism and exhumation-related ductile shearing.~~ Calculated mineral assemblages matching those observed in unsheared samples N5 and 14 (**I THINK IT WOULD BE MUCH BATTER IF YOU PRESENT THE RESULTS FOR THESE TWO SAMPLES SEPARATELY. THEN YOU SHOULD PROPOSE A SINGLE P-T RANGE BY COMPRAING THEM AND SEE WHERE THE BEST MATCHES FOR BOTH SAMPLES OVERLAP**. We disagree – we are grouping samples together according to whether they are sheared or unsheared.) constrain peak *P–T* conditions of subduction-zone metamorphism to ~1.8–2.0 GPa and ~420–560 °C, with the calculated proportions and compositions of major minerals best matching (**THIS IS A VERY VAGUE CONCEPT. I MEAN, HOW DO YOU EVALUATE WHICH ONE IS THE BEST MATCH? GENERALLY SPEAKING, I GUESS YOU CAN SAY THIS IS THE ONE MINIMIZING THE DIFFERENCES BETWEEN THE OBSERVED AND CALCULATED MINERAL ABUNDANCES, BUT MAY BE THIS CAN DONE IN SOME OTHER WAY LIKE, E.G., MINIMIZING THE SQUARED RESIDUALS OF THE DIFFERENCES, OR MAY BE EVEN IN SOME OTHER WAYS. IN ANY CASE I THINK YOU SHOULD EXPLICITLY REPORT WHAT WAS YOUR STRATEGY, ALONG WITH ALL THE OTHER INFORMATION WHICH CAN HELP THE READER FIGURING OUT WHAT WAS DONE**.) observed values at ~1.9 GPa and ~480–520 °C. These conditions lie along the global range of *P–T* conditions predicted to occur at the surface of subducted oceanic crust in modern-day subduction zones (Syracuse *et al*. 2010; Penniston-Dorland *et al*. 2015).

5.1.2. Sheared sample **(STILL WONDERING WHY SAMPLE 11 WAS NOT USED FOR SUCH MODELS)** Preliminary inspection did not reveal it to be useful or

thermobarometry – not all rocks are useful, and this is a trial and error procedure that cannot be easily predicted ahead of time.

In contrast with the undeformed samples, the observed mineral assemblage in sample 7c was calculated to be stable at the notably lower pressure and slightly lower temperature conditions of ~0.2–0.6 GPa and ~420–490 °C, with observed and calculated mineral proportions and compositions matching best at ~0.6 GPa and ~470 °C. ~~These *P*–*T* conditions are far-removed from the slab-top range for modern-day subduction reported by Syracuse *et al.* (2010). The calculated pressures of ~1.9 GPa for peak metamorphism and ~0.6 GPa for retrograde equilibration are approximately equivalent to depths of 60 km and 15 km, respectively, assuming no significant tectonic overpressure~~ **(MAY BE THIS IS MORE APPROPRIATE IN THE DISCUSSION SECTION. HERE YOU SHOULD SIMPLY PRESENT THE RESULTS OF YOUR MODEL. ALSO NOTE THAT THES DEPTH ESTIMATES REFER NOT ONLY TO THE SHEARED SAMPLES, THE SUBJECT OF THIS PARAGRAPH BUT ALSO TO THE UNSHEARED ONES, THE SUBJECT OF THE PREVIOUS PARAGRAPH (I.E., SO WHY NOT REPORTING DEPTH ESTIMATES IN THE FORMER PARAGRAPH FOR THESE LATTER ONES?)**. Semi-independent constraints on *P*–*T* conditions using the avPT function of THERMOCALC (**MAYBE YOU SHOULD EXPLAIN A LITTLE BIT WHAT IS THIS, SO THAT READERS THAT ARE NOT FAMILIAR WITH ALL THE OPTIONS OF THE THERMOCALC SOFTWARE CAN UNDERSTAND WHAT IS THIS FUNCTION AND WHY IT COULD BE USED TO TEST THE RESULTS FROM PSEUDOSECTION. JUST A FEW BRIEF NOTES COULD BE SIFFICIENT. AS FAR AS I KNOW, THIS SHOULD BE FOR MULTIPLE-REACTION THERMOBAROMTRY, BUT I HAVE TO SAY THAT I AM NOT SURE YOU CAN CONSTRAIN BOTH P AND T WITH THE SAME MODEL. HOW ABOUT CONSTRAINING P AND T**

INDEPENDENTLY, USING TWO DIFFERENT MODELS BASED ON MULTIPLE REACTION EQUILIBRIA? TO MY KNOWLEDGE, THERMOCALC SHOULD HAVE ALSO AVP AND AVT FUNCTIONS, EXACTLY FOR SUCH PURPOSES. The avPT function is well known in metamorphic petrology community and is well documented in the source papers. We find the reviewer's comments inconsistent, whereby they ask us to remove some descriptions for being too obvious, but ask other descriptions to be added for things that we also perceive as being 'obvious'.) for each sample produced similar and statistically robust results of 2.05 ± 0.22 GPa and 489 ± 39 °C for N5, 1.95 ± 0.18 GPa and 541 ± 34 °C for 14, and 0.60 ± 0.23 GPa and 464 ± 76 °C for 7c (Supplementary Table 4) **(SEE/ HERE YOU REPORT VALUES FOR SAMPLE N5 AND VALUES FOR SAMPLE 14 SEPERATELY. SO WHY NOT PRESENTING PSEUDOSECTION RESULTS FOR THE TWO SAMPLES SEPERATELY ALSO (AS ASKED IN A PREVIOUS COMMENT)?)** See previous note of grouping samples according to their deformation history., corroborating the results obtained by phase diagram modelling.

6. U–Pb geochronology

U–Pb isotopic analysis of carbonate grains was carried out on metabasite samples 14 (unsheared), 11 (sheared), 3b and 13 (**SO ARE THESE THE MISSING TWO SHEARED SAMPLES? I THINK THESE SHOULD BE TREATED EXACTLY AS THE OTHER SAMPLES (I.E., REPORT PETROGRAPHY, MINERAL CHEMISTRY, WHOLE ROCK COMPOSITION AND PERFORM THERMOBAROMETRIC MODELS), UNLESS, FOR SOME REASON THIS CANNOT BE DONE. BUT IN THIS LATTER INSTANCE, YOU SHOULD GIVE FULL EXPLAINATION ABOUT THIS**), which equilibrated at different stages of the subduction–exhumation cycle. Carbonate crystals within dynamically recrystallised veins were preferentially selected for analyses; however, suitable matrix minerals were also investigated in order to perform a check on the analysed

carbonates, which generally have a low U content. Results of the isotopic composition of the Nagaland blueschists are presented in Supplementary Table 5 and isochrons are shown in Figure 9. Measured $^{207}Pb/^{206}Pb$ ratios range from 0.205 to 0.836 (sample 3b), 0.735 to 0.848 (sample 13), 0.776 to 0.845 (sample 11) and 0.809 to 0.846 (sample 14), and measured $^{238}U/^{206}Pb$ ratios range from 0.361 to 9.752 (sample 3b), 0.043 to 10.53 (sample 13), 0.118 to 5.474 (sample 11) and 0.809 to 0.846 (sample 14)~~, as shown in Figs. 9a, b, c and d~~. All data for each sample lie on a single array on an isochron diagram, indicating that each attained isotopic equilibrium, and give well-defined least squares fit indices with MSWD values of 0.35–1.17 (Figure 9). The U concentrations in the minerals range between 0 and 3 ppb and model Th/U ratios show a wide variation, with most lying between 0.015 and 5, but some reaching up to ~46. ~~Results of the isotopic composition of the Nagaland blueschists are presented in Supplementary Table 5 and isochrons are shown in Fig. 9.~~ These analyses show that unsheared samples 14 and 11 equilibrated at 95.3 ± 5.9 Ma and 93.7 ± 4.0 Ma, respectively, and sheared samples 3b and 13 experienced exhumation-related shear deformation at 90.6 ± 3.4 Ma and 88.8 ± 2.7 Ma, respectively. Although the unsheared sample dataset is within uncertainty of all the sheared sample dates, an overall age progression may be reconstructed from the sheared and unsheared samples. Considering the well-behaved dataset in the studied samples with a low MSWD, it can be broadly inferred that the analysed phases had the same initial isotopic ratio and that the system was at equilibrium during closure of the isotopic system.

7. Discussion and implications

Most natural carbonate occurs in the form of calcite and can be transported to the Earth's interior via subduction of carbonate-rich sediments or metasomatized oceanic crust (Zhang *et al*. 2018). Calcite transforms to aragonite at high pressure. Although may revert back to calcite during exhumation if there are no kinetic limitations. At the *P–T* conditions of peak

metamorphism for samples N5 and 14, the carbonate likely stabilised in the form of aragonite, whereas carbonate in sheared samples 11 and 7c is calcite, which indicates polymorphic transformation following exhumation from peak depths. Representative BSE images showing the analysed spots are presented in Figure 10.

The tectonothermal evolution of the Indo-Myanmar Tethyan ophiolite belt is poorly understood owing to a lack of integrated thermobarometry and geochronology. Here, we have combined microstructurally constrained U–Pb data with *P–T* conditions calculated for peak and retrograde metamorphism in order to constrain the exhumation history of the Nagaland region of this ophiolite complex (Figure ~~10~~11). The ~~samples documented~~ investigated samples show considerable microstructural variation, ranging from largely undeformed (N5 and 14) to sheared (11, 3b, 7c, and 13). The contrasting textures and ages of the studied rocks, together with reported metamorphic recrystallizations ages in the adjoining ophiolite belts in Myanmar (Shi *et al*. 2008; Yui *et al.* 2013; Liu *et al*. 2016) suggest that the terrain has undergone several metamorphic events. In terms of texture, the blueschist facies rocks (N5 and 14) do not show any obvious preferred orientation ~~**The almost intact crystal shapes of the constituent minerals (Fig. 2a) allow us to suggest**~~ that they were formed predominantly under near-hydrostatic conditions, without apparent shear deformation. By contrast, the sheared samples record deformation and post-tectonic (annealing) recrystallization, **as**~~,~~ the constituent minerals display preferred orientation, bending, and curving.

Mineral assemblages in the unsheared samples N5 and 14 constrain peak *P–T* conditions of subduction-zone metamorphism to ~1.8–2.0 GPa and ~420–560 °C, with the calculated proportions and compositions of major minerals matching observed values at ~1.9 GPa and ~480–520 °C (Figure 6) (**I THINK YOU CAN SIMPLY CONCLUDE THAT THE ESTIMATED P-T CONDITIONS ARE THOSE OF THE BEST-MATCH**

ASSEMBLAGES, THERE IS NEED TO REPEAT AGAIN WHAT IS THE TOTAL RANGE FOR THE PEAK ASSEMBLAGE, YOU ALREADY DISCUSSED THIS IN THE PREVIOUS SECTION. I THINK YOU SHOULD REPORT THIS TIGHTER RANGE ALSO IN THE OTHER SECTION OF THE PAPER (E.G., ABSTRACT, CONCLUSIONS) WHERE YOU MENTION THE RESULTS OF YOUR MODELS Done).

By contrast, the observed mineral assemblage in sheared (sample 7c) was calculated to be stable at notably lower *P–T* conditions of ~0.2–0.6 GPa and ~420–490 °C, with observed and calculated mineral proportions and compositions matching best at ~0.6 GPa and ~470 °C (AS **FOR THE PREVIOUS: YOU CAN SIMPLY REPORT 0.6 GPA AND 470°C** Done). The calculated peak metamorphic conditions for the unsheared samples agree with *P–T* conditions previously reported for the area (Chatterjee and Ghose 2010). The *P–T* conditions are far-removed from the slab-top range for modern-day subduction reported by Syracuse *et al*. (2010). The calculated pressures of ~1.9 GPa for peak metamorphism and ~0.6 GPa for retrograde equilibration are approximately equivalent to depths of 60 km and 15 km, respectively, assuming no significant tectonic overpressure. In Figure 10, the ***P–T*** path calculated here is compared with published examples for other blueschist samples from the Naga ophiolites (**NO COMMENT ON THESE? THEY TOOK PRETTY DIFFERENT FROM YOURS (ESPECIALLY THE ONE LABELLED AB14), MAYBE YOU CAN TRY TO PROPOSE SOME EXPLAINATION ABOUT THIS MISMATCH**) and other studies with thermal models of the global active subduction zones (Syracuse *et al*. 2010).

The age of the high-*P* metamorphic event is crucial to the reconstruction of the geological history of this little-known terrain; however, reliable metamorphic age data has been lacking, and ages for the Nagaland ophiolite are poorly resolved whereas it is not so in the Eastern Belt (**AS SAID IN A PREVIOUS COMMENT, I THINK YOU SHOULD SPEND SOME**

ADDITIONAL WORD ON THIS, OTHERWISE IT IS NOT COMPLETELY CLEAR WHY YOU THINK THAT THERE IS SUCH LACK OF RELIABLE AGE DATA ADDED). We have integrated our new age and *P–T* data into a revised tectonic model for the evolution of the Naga ophiolite belt, as shown in Figure 1~~1~~2. Only one whole-rock K–Ar isotopic age of 148 ± 4 Ma (Upper Jurassic) has been reported from a volcanic rock in this area (Sarkar *et al*. 1996), which is supported by a radiolarian age (Baxter *et al*. 2011), whereas recently, a younger U–Pb zircon age of 115 Ma (Lower Cretaceous) has been reported from a plagiogranite (Singh *et al*. 2017). Based on the available geochronological and radiolarian ages, the formation age of the Nagaland ophiolite crust thus likely ranges between Early Cretaceous (Liu *et al*. 2016; our unpublished data) and Late Jurassic (Figure 1~~1~~2a). Past plate reconstructions during this period suggest that early subduction off the coast of Myanmar dipped to the west during the Jurassic, but there was a reversal in polarity immediately prior to the Early Cretaceous (Figure 11b; Bhowmik and Ao, 2015). This reversal caused the proto-Nagaland ophiolite complex oceanic crust to experience subduction along an eastern-dipping convergent margin during the Early Cretaceous, with U–Pb ages of the blueschist associated with the Nagaland ophiolite suggesting that peak high-pressure metamorphism was reached at around this time (Figure 1~~1~~2c).

Utilizing the integrated petrologically constrained *in situ* ages and thermobarometry shows that the unsheared sample 14 yielded a U–Pb age of 95.3 Ma while sheared samples yielded ages ranging between 93.7 Ma (sample 11) and 88.8 Ma (sample 13) Ma, illustrating an age difference between the sheared and unsheared samples. ~~The present study shows~~ This suggests that the Mesozoic ophiolite underwent H*P*–L*T* subduction-related metamorphism c. 95 Ma and that exhumation was a continuous process that lasted until c. 89 Ma (Figure 1~~1~~2d). This age range is in agreement with the Guillot *et al*. (2008)'s ~~reported~~ H*P* metamorphic age inferred from K–Ar whole rock and mineral (phengite, glaucophane) ages of 100 to 80 Ma

(**MAYBE YOU SHOULD ADD SOME DETAIL HOW THIS TIME HAS BEEN ESTIMATED (I.E., IS THIS COMING FROM GEOCHRONOLOGICAL ANALYSES? IF SO, WHAT IS THE METHOD THAT WAS APPLIED**? DONE) for the western Himalayan Tethyan ophiolites. Based on a zircon isotopic study, an older age of 115 Ma has been reported from the garnetiferous amphibolite of the adjoining Myanmar ophiolite (Liu *et al*. 2016). However, no petrological information was presented, making it hard to evaluate the significance of this age. ~~It~~ As a consequence, it is unclear whether the available ages ~~(Liu *et al*. 2016 and our data)~~ record a prolonged emplacement event, discrete metamorphic events or if the older amphibolite represents remnants of metamorphic sole of the ophiolite belt. Although the unsheared sample dataset is within uncertainty of the sheared sample dates, an overall age progression is evident from the studied sheared and unsheared samples. Based on the combined U–Pb age dataset and the calculated *P*–*T* regime**,** it can be inferred that the Nagaland blueschist rocks were exhumed at a rate of ~1 cm/year (~45 km in 5 Ma), which is in the order of rates of plate tectonic processes on the Phanerozoic Earth. However, exhumation along the slab interface would imply overall faster transport rates to achieve this vertical rate. **(I THINK THIS STATEMENT NEEDS SOME APPROPRIATE SUPPORTING REFERENCE. IN ANY CASE, PLEASE NOTE THAT THIS IS CONTRAST WITH WHAT YOU REPORTED IN THE ABSTRACT, WHERE YOU SAID THAT THIS EXHUMATION IS 'A TYPICAL SLOW" (LINE 44). PLEASE CORRECT IN ORDER TO AVOID INCONSISTENCIES** CORRECTED).

U–Pb dating of low-uranium minerals such as calcite, prehnite, epidote, amphibole (**YOU DID NOT SAY YOU MADE U-PB ANALYSES OF SUCH KIND OF MINERALS. SO IAM NOT SURE IT IS APPROPRIATE TO MENTION THESE TOO**, IT HAS BEEN MENTIONED) at small scale is a new and promising

geochronological method. In the present study, we focussed on both carbonate and other cogenetic silicate phases such as prehnite, epidote, amphibole etc. (**SO YOU ACTUALLY PERFORMED U-PB DATINGS ALSO ON OTHER PHASES? IF SO, WHY YOU DIDN'T REPORT THIS IN THE U-PB GEOCHRONOLOGY SECTION? THIS IS GETTING REALLY CONFUSING, I WARMLY INVITE YOU TO ELUCIDATE AND MAKE IT EXTEMELY CLEAR THROUGHOUT THE MANUSCRIPT.** DONE) formed at the same time and the isotopic systems seem to be closed since the metamorphic event. The reported age uncertainty could be improved by using well characterised specific with less scatter age and matrix matched standards (e.g., carbonate minerals normalisation of Pb–Pb isotope is currently achieved using a synthetic glass other than a carbonate, Roberts et al. 2020) ~~standards improved~~ reference materials (both carbonate and silicate phases) (**WHAT DO MEAN BY THIS? IN WHAT SENSE THESE REFERENCE MATERIALS SHOULD BE IMPROVED? I THINK SOME ELUCIDATION MIGHT BE USEFUL,** DONE) Although the behaviour of uranium in carbonates that have undergone high *P*/low *T* is not clear because of the lack of studies in natural and synthetic systems, our study ~~shows~~ suggest that the U–Pb systematics of carbonate can withstand temperatures up to 500 °C without resetting. These data thus encourage the ongoing development of in-situ dating of carbonates and low uranium silicate minerals as a tool to understand the rates and ages of tectonic processes.

Acknowledgements

BM began this work during his visits to JGU Mainz on a BOYSCAST Fellowship and continued during the INSA-DFG Exchange programme visit to Bonn. BM thanks the Council of Scientific and Industrial Research, Government of India for financial support in the form of a project. Sample processing equipment were procured under a Department of Science and

Technology, Government of India FIST program. This is FIERCE contribution XX. BM acknowledges Yhunyulo Tep for the help during the field work. Lorenzo Fedele (Napoli) and four anonymous journal reviewers are appreciated for their insightful comments.

References

Acharyya S.K., 2015, Indo-Burman Ranges: a belt of accreted microcontinents, ophiolites and Mesozoic–Paleogene flyschoid sediments: International Journal of Earth Sciences, v. 104, p. 1235–1251.

Allen, R., Najman, Y., Carter, A., Barfod, D., Bickle, M.J., Chapman, H.J., Garzanti, E., Vezzoli, G., Ando, S., and Parrish, R.R., 2008, Provenance of the Tertiary sedimentary rocks of the Indo-Burman Ranges, Burma (Myanmar): Burman arc or Himalayan-derived?: Journal of the Geological Society of London, v. 165, p. 1045–1057.

Anon., 1986, Geology of Nagaland ophiolite: Geological Survey of India Memoir, v. 119, 113 pp.

Ao, A., Bhowmik, S.K., 2014, Cold subduction of the Neotethys: the metamorphic record from finely banded lawsonite and epidote blueschists and associated metabasalts of the Nagaland Ophiolite Complex, India: Journal of Metamorphic Geology, v. 32, p. 829–860.

Baxter, A.T., Aitchison, J.C., Zyabrev, S.V., and Ali, J.R., 2011, Upper Jurassic radiolarians from the Naga Ophiolite, Nagaland, northeast India: Gondwana Research, v. 20, p. 638–644.

Bhowmik, S.K., and Ao, A., 2016, Subduction initiation in the Neo-Tethys: constraints from counterclockwise P–T paths in amphibolite rocks of the Nagaland Ophiolite Complex, India: Journal of Metamorphic Geology, v. 34, p. 17–44.

Brunnschweiler, R.O., 1966, On the geology of the Indoburman ranges — Arakan Coast and Yoma, Chin Hills, Naga Hills: Journal of the Geological Society of Australia, v. 13, p. 137–194.

Burisch, M., Gerdes, A., Walter, B.F., Neumann, U., Fettel, M. and Markl, G., 2017, Methane and the origin of five-element veins: Mineralogy, age, fluid inclusion chemistry and ore forming processes in the Odenwald, SW Germany: Ore Geology Reviews, v. 81, p. 42–61.

Carswell, D.A., 1990, Eclogite-Facies Rocks. Blackie, London.

Chatterjee, N., and Ghose, N.C., 2010, Metamorphic evolution of the Naga Hills eclogite and blueschist, North India: implications for early subduction of the Indian plate under the Burma microplate: Journal of Metamorphic Geology, v. 28, p. 209–225.

Cloos, M., 1985, Thermal evolution of convergent margins: Thermal modelling and evaluation of isotopic Ar-ages for blueschists in the Franciscan Complex of California: Tectonics, v. 4, p. 421–433.

Coggon, R., and Holland, T.J.B., 2002, Mixing properties of phengitic micas and revised garnet–phengite thermobarometers: Journal of Metamorphic Geology, v. 20, p. 683–696.

Coogan, L.A., Parrish, R.R. and Roberts, N.M., 2016, Early hydrothermal carbon uptake by the upper oceanic crust: Insight from in situ U–Pb dating: Geology, v. 44(2), p. 147–150.

Diener, J.F.A., and Powell, R., 2012, Revised activity–composition models for clinopyroxene and amphibole: Journal of Metamorphic Geology, v. 30, p. 131–142.

Ernst, W.G., 1973, Blueschist metamorphism and P–T regimes in active subduction zones: Tectonophysics, v. 17, p. 255–272.

Gansser, A., 1980, The significance of the Himalayan suture zone: Tectonophysics, v. 62, p. 37–52.

Gilley, L.D., Harrison, T.M., Leloup, P.H., Ryerson, F.J., Lovera, O.M. and Wang, J.H., 2003, Direct dating of left-lateral deformation along the Red River shear zone, China and Vietnam: Journal of Geophysical Research: Solid Earth, v. 108(B2), 2127.

Guillot, S., Mahéo, G., de Sigoyer, J., Hattori, K.H. and Pêcher, A., 2008, Tethyan and Indian subduction viewed from the Himalayan high- to ultrahigh-pressure metamorphic rocks: Tectonophysics, v. 451, p. 225–241.

Hansman, R.J., Albert, R., Gerdes, A., and Ring, U., 2018, Absolute ages of multiple generations of brittle structures by U-Pb dating of calcite: Geology, v. 6(3), p. 207–210.

Hawthorne, F.C., Oberti, R., Harlow, G.E., Maresch, W.V., Martin, R.F., Schumacher, J.C. and Welch, M.D., 2012. Nomenclature of the amphibole supergroup. American Mineralogist, v. 97, p. 2031–2048.

Hernández-Uribe, D., Palin, R.M., Cone, K.A. and Cao, W., 2020. Petrological implications of seafloor hydrothermal alteration of subducted mid-ocean ridge basalt: Journal of Petrology, v. 9, p. egaa086, doi: 10.1093/petrology/egaa086

Holland, T.J.B., 2009, AX: A program to calculate activities of mineral end-members from chemical analyses. http://www.esc.cam.ac.uk/research/research-groups/holland/ax. Accessed June 2015.

Holland, T.J.B., and Powell, R., 1998, An internally consistent thermodynamic dataset for phases of petrological interest: Journal of Metamorphic Geology, v. 16, p. 309–344.

Holland, T.J.B., and Powell, R., 2003, Activity-composition relations for phases in petrological calculations: an asymmetric multicomponent formulation: Contributions to Mineralogy and Petrology, v. 145, p. 492–501.

Holland, T.J.B., Baker, J.M., and Powell, R., 1998, Mixing properties and activity–composition relationships of chlorites in the system MgO–FeO–Al_2O_3–SiO_2–H_2O: European Journal of Mineralogy, v. 10, p. 395–406.

Holt, W.E., Ni, J.F., Wallace, T.C., and Haines, A.J., 1991, The active tectonics of the Eastern Himalayan syntaxis and surrounding regions: Journal of Geophysical Research, v. 96, p. 14595–14632.

Johannes, W., and Puhan, D., 1971, The calcite-aragonite transition, reinvestigated. Contributions to Mineralogy and Petrology, v. 31(1), p. 28–38.

Kretz, R., 1983, Symbols for rock-forming minerals: American Mineralogist, 68, 277–279.

Khogenkumar, S., Singh, A.K., Kumar, S., Lakhan, N., Chaubey, M., Imtisunep, S., Dutt, A. and Oinam, G., 2021, Subduction versus non-subduction origin of the Nagaland-Manipur Ophiolites along the Indo-Myanmar Orogenic Belt, northeast India: Fact and fallacy. Geological Journal, v. 56(4), p. 1773-1794.

Li, Q., Parrish, R.R., Horstwood, M.S.A., and McArthur, J.M., 2014, U–Pb dating of cements in Mesozoic ammonites: Chemical Geology, v.376, p. 76–83.

Liu, C.-Z., Chung, S.-L., Wu, F.-Y., Zhang, C., Xu, Y., Wang, J.-G., Chen, Y. and Guo, S., 2016, Tethyan suturing in Southeast Asia: Zircon U–Pb and Hf–O isotopic constraints from Myanmar ophiolites: Geology, v. 44, p. 311–314.

Ludwig, K., 2007, Isoplot 3.62, Berkley Geochronology Centre Special Publication 4, p. 70.

Morimoto, N. *et al*. 1988, Nomenclature of pyroxenes: American Mineralogist, v. 73, p. 1123–1133.

Millonig, L.J., Gerdes, A., and Groat, L.A., 2012, U–Th–Pb geochronology of meta-carbonatites and meta-alkaline rocks in the southern Canadian Cordillera: a geodynamic perspective: Lithos, v. 152, p. 202–217.

Mitchell, A.H.G., 1993, Cretaceous–Cenozoic tectonic events in the western Myanmar–Assam region: Journal of the Geological Society of London, v. 150, p. 1089–1102.

Mitchell, A.H.G., Htay, M.T., Htun, K.M., Win, M.N., Oo, T., and Hlaing, T., 2007, Rock relationships in the Mogok Metamorphic Belt, Tatkon to Mandalay, central Myanmar: Journal of Asian Earth Sciences, v. 29, p. 891–910.

Mitchell, A.H.G., Chung, S.-L., Oo, T., Lin, T.-H., and Hung, C-H., 2012, Zircon U-Pb ages in Myanmar: magmatic-metamorphic events and the closure of a Neo-Tethys Ocean?: Journal of Asian Earth Sciences, v. 56, p. 1–23.

Miyashiro, A., 1961, Evolution of metamorphic belts. Journal of Petrology, v. 2, p. 277–311.

Palin, R.M., and White, R.W., 2016, Emergence of blueschists on Earth linked to secular changes in oceanic crust composition: Nature Geoscience, v. 9, p. 60–64.

Palin, R.M., Weller, O.M., Waters, D.J., and Dyck, B., 2016, Quantifying geological uncertainty in metamorphic phase equilibria modelling; a Monte Carlo assessment and implications for tectonic interpretations: Geoscience Frontiers, v. 7, p. 591–607.

Penniston-Dorland, S. C., Kohn, M. J., and Manning, C. E., 2015, The global range of subduction zone thermal structures from exhumed blueschists and eclogites: Rocks are hotter than models: Earth and Planetary Science Letters, v. 428, p. 243–254.

Powell, R., and Holland, T.J.B., 1988, An internally consistent thermodynamic dataset with uncertainties and correlations: 3. Application to geobarometry, worked examples, and a computer program: Journal of Metamorphic Geology, v. 6, p. 173–204.

Powell, R., and Holland, T.J.B., 1994, Optimal geothermometry and geobarometry: American Mineralogist, v. 79, p. 120–133.

Rasbury, E.T., Cole, J.M., 2009, Directly dating geologic events: U–Pb dating of carbonates: Reviews of Geophysics v. 47, RG3001.

Ring, U., and A. Gerdes, 2016, Kinematics of the Alpenrhein-Bodensee graben system in the Central Alps: Oligocene/Miocene transtension due to formation of the Western Alps arc: Tectonics, v. 35, doi:10.1002/2015TC004085.

Robb, L.J., Armstrong, R.A., and Waters, D.J., 1999, The history of granulite-facies metamorphism and crustal growth from single zircon U–Pb geochronology: Namaqualand, South Africa: Journal of Petrology, v. 40, p. 1747–1770.

Roberts, N.M.W. and Walker, R.J., 2016. U-Pb geochronology of calcite-mineralized faults: Absolute timing of rift-related fault events on the northeast Atlantic margin: Geology, v. 44, p. 531–534.

Roberts, N.M.W., Drost, K., Horstwood, M.S.A., Condon, D.J., Chew, D., Drake, H., Milodowski, A.E., McLean, N.M., Smye, A.J., Walker, R.W., Haslam, R., Hodson, K., Imber, J., Beaudoin, N., and Lee, J.K., 2020. Laser ablation inductively coupled plasma mass spectrometry (LA-ICP-MS) U–Pb carbonate geochronology: strategies, progress, and limitations: Geochronology, v. 2, p. 33–61,

Roduit, N., 2010. JMicroVision: un logiciel d'analyse d'images pétrographiques innovant: Étude sur différentes méthodes de quantification et de caractérisation des roches. Éditions universitaires Européennes, 136 pp.

Rubatto, D., and Hermann, J., 2001, Exhumation as fast as subduction?: Geology, v. 29, p. 3–6.

Rubatto, D., Williams, I.S. and Buick, I.S., 2001, Zircon and monazite response to prograde metamorphism in the Reynold Range, Central Australia: Contribution to Mineralogy and Petrology, v. 140, p. 458–468.

Sarkar, A., Datta, A.K., Poddar, B.C., Bhattacharyya, B.K., Kollapuri, V.K., and Sanwal, R., 1996, Geochronological studies of Mesozoic igneous rocks from eastern India: Journal of Southeast Asian Earth Sciences, v. 13, p. 77–81.

Salih, N., Mansurbeg, H., Kolo, K., Gerdes, A., and Préat, A., 2019, In situ U-Pb dating of hydrothermal diagenesis in tectonically controlled fracturing in the Upper Cretaceous Bekhme Formation, Kurdistan Region-Iraq: International Geology Review, v. 62, p. 2261–2279.

Schmidt, M.W., and Poli, S., 1998, Experimentally based water budgets for dehydrating slabs and consequences for arc magma generation: Earth and Planetary Science Letters, v. 163, p. 361–379.

Searle, M.P., Noble, S.R., Cottle, J.M., Waters, D.J., Mitchell, A.H.G., Hlaing, T., and Horstwood, M.S.A., 2007, Tectonic evolution of the Mogok metamorphic belt, Burma (Myanmar) constrained by U–Th–Pb dating of metamorphic and magmatic rocks: Tectonics, v. 26, p. TC3014.

Sengupta, S., Ray, K.K., Acharyya, S.K., and de Smeth, J.B., 1990, Nature of ophiolite occurrence along eastern margin of Indian plate and their tectonic significance: Geology, v. 18, p. 439–442.

Shi, G.H., Cui, W.Y., Cao, S.M., Jiang, N., Jian, P., Liu, D.Y., Miao, L.C., and Chu, B.B., 2008, Ion microprobe zircon U–Pb age and geochemistry of the Myanmar jadeitite: Journal of the Geological Society of London, v. 165, p. 221–234.

Shi, G., Lei, W., He, H., Nok Ng, Y., Liu, Y., Liu Y., Yuan, Y., Kang, Z., and Xie, G., 2014, Superimposed tectono-metamorphic episodes of Jurassic and Eocene age in the jadeite uplift, Myanmar, as revealed by $^{40}Ar/^{39}Ar$ dating. Gondwana Research, v. 26, p. 464–474.

Singh, A.K., Chung, S.L., Bikramaditya, R.K. and Lee, H.Y., 2017, New U–Pb zircon ages of plagiogranites from the Nagaland-Manipur Ophiolites, Indo-Myanmar Orogenic Belt, NE India: Journal of Geological Society of London, v. 174, p. 170–179.

St-Onge, M.R., Rayner, N., Palin, R.M., Searle, M.P., Waters, D.J., 2013, Integrated pressure-temperature-time constraints for the Tso Morari dome (NW India): Implications for the burial and exhumation path of UHP units in the western Himalaya: Journal of Metamorphic Geology, v. 31, p. 469–504.

Stacey, J.S., and Kramers, J.D., 1975, Approximation of terrestrial lead isotope evolution by a two-stage model: Earth and Planetary Science Letters, v. 26, p. 207–221.

Syracuse, E.M., van Keken, P.E., and Abers, G.A., 2010, The global range of subduction zone thermal models. Physics of the Earth and Planetary Interiors, v. 183, p. 73–90.

Terry, M.P., Robinson, P. and Ravna, K., 2000, Kyanite eclogite thermobarometry and evidence for thrusting of UHP over HP metamorphic rocks, Nordøyane, Western Gneiss Region, Norway: American Mineralogist, v. 85, p. 1637–1650.

Wang, X. and Griffin, W.L., 2004, Unusual Hf contents in metamorphic zircon from coesite-bearing eclogites of the Dabie Mountains, east-central China: implications for the dating of ultrahigh-pressure metamorphism: Journal of Metamorphic Geology, v. 22, p. 629–637.

Wang, Y., and Foley, S.F., 2020, The role of blueschist stored in shallow lithosphere in the generation of post-collisional orogenic magmas: Journal of Geophysical Research, v. 125, doi.org/10.1029/2020JB019910.

White, R.W., Powell, R., and Holland, T.J.B., 2007, Progress relating to calculation of partial melting equilibria for metapelites: Journal of Metamorphic Geology, v. 25, p. 511–527.

White, R.W., Powell, R., Holland, T.J.B., and Worley, B.A., 2000, The effect of TiO_2 and Fe_2O_3 on metapelitic assemblages at greenschist and amphibolite facies conditions: mineral equilibria calculations in the system K_2O–FeO–MgO–Al_2O_3–SiO_2–H_2O–TiO_2–Fe_2O_3: Journal of Metamorphic Geology, v. 18, p. 497–511.

Williams, I.S., and Claesson, S., 1987, Isotopic evidence for Precambrian provenance and Caledonian metamorphism of high grade paragneisses from the Seve Nappes, Scandanavian Caledonides. II, Ion microprobe zircon U-Th-Pb: Contribution to Mineralogy and Petrology, v. 97, p. 205–217.

Yui, T.F., Fukoyama, M., Iizuka, Y., Wu, C.M., Wu, T.W., Liou, J.G. and Grove, M., 2013, Is Myanmar jadeitite of Jurassic age?: A result from incompletely recrystallised inherited zircon. Lithos, v. 160–161, p. 268–282.

Zhang, Zh., Mao, Zh., Liu, X., Zhang, Y., and Brodholt, J., 2018, Stability and Reactions of $CaCO_3$ Polymorphs in the Earth's Deep Mantle: Journal of Geophysical Research, Solid Earth, v. 123(8), p. 6491–6500.

Figure captions

Figure 1. (A) Regional geological map of Indo-Myanmar Range and part of Myanmar (after Acharyya 2015). (B) Geological map of the Indo-Myanmar ophiolite belt (after Geological Survey of India M.N.C. DRG No. 42/87) (C) Geological map of the Nagaland ophiolite belt showing sample locations (after Anon. 1986, Ao and Bhowmick, 2016). (D) Field photographs (1) Unfoliated/Unsheared sample occur as boulders. Person for reference. (2) Unsheared sample showing the slicken sided face, chisel is for reference. (3) Blueschist samples present as blocky boulders. (4) Sheared sample showing foliation on a freshly broken face. Pen shows the foliation trend.

Figure 2. Thin-section photomicrographs showing representative mineral assemblages and microstructures for undeformed samples N5 (a–b) and 14 (c–d). All thin section images are shown under plane-polarized light. Scale bar is 1 mm. (a–b) Glaucophane- and epidote-rich matrix in sample N5, with minor garnet porphyroblasts associated with quartz and muscovite.

(c) Small millimetre-scale garnet in sample 14 mostly occurs in quartz-rich domains that are relatively epidote- and barroisite-poor. (d) Barroisite grains enclose epidote crystals. Mineral use in 2(a) Gln – Glaucophane, Grt – Garnet, Ep – Epidote, Ms – Muscovite. 2(b) Gln – Glaucophane, Grt – Garnet, Ep – Epidote, Ms – Muscovite, Qtz – quartz, 2(c) Brs – Barroisite, Carb – Carbonate, Grt – Garnet, Ep – Epidote. 2(d) Brs – Barroisite, Ep – Epidote, Ms – Muscovite, Qtz – quartz, Ttn – Titanite.

Figure 3. Thin-section photomicrographs showing representative mineral assemblages and microstructures in sheared samples 7c (a–b) and 11 (c–f). All thin section images are shown under plane-polarized light (unless stated otherwise) and oriented perpendicular to the dominant metamorphic foliation. Scale bar is 1 mm. (a) The metamorphic foliation in sample 7c is defined by aligned crystals of epidote, sodic-calcic amphibole, and calcic amphibole, (b) and is crosscut by quartz- and carbonate-filled veins that also cause localized deflections at their intersections. Sample 11 contains olive-green aegirine–augite (c) and garnet (d) porphyroblasts that are wrapped by a glaucophane–magnesioriebeckite foliation defined by alternating glaucophane- and quartz-rich bands. Sheared veins filled with carbonate (e) and quartz (f) exhibit ductile deformation microstructures and dynamic recrystallization. Mineral abbreviation use in Figure 3(a) Brs – Wnc: Barroisite – Winchite, Ep – Epidote, Prg – Ed: Pargsite – Edinite, Ttn: Titanite, Figure 3(b) Qtz – Quartz, Carb – Carbonate, Brs – Barroisite, Wnc – Winchite, Ep – Epidote, Ms – Muscovite, Kfs – K-feldspar, Ab – Albite, 3(c) Agt – Aegirine augite, Gln: Glaucophane, Fgl – Ferroglacuphane, Grt – Garnet, Qtz – Quartz, Ms – Muscovite, Figure 3(d) Alb – Albite, Carb – Carbonate, Gln – Glaucophane, Fgl – Ferroglaucophane, Quartz – Quartz, Figure 3(e) Carb – Carbonate, Ms – Muscovite, Qtz – Quartz, Figure 3(f) Carb – Carbonate, Qtz – Quartz.

Figure 4. ~~Garnet c~~Compositional line profile for a garnet porphyroblast of from the unsheared sample N5, running from rim to rim ~~across a representative-sized euhedral grain~~ (~0.75 mm diameter). (a) Cation mole fractions of divalent cations. (b) X-ray compositional map of divalent cations showing relative concentrations from core to rim. Colours do not represent equivalent cation concentrations between images.

Figure 5. Compositions of amphiboles from all studied samples, ~~categorized~~ classified according to the classification scheme of Hawthorne *et al*. (2012). Discrimination between calcic (group 2), calcic-sodic (group 3), and sodic (group 4) amphiboles is based upon the Na content of the M4 crystallographic site, with the ranges <0.5, 0.5–1.5, and >1.5, respectively for a 23-oxygen recalculation. Representative compositions are given in Supplementary Table 2.

Figure 6. Results of mineral equilibria modelling for unsheared sample N5. (a) Pressure–temperature (*P*–*T*) pseudosection constructed for the bulk composition given in Supplementary Table 3. Dotted overlay represents the global range of *P*–*T* conditions modelled to occur at the surface of subducting ocean crust in present-day subduction zones (Syracuse *et al*. 2010). Gray star and associated dashed ellipses represent the results of avPT calculations (Supplementary Table 4) and are shown at 1 and 2 S.D. Bold line marks the extent of H_2O-bearing assemblage fields. Numbered fields are as follows: 1 – Grt Ms Cld Tlc Omp, 2 – Grt Ms Cld Tlc Omp Gln, 3 – Grt Ms Cld Tlc Omp Gln Lws, 4 – Grt Ms Cld Tlc Omp Ky Lws, 5 – Grt Ms Act Cld Tlc Ky Lws, 6 – Grt Ms Bt Cld Act Gln, 7 – Grt Chl Bt Cld Act Gln, 8 – Grt Bt Act Gln Mag, 9 – Grt Bt Chl Hbl Gln, 10 – Bt Omp Hbl Pl H_2O, 11 – Bt Omp Hbl Pl Ab H_2O, 12 – Grt Ms Omp Hbl H_2O, 13 – Grt Ms Gln H_2O, 14 – Grt Chl Ms Omp Gln, 15 – Grt Chl Ms Brs Gln, 16 – Grt Chl Ms Omp Gln Lws, 17 – Grt Ms Cld Omp

Gln Lws. Some small, minor fields are unlabelled for clarity. (b) Interpreted peak assemblage field showing isolines of ~~molar~~ modal proportions of selected phases. Red star indicates the best match between observed and calculated mineral abundances. Dashed line labelled $XNaM_4Act = 0.25$ marks the division between actinolite (<0.25) at low-T and barroisite (>0.25) at high-*T*. (c) Bar chart showing degree of correlation between observed volume proportions (%) of minerals and calculated proportions at 1.9 GPa and 485 °C (red star in ~~part~~ b). ~~(d) Graphical representation of the calculated (Calc. vol.%) and observed (Obs. Vol%) volume proportions for sample N5 at 1.9 GPa and 485 °C.~~

Figure 7. Results of mineral equilibria modelling for unsheared sample 14. (a) Pressure–temperature (*P*–*T*) pseudosection constructed for the bulk composition given in Supplementary Table 3. Dotted overlay represents the global range of P–T conditions modelled to occur at the surface of subducting ocean crust in present-day subduction zones (Syracuse *et al*. 2010). Gray star and associated dashed ellipses represent the results of avPT calculations (Table 4) and are shown at 1 and 2 S.D. Bold line marks the extent of H_2O-bearing assemblage fields. Numbered fields are as follows: 1 – Grt Ms Pg Omp Act Gln, 2 – Grt Ms Bt Omp Act Gln, 3 – Grt Bt Omp Act Gln Ab, 4 – Grt Bt Omp Act Gln Ilm Mag Ab (–Rt), 5 – Grt Bt Omp Act Gln Mag Ab (–Rt), 6 – Grt Bt Omp Brs Gln Mag, 7 – Bt Omp Brs Gln Hbl Mag, 8 – Grt Bt Omp Brs Hbl, 9 – Bt Di Brs Hbl H_2O, 10 – Bt Di Hbl Ttn H_2O (–Rt), 11 – Bt Di Hbl, 12 – Grt Ms Bt Omp Act H_2O, 13 – Grt Ms Tlc Omp Act H_2O, 14 – Grt Ms Tlc Omp H_2O, 15 – Grt Ms Tlc Omp Brs Lws, 16 – Grt Chl Ms Omp Brs, 17 – GrtChl Ms Omp Brs H_2O. Some small, minor fields are unlabelled for clarity. (b) Red star indicates the best match between observed and calculated mineral abundances. Interpreted peak assemblage field showing isolines of ~~molar~~ modal proportions of selected phases. Dashed line labelled $XNaM_4Act = 0.25$ marks the division between actinolite (<0.25) at low-T and

barroisite (>0.25) at high-T. (c) Bar chart showing degree of correlation between observed volume proportions (%) of minerals and calculated proportions at 2.0 GPa and 525 °C (red star in part b). ~~(d) Graphical representation of the calculated (Calc. vol.%) and observed (Obs. Vol%) volume proportions for sample 14 at 2.0 GPa and 525 °C.~~

Figure 8. Results of phase equilibria modelling for sheared sample 7c. (a) Pressure–temperature (*P–T*) pseudosection constructed for the bulk composition given in Supplementary Table 3. Dotted overlay represents the global range of P–T conditions modelled to occur at the surface of subducting ocean crust in present-day subduction zones (Syracuse *et al*. 2010). Gray star and associated dashed ellipses represent the results of avPT calculations (Table 4) and are shown at 1 and 2 S.D. Bold line marks the extent of H_2O-bearing assemblage fields. Numbered fields are as follows: 1 – Omp Act Gln Mag Rt Hem (–Ttn), 2 – Omp Act Gln Mag Rt, 3 – Omp Act Gln Mag, 4 – Omp Act Gln Mag Ab, 5 – Act Gln Mag Ab, 6 – Omp Act Hbl Gln Mag Rt (–Ttn), 7 – Omp Act Hbl Gln Ab, 8 – Act Hbl Gln Mag Ab, 9 – Chl Act Hbl Mag Ab, 10 – Chl Act Hbl Ab H_2O, 11 – BrsHbl Ab, 12 – Omp Act Hbl Ab, 13 – Di Act Hbl Ab H_2O, 14 – Di Hbl Ab H_2O, 15 – Di Act Hbl Pl, 16 – Di Hbl Pl Mag Hem (–Ttn, Ep), 17 – Omp Act Hbl Gln Rt Hem (–Ttn), 18 – Omp Brs Hbl Gln Rt Hem (–Ttn), 19 – Omp Brs Hbl Gln Rt (–Ttn), 20 – Omp Act Hbl Gln Rt (–Ttn), 21 – Omp Brs Hbl Gln, 22 – Omp Act Hbl Gln, 23 – Omp Brs Gln Rt Hem (–Ttn), 24 – Omp Act Hem (–Ttn), 25 – Omp Act (–Ttn). Some small, minor fields are unlabelled for clarity. (b) Red star indicates the best match between observed and calculated mineral abundances. Interpreted peak assemblage field showing isolines of ~~molar~~ modal proportions of selected phases. Dashed line labelled $XNaM_4Act = 0.25$ marks the division between actinolite (<0.25) at low-T and barroisite (>0.25) at high-T. (c) Bar chart showing degree of correlation between observed volume proportions (%) of minerals and calculated proportions at 0.6 GPa

and 465 °C (red star in part b). ~~(d) Graphical representation of the calculated (Calc. vol.%) and observed (Obs. Vol%) volume proportions at 0.6 GPa and 465 °C.~~

Figure 9. Isochrons for all dated samples. A: Unsheared sample 14. B: Sheared sample 11. C: Sheared sample 3b. D: Sheared sample 13. All ellipses are shown at the 2σ confidence interval and n = number of analyses.

Figure 10. Representative back scattered electron images of analysed samples 14 (a), 11 (b), 3b (c) and 13 (d). U–Pb analysed spots are showing in ellipse (white: silicate phases and yellow: carbonates).

Figure 1~~0~~1. Pressure–temperature ~~–time (*P–T–t*)~~ diagram summarizing the ~~history~~ proposed model for the tectonometamorphic evolution of blueschist-facies rocks from the Nagaland ophiolite complex. Red boxes represent calculated conditions of metamorphism and thick grey arrow represents the interpreted *P–T–t* evolution. Paths for Nagaland blueschists reported by Chatterjee and Ghose (2010) and Ao and Bhowmik (2014) are shown (CG10 and AB14, respectively) for comparison. Aragonite-calcite stability curve is from Johannes and Puhan (1971).

Figure 1~~1~~2. Schematic tectonic model for formation and exhumation of the Nagaland ophiolite belt and its metamorphic suite. ~~Final tectonic configuration of tectonostratigraphic slices is modified after Khogenkumar et al. (2020).~~ (a) Westward-dipping subduction away from Myanmar during the Jurassic, with future Nagaland ophiolite belt oceanic crust on the overlying plate. (b) Reversal in the subduction dip direction prior to the Early Cretaceous, leading to burial of future Nagaland ophiolitic crust and mantle. (c) Peak metamorphism of the studied samples was achieved during the Middle Cretaceous, with (d) slab ~~breakaway~~

break-off and buoyancy-driven exhumation and associated shearing of these units during the Middle to Late Cretaceous. (e) the final configuration of the Indo-Myanmar plates and suture zone between following collisional orogenesis (modified after Khogenkumar *et al*. 2021). Yellow star indicates locations of the studied samples during metamorphism and deformation.